



Norwegian University of
Science and Technology

Wind-Induced Response of Long-Span Suspension Bridges Subjected to Span- Wise Non-Uniform Winds: A Case Study

Erlend Munkeby Forbord
Hallvard Hjellvik

Master of Science in Engineering and ICT

Submission date: June 2017

Supervisor: Ole Andre Øiseth, KT

Co-supervisor: Aksel Fenerci, KT
Tor Martin Lystad, KT

Norwegian University of Science and Technology
Department of Structural Engineering



MASTER THESIS 2017

SUBJECT AREA: Dynamic response of structures	DATE: 11 June 2017	NO. OF PAGES: 18 + 96 + 27
---	-----------------------	-------------------------------

TITLE:

Wind-induced response of long-span suspension bridges subjected to span-wise non-uniform winds: A case study

Vindindusert respons av hengebruer med langt spenn utsatt for varierende vind langs bruspenntet: Et case-studie

BY:

Erlend Munkeby Forbord

Hallvard Hjellvik



SUMMARY:

The Hardanger Bridge has a main span of 1 310 meters which makes it the longest suspension bridge in Norway and among the top 15 longest in the world as of 2017. The bridge consists of only two traffic lanes and one pedestrian lane, which makes the bridge deck very slender. The bridge is located in a fjord in western Norway and the surroundings consist of mountains over 1 000 meters high. The mountains affect the wind field and make the wind characteristics at the bridge site span-wise non-uniform.

To verify the accuracy of dynamic response calculation methods of slender suspension bridges, a comprehensive measurement system was installed on the Hardanger Bridge after the opening in 2013. In this thesis, the main scope will be on the span-wise non-uniformity of the wind field. It will be investigated whether non-uniform wind profiles can predict the response of the bridge more accurately than uniform profiles with respect to the measured response.

A numerical study was carried out to investigate the influence of non-uniform wind speed and turbulence on the response prediction. Several profiles were studied and the concluding remarks were that the response increased for a non-uniform compared to a uniform wind speed profile. A non-uniform turbulence profile with the opposite shape of the wind profile decreased the response compared to the uniform turbulence profile. When the wind speed profile is non-uniform, the self-excited forces may also be taken as non-uniform. It was seen that for low wind speeds, the influence of including the non-uniform self-excited forces on the response was small, while for very high wind speeds the response got more unstable and the influence was larger.

The response has also been predicted using wind data from the Hardanger Bridge, and the predictions have been compared to the measured response. Uniform profiles of wind speed and turbulence have been given different values based on the measured data, more specifically the mean value of all sensors and the value from the midmost wind sensor. It is seen that the choice of value does not affect the accuracy of response predictions. No matter what values are chosen, the predictions are quite inaccurate in general. Introducing a non-uniform profile of mean wind speed makes the predictions slightly better in some cases, but not noteworthy, and the accuracy is still relatively low. When also including the non-uniformity of turbulence in the response calculations, the predicted response is reduced and the accuracy worsened with respect to the measured response. Accounting for the non-uniformity of self-excited forces shows almost no effect on the predictions. It is concluded that non-uniform wind profiles do not improve the accuracy of predicted bridge response, and that other uncertainties in the calculation methods have larger impact on the predictions than whether the non-uniform profiles are included or not.

RESPONSIBLE TEACHER: Associate Professor Ole Andre Øiseth

SUPERVISOR(S): Associate Professor Ole Andre Øiseth, PhD candidate Aksel Fenerci and PhD candidate Tor Martin Lystad

CARRIED OUT AT: The Department of Structural Engineering, NTNU.

MASTEROPPGAVE 2017

for

Erlend Munkeby Forbord og Hallvard Hjellvik

Vindindusert respons av hengebruer med langt spenn utsatt for varierende vind langs bruspennet: Et case-studie

Wind-induced response of long-span suspension bridges subjected to span-wise non-uniform winds: A case study

I forbindelse med prosjektet ferjefri E39 er Hardangerbrua instrumentert for å undersøke nøyaktigheten til metodene som benyttes for å beregne dynamisk respons av slanke brukonstruksjoner utsatt for vindlaster.

Denne oppgaven dreier seg om analyse av måledata og beregning av dynamisk respons av Hardangerbrua for å studere nøyaktigheten til metodene. Hovedfokuset vil være å undersøke om å inkludere varierende vindlaster langs bruspennet i responsberegningene kan øke nøyaktigheten til metodene.

Opgaven bør inneholde følgende temaer:

- Det skal gjennomføres et litteraturstudium knyttet opp mot dynamisk respons av hengebruer med varierende vind langs bruspennet.
- Gjeldende beregningsmetoder skal modifiseres til å ta hensyn for varierende vindlaster langs konstruksjoner.
- Det skal gjennomføres en numerisk studie for å undersøke effektene ved å inkludere varierende vindhastigheter og turbulens langs bruspennet i responsberegningene.
- Beregning av dynamisk respons ved bruk av målt vinddata.
- Det skal undersøkes om den predikerte dynamiske responsen blir beregnet mer nøyaktig i forhold til målt respons av brua ved å inkludere varierende vind langs bruspennet i responsberegningene.

Besvarelsen organiseres i henhold til gjeldende retningslinjer.

Veileder(e): Ole Andre Øiseth, Aksel Fenerci og Tor Martin Lystad

Besvarelsen skal leveres til Institutt for konstruksjonsteknikk innen 11. juni 2017.

NTNU, 15. januar, 2017

Ole Andre Øiseth
faglærer

Preface

This thesis is composed at the Department of Structural Engineering at the Norwegian University of Science and Technology, Spring 2017. The authors of this thesis have a background from the study programs Civil and Environmental Engineering and Engineering and ICT, respectively, both within the field of study in structural engineering. The thesis presents the final work of the last semester at these two 5-year study programs at NTNU.

The thesis is developed in collaboration with the Norwegian Public Road Administration which has several projects regarding bridge crossings over larger fjords. The thesis comprises a field in the dynamic engineering which has not been researched much before, and include tasks like calculating the buffeting response of a bridge using measured wind data and signal processing. This has made the work exciting and educational .

We want to thank our supervisor Associate Professor Ole Øiseth and co-supervisors PhD candidates Aksel Fenerci and Tor Martin Lystad for the good guidance, the follow-up and for answering all our questions through the work. Also, we want to thank the Norwegian Public Road Administration for the financial support for this thesis and providing the data. Lastly, we would like to thank our friends and fellow students for inspiring discussions and good company throughout the time at NTNU.

Erlend Munkeby Forbord

Hallvard Hjellvik

Trondheim, 2017-06-11



Abstract

The Hardanger Bridge has a main span of 1 310 meters which makes it the longest suspension bridge in Norway and among the top 15 longest in the world as of 2017. The bridge consists of only two traffic lanes and one pedestrian lane, which makes the bridge deck very slender. The bridge is located in a fjord in western Norway and the surroundings consist of mountains over 1 000 meters high. The mountains affect the wind field and make the wind characteristics at the bridge site span-wise non-uniform.

To verify the accuracy of dynamic response calculation methods of slender suspension bridges, a comprehensive measurement system was installed on the Hardanger Bridge after the opening in 2013. In this thesis, the main scope will be on the span-wise non-uniformity of the wind field. It will be investigated whether non-uniform wind profiles can predict the response of the bridge more accurately than uniform profiles with respect to the measured response.

A numerical study was carried out to investigate the influence of non-uniform wind speed and turbulence on the response prediction. Several profiles were studied and the concluding remarks were that the response increased for a non-uniform compared to a uniform wind speed profile. A non-uniform turbulence profile with the opposite shape of the wind profile decreased the response compared to the uniform turbulence profile. When the wind speed profile is non-uniform, the self-excited forces may also be taken as non-uniform. It was seen that for low wind speeds, the influence of including the non-uniform self-excited forces on the response was small, while for very high wind speeds the response got more unstable and the influence was larger.

The response has also been predicted using wind data from the Hardanger Bridge, and the predictions have been compared to the measured response. Uniform profiles of wind speed and turbulence have been given different values based on the measured data, more specifically the mean value of all sensors and the value from the midmost wind sensor. It is seen that the choice of value does not affect the accuracy of response predictions. No matter what values are chosen, the predictions are quite inaccurate in general. Introducing a non-uniform profile of mean wind speed makes the predictions slightly better in some cases, but not noteworthy, and the accuracy is still relatively low. When also including the non-uniformity of turbulence in the response calculations, the predicted response is reduced and the accuracy worsened with respect to the measured response. Accounting for the non-uniformity of self-excited forces shows almost no effect on the predictions. It is concluded that non-uniform wind profiles do not improve the accuracy of predicted bridge response, and that other uncertainties in the calculation methods have larger impact on the predictions than whether the non-uniform profiles are included or not.

Sammendrag

Hardangerbrua har et hovedspenn på 1 310 meter som gjør den til Norges lengste hengebru og blant de topp 15 lengste hengebruer i verden per 2017. Brua består av kun to kjørefelt i tillegg til et gangfelt, noe som gjør at brudekket er meget slankt. Brua spenner over Hardangerfjorden vest i Norge og omgivelsene består av høye fjell på over 1 000 meter. Fjellene påvirker vindfeltet og gjør at vindens egenskaper varierer langs bruspennet.

For å verifisere nøyaktigheten til metodene som benyttes for å estimere dynamisk respons av hengebruer, ble det installert et omfattende målesystem på Hardangerbrua etter åpningen i 2013. I denne masteroppgaven vil hovedfokuset være på det varierende vindfeltet langs brua. Det vil bli undersøkt om responsberegningne blir mer nøyaktige dersom de varierende egenskapene til vindfeltet blir inkludert i stedet for å bruke et uniformt vindfelt.

Et numerisk studie har blitt gjennomført for å undersøke påvirkningen av varierende vindhastigheter og turbulens på responsberegningene. Flere forskjellige profiler har blitt testet og resultatene viser at responsen blir større med bruk av varierende vindhastigheter i forhold til et uniformt vindhastighetsprofil langs brua. Varierende turbulensprofil langs brua med motsatt form av det varierende vindhastighetsprofilen viser seg å redusere responsen i forhold til når et uniformt turbulensprofil blir brukt. Når vindhastighetsprofilen varierer langs bruspennet vil også noen av de aerodynamiske egenskapene gjøre det samme, og dette kan inkluderes i responsberegningene. For lave vindhastigheter viser det seg at påvirkningen av varierende aerodynamiske egenskaper er liten, mens for veldig høye vindhastigheter blir responsen ustabil og påvirkningen større.

Responsen har også blitt estimert ved bruk av målt vinddata på Hardangerbrua, og den estimerte responsen har blitt sammenlignet med målt respons. Uniforme profiler for vindhastighet og turbulens har blitt gitt ulike verdier basert på målt data, nærmere bestemt gjennomsnittlig vindhastighet fra alle sensorene og vindhastigheten fra sensoren nærmest midten av bruspennet. Nøyaktigheten til responsen viser seg å ikke bli påvirket av hvilken av verdiene som er valgt for et uniformt profil. Uansett hvilken verdi som blir brukt er estimert respons forholdsvis unøyaktig. Ved å inkludere varierende vindhastigheter blir responsberegningene noe bedre, men ikke nevneverdig, og nøyaktigheten er fremdeles nokså lav. Når i tillegg varierende turbulens blir introdusert i beregningene, blir den estimerte responsen redusert og mer unøyaktig i forhold til den målte responsen. Å inkludere de varierende aerodynamiske egenskapene langs bruspennet har nesten ingen påvirkning på den estimerte responsen. Det blir konkludert med at varierende profiler for vindhastighet og turbulens ikke forbedrer nøyaktigheten til den estimerte responsen, og at andre usikkerheter knyttet til beregningene har større innvirkning på estimatene enn om de varierende profilene blir inkludert eller ikke.

Contents

- Preface v
- Abstract vii
- Nomenclature xv

- 1 Introduction 1**

 - 1.1 Background 1
 - 1.2 Structure of the thesis 4

- 2 Theory 5**

 - 2.1 Random vibration theory 5
 - 2.2 Dynamic response prediction 11
 - 2.3 Modifications to account for the non-uniformity 16
 - 2.4 Data handling and signal processing 18

 - 2.4.1 Acceleration data 18
 - 2.4.2 Wind data 19

- 3 The Hardanger Bridge and monitoring system 21**

3.1	Description of the Hardanger Bridge	21
3.2	Measurement system	23
4	Wind field characteristics	25
4.1	Mean wind speeds	26
4.2	Turbulence components	30
5	Calculation basis	33
5.1	Constants	33
5.2	Modes	35
5.3	Aerodynamic derivatives	36
5.4	Wind profiles	38
6	Numerical study	41
6.1	Influence of non-uniform wind speed profile	41
6.2	Influence of non-uniform turbulence standard deviations	52
6.3	Influence of non-uniform self-excited forces	56
6.4	Conclusion	67
7	Comparison with measured response	69
7.1	Uniform profiles	71
7.1.1	Step 1: Wind speed	71
7.1.2	Step 2: Standard deviation of turbulence components	74
7.2	Non-uniform profiles	79

<i>CONTENTS</i>	xiii
7.2.1 Step 3: Wind speed	79
7.2.2 Step 4: Standard deviation of turbulence components	82
7.2.3 Step 5: Self-excited forces	86
8 Summary	91
8.1 Summary and Conclusions	91
8.2 Recommendations for Further Work	94
References	95
A Wind data	97
A.1 Horizontal wind profiles	97
A.2 Standard deviation of turbulence components	101
A.3 Wind characteristics	104
B Predicted response	105
B.1 Uniform compared with non-uniform mean wind speed	105
B.2 Uniform compared with non-uniform turbulence std	115

Nomenclature

Abbreviations

AD Aerodynamic derivatives

DFT Discrete Fourier transformation

FEM Finite Element Method

FFT Fast Fourier transformation

NPRA Norwegian Public Road Administration

NTNU Norwegian University of Science and Technology

pp percentage points

std standard deviation

List of symbols

η generalised coordinate

\mathbf{B}_q buffeting load coefficient matrix

\mathbf{H} frequency response matrix

$\mathbf{r}, \dot{\mathbf{r}}, \ddot{\mathbf{r}}$ displacement velocity and acceleration vector

μ mean value

ω radian frequency

ϕ mode shape

ρ air density

- σ standard deviation
- C** damping matrix
- K** stiffness matrix
- M** mass matrix
- q** load vector
- θ wind direction
- A_n^*, H_n^*, P_n^* aerodynamic derivatives
- A_{mn} aerodynamic admittance function
- B width of the girder
- C_D, C_L, C_M drag, lift and moment force coefficient
- D height of the girder
- f frequency vector
- $f_{Nyquist}$ Nyquist frequency
- G_n, \mathbf{G}_n the Fourier transform of a variable n , a vector
- K reduced frequency
- L span length
- S or \mathbf{S} auto or cross-spectral density, cross-spectral density matrix
- T natural period
- t time
- V horizontal mean wind velocity
- V_r reduced wind velocity
- z height above water
- Subscripts/superscripts**
- \sim modal property
- $*$ complex conjugate
- mean value

-1	matrix inverse
0	still air
ae	aerodynamic/aero-elastic
buff	buffeting
r	response position
T	transpose
u, w	along wind, across-wind vertically
V	wind property
y, z, θ	horizontal, vertical, rotation

Introduction

1.1 Background

Bridges can be constructed in many different ways, but suspension bridges stand out in the way that they can span long distances. Today, the Akashi Kaikyo Bridge in Japan is the longest suspension bridge in the world with a main span length of 1 990 meters [1]. Suspension bridges represent an attractive bridge concept because of the possibility of a long main span, and modern bridge design is trying to cross even longer distances. With the increasing span lengths, the study of wind effects on bridges is of growing importance.

Wind effects on large structures have been studied for a long time, and several factors have increased the interest in this field during the years. Longer and higher structures, smaller member sizes due to stronger materials and reduced structural damping due to new production methods are all factors that have increased the vulnerability to wind actions. A final triggering factor was the collapse of Tacoma Narrows Bridge in 1940 under a rather low wind speed of 19 m/s. During the decades after this incident, there was an increase in research within the field of bridge engineering. In 1961, Davenport stated that the wind load on buildings is determined by combined effects of wind climate, local terrain, aerodynamic characteristics of the structure, load amplification from wind-induced resonant vibrations and certain criteria determined by the use of the particular building [2]. To calculate the wind-induced loads and responses of structures, Davenport turned to statistics and stochastic vibration theory. The response was analysed mode by mode, based on the strip theory of aerodynamics, and described in his paper about gust effect loading (1967) [3].

In 1971, Scanlan et al. published an article on airfoil and bridge deck flutter derivatives that correctly explained the cause of the collapse of the Tacoma Narrows Bridge [4]. The publication laid the foundation for further bridge flutter analyses, and their formulations are still used in today's methods.

Currently, the state of the art is the multimode method, where the coupling effects from several still-air vibration modes are taken into account in the response calculation (Jain et al. 1996b) [5]. Several vibration modes may interact, and the multimode effects can stabilise or destabilise the structure, which has been shown by Katsuchi et al. (1999) [6].

The Norwegian Public Road Administration (NPRA) has started a project to replace the ferries with bridges west in Norway. Several fjords wider than 2000 m need to be crossed, including the Sognefjord which in addition to its large width has a complex surrounding terrain with steep mountains over 500 meters high which can affect the wind field at the site and make it span-wise non-uniform. The Hardanger Bridge, opened in 2013, has a surrounding terrain which is comparable to the Sognefjord and has been installed with a measurement system which enables verification of the methods used when calculating dynamic response of long-span bridges. In this thesis, the measurement system will be used to study the influence of a non-uniform wind field on the bridge response. Uniform and non-uniform profiles of mean wind speed and turbulence standard deviations will be made based on the measured wind data and used to predict the response of the Hardanger bridge. The predicted responses will be compared with each other and with the measured response to investigate if a non-uniform wind profile can predict the response more accurately than a uniform profile.

As the span lengths of suspension bridges get longer, the interest of studying certain aspects of wind-induced response more thoroughly has emerged. The effect of span-wise non-uniform wind fields on the response of suspension bridges is one of the topics that has become subject to research the recent years. Non-uniformity of the mean wind speed is what has been studied the most so far, and publications about its effect on both static response [7, 8], dynamic precritical response [9, 10, 8] and critical flutter speed [7, 10] has been made. The non-uniformity has been included through arbitrary functions [7, 10, 9] and use of wind tunnel measurements on a terrain model [8]. The studies of Cheynet (2016) [9] and Hu et al. (2017) [8] both show that their non-uniform mean wind speed profiles result in only small changes ($\leq 3\%$) of dynamic response compared to an energy equivalent uniform profile. However, their non-uniform profiles do not differ more than 10% from the uniform profiles. Arena et al. (2014) [10] show that the critical flutter speed might be affected by non-uniformity of the mean wind speed; however, it is reduced by only 3 % in their worst case. Arena et al. (2014) also discusses non-uniform vertical gusts, which are shown to increase the transient response in the vertical direction by over 100% at most compared to energy equivalent uniform gusts. Currently, this is the most significant result found in the literature regarding the effect of non-uniform wind fields on bridge response. Zhang (2006) [7] also finds large effects of non-uniform mean wind speeds, but the span-wise wind profiles compared have different energy content from each other, and the results are mainly attributed to this fact and not the non-uniformity of the wind.

What remains to be studied, at least to the authors' knowledge, are the effects of span-wise non-uniformity of turbulence. In this thesis, we will try to approach this aspect, in addition to the effect of non-uniform mean wind speeds. Both span-wise wind profiles described by arbitrary functions and real wind data from the Hardanger Bridge site will be used to study the response to non-uniform

winds. A larger variation of wind profiles than could be found in the literature will be analysed, including linear and exponential span-wise variations. The effect of including span-wise non-uniform self-excited forces in the calculations will also be investigated.

1.2 Structure of the thesis

The report is structured in the following way:

Chapter 2 - Theory: First, an introduction to the random vibration theory will be made. Then the theory behind the calculation of buffeting response is shown, together with the modifications made to account for the Hardanger Bridge and to account for non-uniformity of mean wind speed and turbulence standard deviations. Finally, the signal processing of the measurement data, both wind speeds and accelerations, is explained.

Chapter 3 - The Hardanger Bridge and the measurement system: Chapter 3 presents the Hardanger Bridge, the surrounding terrain and the measurement system installed on the bridge.

Chapter 4 - Wind characteristics: This chapter shows the general wind conditions at the site for the recordings used in this report. Some span-wise profiles of mean wind speed and standard deviation of the turbulence components at the bridge site are shown to illustrate the non-uniformity at the site.

Chapter 5 - Calculation basis: The constants, modes and calculation methods used in this thesis is described in this chapter.

Chapter 6 - Numerical study: The analysis in this report are divided into two parts. In this chapter, the results from the first part will be presented. The buffeting response is calculated from arbitrary mean wind speed and turbulence standard deviation profiles to study how the response react to the non-uniform profiles.

Chapter 7 - Comparison with measured response: In this part, the buffeting response calculated from the actual wind data and the results from the signal processing of acceleration data will be presented. Several different span-wise profiles for the mean wind speed and turbulence standard deviation obtained from the wind recordings will be compared and discussed.

Chapter 8 - Summary: Conclusions will be made based on the results from Chapter 6 and Chapter 7, and recommendations for further work will be given.

Theory

In this chapter, the theory used in this thesis will be presented. It starts with an introduction to the theory of random vibrations. The calculation of the dynamic response is presented next and mainly consists of three steps. The first step is to calculate the frequency response matrix, then the load matrix and finally the matrix of the response spectra. The method and formulas used for calculating the dynamic response for uniform wind fields will be shown, before explaining the adjustments made to account for non-uniform wind fields. Finally, a presentation will be given of the theory and formulas used for calculating the dynamic response from the measured data and for the signal processing of the wind data.

2.1 Random vibration theory

A stochastic process is an ensemble of random variables. Each variable can represent a variable at a certain time. A physical process, such as wind, can be taken as a stochastic process if the wind value is random at a certain time or position and the future behaviour can only be predicted with a certain probability [11]. A stochastic process can consist of an ensemble, which is an ensemble of samples. Each sample is a time series of a physical phenomenon.

The average value of a stochastic process with N number of samples at the time t_1 , can be taken as the sum of all the sampling points at time t_1 from all the samples, and divided by the total number of samples:

$$\mu_x(t_1) = \lim_{N \rightarrow \infty} \frac{1}{N} \sum_{n=0}^N x_n(t_1) \quad (2.1)$$

If the $\mu_x(t_1)$ do not vary when t_1 vary, the process is said to be weakly stationary [12]. A process

can either be a stationary or a non-stationary process. The weakly term indicate that only the first- and second-order probability distributions are independent of time, while a strictly stationary process indicates that all the probability distributions are independent of time. The average of each sample can be defined as:

$$\mu_x(n) = \lim_{T \rightarrow \infty} \frac{1}{T} \int_0^T x_n(t) dt \quad (2.2)$$

In an ergodic process, the statistical properties of a sample must represent the statistical properties of the entire process. Hence, $\mu_x(n)$ does not change for the different samples, $\mu_x = \mu_x(n)$. A process always has to be stationary to be an ergodic process, and each sample is representative of all the samples in this stochastic process [12].

Nyquist frequency

The Nyquist frequency is the maximum frequency which can be detected in a signal with sample rate of f_s . The sampling frequency has to be twice as high as the highest frequency contained in the signal, so if a signal has a maximum frequency of $10Hz$, the sampling frequency has to be $20Hz$. The Nyquist frequency indicates a minimum number of discrete values that need to be extracted to sufficiently represent the signal. The frequency is given by [12]:

$$f_{Nyquist} = \frac{f_s}{2} \quad (2.3)$$

If the sampling rate is chosen too low, aliasing occurs, and information will be lost. Figure 2.1 shows an example of a sufficiently sampled and a not sufficiently sampled signal. The signal which is not sufficiently sampled loses information by not including all peaks, and aliasing occurs.

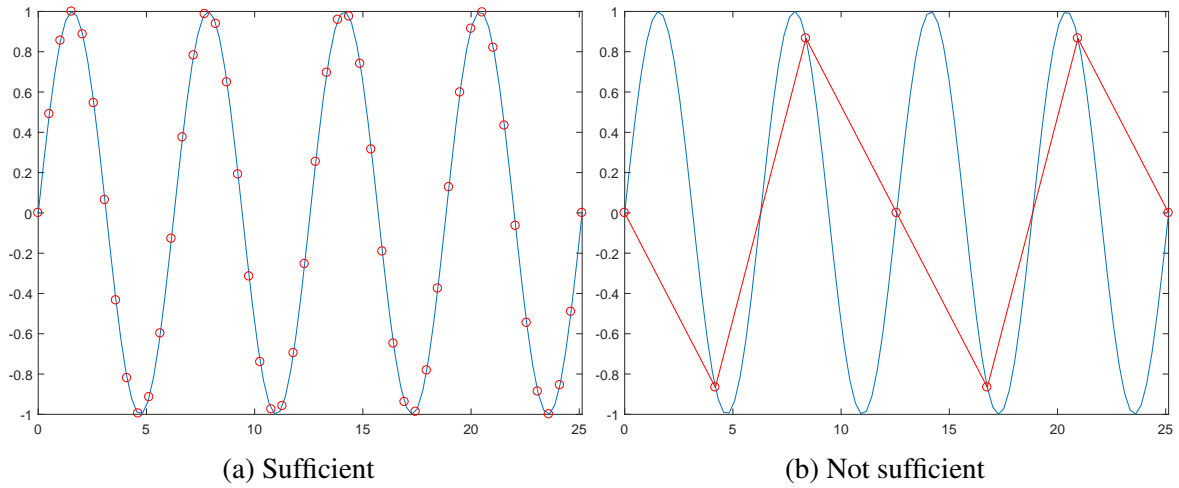


Figure 2.1: Sampling rate

Standardisation

All signals consist of a static and a fluctuating component, where the static component is the expected value of the signal. For a digitised signal, x_n , the expected value is defined as:

$$\bar{x} = \frac{1}{N} \sum_{n=1}^N x_n = \mu_x \quad (2.4)$$

The fluctuating component can be defined as a new signal varying around an equilibrium line equal zero:

$$y_n = x_n - \bar{x} \quad (2.5)$$

Fourier transformation and fast Fourier transformation

The most important task for a Fourier transformation is to convert a function from the time domain to the frequency domain. The Discrete Fourier Transform (DFT) is an approximated method for transforming the function to the frequency domain. This method is accurate for all frequencies which is below half the sampling rate, also called the Nyquist frequency [13].

A Fourier transformation comes from a Fourier series. If $x(t)$ is a continuous periodic function with period T , the Fourier series of the function is given by [12]:

$$x(t) = a_0 + 2 \sum_{k=1}^{\infty} \left(a_k \cos \frac{2\pi kt}{T} + b_k \sin \frac{2\pi kt}{T} \right) \quad (2.6)$$

The factors, a_0 , a_k and b_k , is the Fourier coefficients. The Fourier transform to the continuous function $x(t)$ is in complex notation defined as [12]:

$$X_k = \frac{1}{T} \int_0^T x(t) e^{-i(2\pi kt/T)} dt \quad (2.7)$$

If the signal consists of a discrete series with a finite number, N , of discrete elements, the Fourier transform is replaced by the sum and will be an approximation. The DFT is defined by [12]

$$X_k = \frac{1}{N} \sum_{r=0}^{N-1} x_r e^{-i(2\pi kr/N)} \quad (2.8)$$

Spectral density

Given a pair of arbitrary sample records, $x_k(t)$ and $y_k(t)$, the common statistical properties can be obtained with the spectral densities. The Fourier transform of the two sample records with finite duration T on the continuous form is given by:

$$\begin{aligned} X_k &= \int_0^T x_k(t) e^{-i\omega t} dt \\ Y_k &= \int_0^T y_k(t) e^{-i\omega t} dt \end{aligned} \quad (2.9)$$

The two-sided auto- and cross-spectral densities are defined by [13].

$$\begin{aligned} S_{xx}(\omega) &= \lim_{T \rightarrow \infty} E \left[\frac{1}{T} X_k^*(\omega, T) X_k(\omega, T) \right] \\ S_{yy}(\omega) &= \lim_{T \rightarrow \infty} E \left[\frac{1}{T} Y_k^*(\omega, T) Y_k(\omega, T) \right] \\ S_{xy}(\omega) &= \lim_{T \rightarrow \infty} E \left[\frac{1}{T} X_k^*(\omega, T) Y_k(\omega, T) \right] \end{aligned} \quad (2.10)$$

where * indicate the complex conjugate. Since the Fourier transform has a complex form, it is defined for $\omega \in (-\infty, \infty)$, hence the spectral density is also defined in the same frequency domain. The two-

sided spectra is symmetric around zero and can therefore be transformed to the one-sided spectra, $G(\omega)$, with ω defined in the range $(0, \infty)$ by [13]:

$$G_{nm}(\omega) = 2S_{nm}(\omega), \quad n, m \in \{x, y\} \quad (2.11)$$

The integrated spectral density in the frequency domain contains the variance of the process x , and is defined as [11]:

$$\text{Var}(x) = \sigma_x^2 = \int_0^{\infty} G_x(\omega) d\omega \quad (2.12)$$

Spectral density estimation

The most simple estimation method to calculate the spectra of a signal is by using the Discrete Fourier Transform. The spectra are estimated from a long signal, and measured signals may contain noise which influences the spectral density. The amount of noise in the signal can be reduced by different methods, which are all modifications of the periodogram. By using the convolution theorem, the periodogram is defined as follows for a signal $x(t)$ [14]:

$$\hat{P}_{xx}(\omega) = \frac{1}{N} X_N^*(\omega) X_N(\omega) \quad (2.13)$$

where $X_N(\omega)$ is the Fourier transform defined as

$$X_N(\omega) = \sum_{n=-\infty}^{\infty} x_N(n) e^{-i\omega n} \quad \text{where} \quad x_N(n) = w(n)x(n) \quad (2.14)$$

where n is the number of discrete elements in the signal and $w(n)$ is the window function. The window function may have different shapes, and in Figure 2.2 a Hamming window is shown. The modified periodogram is defined as [14]:

$$\hat{P}_{xx}(\omega) = \frac{1}{N} |X_N(\omega)|^2 = \frac{1}{N} \left| \sum_{n=-\infty}^{\infty} x(n)w(n)e^{-i\omega n} \right|^2 \quad (2.15)$$

Welch's method is using the modified periodogram method for each segment. The sample series of length N is first divided into K sequences with the same length. Then, the modified periodogram method is used to obtain the spectral density for each segment, before all segments are averaged to find the assembled estimated spectrum. The Hamming window is one window type that moderates the

transition between each segment. In Figure 2.2 an example of Hamming window applied on Welch's method, with segment length $L = N/2$ and 50% overlap, is shown.

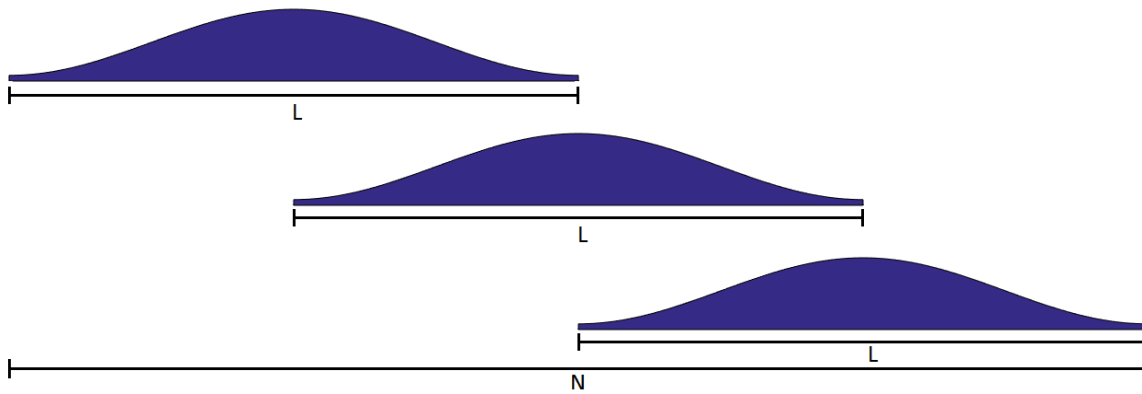


Figure 2.2: Welch's method with Hamming window

2.2 Dynamic response prediction

In this section the general relations and methods used in calculation of the dynamic response will be presented. It is assumed that the bridge may be treated as a line-like structure. The solution is based on a modal superposition approach introducing the mode shapes as generalised coordinates. Axial displacements in the longitudinal direction is disregarded. This method requires a sufficient number of natural modes and corresponding undamped natural frequencies. The equation of motion is introduced with displacement in Cartesian coordinates.

$$\mathbf{M}_0 \ddot{\mathbf{r}}(x, t) + (\mathbf{C}_0 - \mathbf{C}_{ae}(V, \omega)) \dot{\mathbf{r}} + (\mathbf{K}_0 - \mathbf{K}_{ae}(V, \omega)) \mathbf{r} = \mathbf{q}(x, t) \quad (2.16)$$

where \mathbf{M}_0 , \mathbf{C}_0 and \mathbf{K}_0 are the mass-, damping- and stiffness matrices in still-air conditions, and \mathbf{C}_{ae} and \mathbf{K}_{ae} are the aerodynamic damping- and stiffness matrices. $\mathbf{q}(x, t)$ is the wind load on the structure. The displacement in Cartesian coordinates can be expressed by the sum of the products of selected natural mode shapes, ϕ_i , and the corresponding generalised coordinates, η_i , as follows:

$$\begin{aligned} \mathbf{r}(x, t) &= \mathbf{\Phi}(x) \boldsymbol{\eta}(t) \\ \mathbf{\Phi}(x) &= [\phi_1 \dots \phi_i \dots \phi_{N_{mod}}] \\ \boldsymbol{\eta}(t) &= [\eta_1 \dots \eta_i \dots \eta_{N_{mod}}] \\ \phi_i &= [\phi_y \quad \phi_z \quad \phi_\theta] \end{aligned} \quad (2.17)$$

where ϕ_n , $n \in \{y, z, \theta\}$, symbolises the horizontal, vertical and torsional components of the mode shapes along the girder. Replacing the Cartesian coordinates by the mode shapes and the generalised coordinates, the equation of motion in the modal form is obtained as

$$\tilde{\mathbf{M}}_0 \ddot{\boldsymbol{\eta}}(x, t) + (\tilde{\mathbf{C}}_0 - \tilde{\mathbf{C}}_{ae}(V, \omega)) \dot{\boldsymbol{\eta}} + (\tilde{\mathbf{K}}_0 - \tilde{\mathbf{K}}_{ae}(V, \omega)) \boldsymbol{\eta} = \tilde{\mathbf{Q}}(t) \quad (2.18)$$

where the superscript \sim denotes the modal forms, which are defined as:

$$\begin{aligned}
\tilde{\mathbf{Q}}(t) &= \int_L \mathbf{\Phi}(x) \mathbf{q}(x, t) dx \\
\tilde{\mathbf{M}}_0 &= \int_L \mathbf{\Phi}^T(x) \mathbf{M}_0 \mathbf{\Phi}(x) dx \\
\tilde{\mathbf{C}}_0 &= \int_L \mathbf{\Phi}^T(x) \mathbf{C}_0 \mathbf{\Phi}(x) dx \\
\tilde{\mathbf{K}}_0 &= \int_L \mathbf{\Phi}^T(x) \mathbf{K}_0 \mathbf{\Phi}(x) dx \\
\tilde{\mathbf{K}}^{(ae)}(V, \omega) &= \int_L (\mathbf{\Phi}^T(x) \mathbf{K}_{ae}(V, \omega) \mathbf{\Phi}(x)) dx \\
\tilde{\mathbf{C}}^{(ae)}(V, \omega) &= \int_L (\mathbf{\Phi}^T(x) \mathbf{C}_{ae}(V, \omega) \mathbf{\Phi}(x)) dx
\end{aligned} \tag{2.19}$$

where L is the total length of the structure. The transformation from the time domain to the frequency domain is done by a Fourier transformation of $\boldsymbol{\eta}(x, t)$ and $\tilde{\mathbf{Q}}(x, t)$:

$$\begin{aligned}
\boldsymbol{\eta}(x, t) &= \sum_{\omega} \mathbf{G}_{\eta}(\omega) e^{i\omega t} \\
\tilde{\mathbf{Q}}(x, t) &= \sum_{\omega} \mathbf{G}_{\tilde{\mathbf{Q}}}(\omega) e^{i\omega t}
\end{aligned} \tag{2.20}$$

where $\mathbf{G}_{\eta}(\omega)$ and $\mathbf{G}_{\tilde{\mathbf{Q}}}(\omega)$ are the Fourier transforms of the generalised deformations and the modal load matrix, respectively. The generalised deformation and the modal load matrix in Equation (2.18) can then be replaced by their Fourier transforms to obtain the equation of motion on the following form:

$$\begin{aligned}
[-\tilde{\mathbf{M}}_0 \omega^2 + (\tilde{\mathbf{C}}_0 - \tilde{\mathbf{C}}_{ae}(V, \omega)) i\omega + (\tilde{\mathbf{K}}_0 - \tilde{\mathbf{K}}_{ae}(V, \omega))] \mathbf{G}_{\eta} &= \mathbf{G}_{\tilde{\mathbf{Q}}} \\
\tilde{\mathbf{H}}_{\eta}^{-1}(V, \omega) \mathbf{G}_{\eta} &= \mathbf{G}_{\tilde{\mathbf{Q}}}
\end{aligned} \tag{2.21}$$

$\tilde{\mathbf{H}}_{\eta}(V, \omega)$ denote the generalised frequency response matrix, which describes the relation between the load and the deformation of the structure for the given load.

Frequency response matrix

The frequency response matrix is defined as follows:

$$\tilde{\mathbf{H}}_{\eta}(V, \omega) = [-\tilde{\mathbf{M}}_0 \omega^2 + (\tilde{\mathbf{C}}_0 - \tilde{\mathbf{C}}_{ae}(V, \omega)) i\omega + (\tilde{\mathbf{K}}_0 - \tilde{\mathbf{K}}_{ae}(V, \omega))]^{-1} \tag{2.22}$$

The modal still-air and aerodynamic matrices are defined in Equation (2.19).

Damping and stiffness matrix

The aerodynamic damping and stiffness matrices can be obtained by following the notations of Scanlan and Tomko [11], as follows:

$$\begin{aligned}\hat{\mathbf{C}}_{ae}(V, \omega) &= \begin{bmatrix} P_1^* & P_5^* & BP_2^* \\ H_5^* & H_1^* & BH_2^* \\ BA_5^* & BA_1^* & B^2A_2^* \end{bmatrix} \\ \hat{\mathbf{K}}_{ae}(V, \omega) &= \begin{bmatrix} P_4^* & P_6^* & BP_3^* \\ H_6^* & H_4^* & BH_3^* \\ BA_6^* & BA_4^* & B^2A_3^* \end{bmatrix}\end{aligned}\quad (2.23)$$

where B is the width of the girder and $P_n^*, H_n^*, A_n^*, n \in \{1, 2, \dots, 6\}$ are the dimensionless aerodynamic derivatives which are functions of the frequency and the mean wind velocity. It has been considered convenient to normalise the aerodynamic damping and stiffness matrix in the following way

$$\mathbf{C}_{ae} = \frac{\rho B^2}{2} \omega \hat{\mathbf{C}}_{ae}, \quad \mathbf{K}_{ae} = \frac{\rho B^2}{2} \omega \hat{\mathbf{K}}_{ae} \quad (2.24)$$

where ρ is the air density, ω is the circular frequency and B is the width of the girder. The aerodynamic derivatives can be taken from the quasi-steady theory [11] and are functions of the reduced frequency $K = (\omega_i B)/V$, or the reduced velocity $V_{red} = 1/K$.

$$\begin{bmatrix} P_1^* & H_1^* & A_1^* \\ P_2^* & H_2^* & A_2^* \\ P_3^* & H_3^* & A_3^* \\ P_4^* & H_4^* & A_4^* \\ P_5^* & H_5^* & A_5^* \\ P_6^* & H_6^* & A_6^* \end{bmatrix} = \begin{bmatrix} -2\bar{C}_D \frac{D}{B} \frac{V}{B\omega_i} & -(C'_L + \bar{C}_D \frac{D}{B}) \frac{V}{B\omega_i} & -C'_M \frac{V}{B\omega_i} \\ 0 & 0 & 0 \\ C'_D \frac{D}{B} \left(\frac{V}{B\omega_i}\right)^2 & C'_L \left(\frac{V}{B\omega_i}\right)^2 & C'_M \left(\frac{V}{B\omega_i}\right)^2 \\ 0 & 0 & 0 \\ (\bar{C}_L - C'_D \frac{D}{B}) \frac{V}{B\omega_i} & -2\bar{C}_L \frac{V}{B\omega_i} & -2\bar{C}_M \frac{V}{B\omega_i} \\ 0 & 0 & 0 \end{bmatrix} \quad (2.25)$$

where C_D, C_L and C_M are force coefficients. The aerodynamic derivatives may also be derived experimentally from wind tunnel measurements of the cross section.

Load matrix

The actual wind load on the structure needs to be described in order to obtain the load matrix. The wind load on a body is described through the turbulence components. The cross-spectral density matrix for the turbulence component can be established as

$$\mathbf{S}_V^+(\Delta x, \omega) = \begin{bmatrix} \mathbf{S}_{uu}^+(\Delta x, \omega) & \mathbf{S}_{uw}^+(\Delta x, \omega) \\ \mathbf{S}_{wu}^+(\Delta x, \omega) & \mathbf{S}_{ww}^+(\Delta x, \omega) \end{bmatrix} \quad (2.26)$$

where \mathbf{S}_{uu}^+ represents the cross-spectral density of the horizontal wind component, \mathbf{S}_{ww}^+ is the cross-spectral density of the vertical component and $\mathbf{S}_{uw}^+ = \mathbf{S}_{wu}^+$ is the cross-spectral density of the horizontal and vertical components between two points with Δx as the distance between them. The cross spectral densities are expressed as

$$\begin{aligned} \mathbf{S}_{uu}^+(\Delta x, \omega) &= \mathbf{S}_u^+(\omega) \exp\left(-C_u \frac{\omega \Delta x}{V}\right) \\ \mathbf{S}_{ww}^+(\Delta x, \omega) &= \mathbf{S}_w^+(\omega) \exp\left(-C_w \frac{\omega \Delta x}{V}\right) \\ \mathbf{S}_{uw}^+(\Delta x, \omega) &= \mathbf{S}_{wu}^+(\Delta x, \omega) \approx 0 \end{aligned} \quad (2.27)$$

Here, \mathbf{S}_u^+ and \mathbf{S}_w^+ are the single point spectral densities of the turbulence. The cross terms \mathbf{S}_{uw}^+ and \mathbf{S}_{wu}^+ are often neglected. A transfer function is introduced to transform the turbulence into load on a body. The transfer function matrix is defined as

$$\mathbf{B}_q(\omega) = \frac{\rho V B}{2} \begin{bmatrix} 2(D/B)\bar{C}_D A_{yu}(\omega) & ((D/B)C'_D - \bar{C}_L)A_{yw}(\omega) \\ 2\bar{C}_L A_{zu}(\omega) & (C'_L + (D/B)\bar{C}_D)A_{zw}(\omega) \\ 2B\bar{C}_M A_{\theta u}(\omega) & BC'_M A_{\theta w}(\omega) \end{bmatrix} \quad (2.28)$$

where B and D denotes the width and height of the girder; $A_{nm}(\omega)$, $n \in \{y, z, \theta\}$ and $m \in \{u, w\}$, are the admittance functions and \bar{C}_n , C'_n , $n \in \{D, L, M\}$ are the mean value and the derivative of the static force coefficient. By the use of the transfer function matrix and the cross spectral density matrix of the turbulence components, the wind load spectral matrix can be calculated by

$$\mathbf{S}_q(\Delta x, \omega) = \mathbf{B}_q(V, \omega) \mathbf{S}_V(\Delta x, \omega) \mathbf{B}_q^T(V, \omega) \quad (2.29)$$

The modal wind load spectral density can be defined using the matrix of mode shapes, Φ [15]:

$$\mathbf{S}_{\tilde{Q}Buf}^+(\omega) = \int_L \int_L \mathbf{\Phi}^T(x_1) \mathbf{B}_q(\omega) \mathbf{S}_V^+(\Delta x, \omega) \mathbf{B}_q^T(\omega) \mathbf{\Phi}(x_2) dx_1 dx_2 \quad (2.30)$$

Spectral response matrix

The last calculation is to obtain the spectral response matrix, containing the auto- and cross-spectra of the response components, and the spectral density matrix of the modal response is defined as

$$\mathbf{S}_\eta(\omega) = \tilde{\mathbf{H}}^*(\omega) \mathbf{S}_{\tilde{Q}}(\omega) \tilde{\mathbf{H}}^T(\omega) \quad (2.31)$$

Here, $\tilde{\mathbf{H}}$ is the generalised frequency response matrix, $\mathbf{S}_{\tilde{Q}}$ is the modal wind load spectral matrix as defined previously, and $*$ denotes the complex conjugate. The modal response is converted back to the real coordinates to obtain the response spectrum in the following way using the mode shapes:

$$\mathbf{S}_R(x_r, \omega) = \mathbf{\Phi}(x_r) \mathbf{S}_\eta(\omega) \mathbf{\Phi}^T(x_r) \quad (2.32)$$

where $\mathbf{\Phi}$ is the mode shape matrix and \mathbf{S}_η is the modal response spectral matrix. The variances and covariances of the response components at the point x_r can be found by integrating the spectral response matrix in the frequency domain as follows [11]:

$$\text{VAR}(R(x_r)) = \boldsymbol{\sigma}^2(x_r) = \int_{\omega} \mathbf{S}_R^+(\omega, x_r) d\omega \quad (2.33)$$

The standard deviations σ_{ii} , where $i \in \{y, z, \theta\}$, and the correlation coefficients ρ_{ij} , where $i, j \in \{y, z, \theta\}$, at the point x_r are then given by

$$\text{STD}(R(x_r)) = \boldsymbol{\sigma}(x_r) = \sqrt{\boldsymbol{\sigma}^2(x_r)} \quad (2.34)$$

where

$$\boldsymbol{\sigma}(x_r) = \begin{bmatrix} \sigma_{yy} & \rho_{yz} & \rho_{y\theta} \\ \rho_{zy} & \sigma_{zz} & \rho_{z\theta} \\ \rho_{\theta y} & \rho_{\theta z} & \sigma_{\theta\theta} \end{bmatrix} \quad (2.35)$$

2.3 Modifications to account for the non-uniformity

In this section, the modified equations for calculating the dynamic response to non-uniform wind velocity and turbulence standard deviation profiles are shown. The components in the modal wind load spectral matrix and the frequency response matrix are changed to account for the non-uniform wind field. The modal wind load spectral matrix is then defined as follows:

$$\mathbf{S}_{\hat{Q}Buf}^+(\omega) = \int_L \int_L \Phi_i^T(x_1) \mathbf{B}_q(x_1, x_2, \omega) \mathbf{S}_V^+(x_1, x_2, \omega) \mathbf{B}_q^T(x_1, x_2, \omega) \Phi_j(x_2) dx_1 dx_2 \quad (2.36)$$

Both the buffeting load coefficient matrix and the cross-spectral densities of the turbulence components become functions of the location, x , because the uniform mean wind velocity component, V , is replaced by the non-uniform wind velocity function, $V(x)$. The buffeting load coefficient matrix is now a function of x , in addition to ω , with the same coefficients as explained previously, and is defined as follows:

$$\mathbf{B}_q(x_1, x_2, \omega) = \frac{\rho(V(x_1) + V(x_2)/2)B}{2} \begin{bmatrix} 2(D/B)\bar{C}_D A_{yu}(\omega) & ((D/B)C'_D - \bar{C}_L)A_{yw}(\omega) \\ 2\bar{C}_L A_{zu}(\omega) & (C'_L + (D/B)\bar{C}_D)A_{zw}(\omega) \\ 2B\bar{C}_M A_{\theta u}(\omega) & BC'_M A_{\theta w}(\omega) \end{bmatrix} \quad (2.37)$$

The cross-spectral densities of the turbulence components of the wind field are changed to be functions of x_1 and x_2 , instead of functions of the separation between the two points. They are now calculated from two different single point spectral densities of the turbulence, and the wind speed component is taken as the average mean wind speed at the two points. The cross-spectral density matrix is then expressed as

$$\mathbf{S}_V^+(x_1, x_2, \omega) = \begin{bmatrix} \mathbf{S}_{uu}^+(x_1, x_2, \omega) & \mathbf{S}_{uw}^+(x_1, x_2, \omega) \\ \mathbf{S}_{wu}^+(x_1, x_2, \omega) & \mathbf{S}_{ww}^+(x_1, x_2, \omega) \end{bmatrix} \quad (2.38)$$

where

$$\begin{aligned} \mathbf{S}_{uu}^+(x_1, x_2, \omega) &= \sqrt{\mathbf{S}_u^+(x_1, \omega) \mathbf{S}_u^+(x_2, \omega)} \exp\left(-C_u \frac{\omega \Delta x}{0.5(V(x_1) + V(x_2))}\right) \\ \mathbf{S}_{ww}^+(x_1, x_2, \omega) &= \sqrt{\mathbf{S}_w^+(x_1, \omega) \mathbf{S}_w^+(x_2, \omega)} \exp\left(-C_w \frac{\omega \Delta x}{0.5(V(x_1) + V(x_2))}\right) \\ \mathbf{S}_{uw}^+(\Delta x, \omega) &= \mathbf{S}_{wu}^+(\Delta x, \omega) \approx 0 \end{aligned} \quad (2.39)$$

The single point wind spectra used in dynamic response calculations in this thesis are modifications of the Kaimal wind spectrum [11] and are dependant on both location along the bridge axis and

frequency:

$$\begin{aligned} \mathbf{S}_u^+(x, \omega) &= \frac{\sigma_u^2(x)}{2\pi f} \frac{A_u(fz/V(x))}{(1 + 1.5A_u fz/V(x))^{5/3}} \\ \mathbf{S}_w^+(x, \omega) &= \frac{\sigma_w^2(x)}{2\pi f} \frac{A_w(fz/V(x))}{(1 + 1.5A_w fz/V(x))^{5/3}} \end{aligned} \quad (2.40)$$

Since the unit of frequency in these spectra is Hz, the spectra are divided by 2π so that the frequency variable can be changed to $\omega = 2\pi f$, as used in other equations.

The components that are dependent on x in the wind spectra are the horizontal mean wind velocity and the standard deviations of the horizontal and vertical turbulence components. By defining the wind spectra like this, the non-uniformity of the mean wind speed and turbulence standard deviations can be taken account for in the calculation of the modal wind load spectral matrix $\mathbf{S}_{\tilde{Q}Buf}^+(\omega)$ (Eq. (2.36)).

The non-uniformity of the mean wind speed also influences the frequency response function, through the aerodynamic damping and stiffness matrices which are dependant on the mean wind speed. The generalised frequency response matrix is then expressed as

$$\tilde{\mathbf{H}}_\eta(V(x), \omega) = [-\tilde{\mathbf{M}}_0 \omega^2 + (\tilde{\mathbf{C}}_0 - \tilde{\mathbf{C}}_{ae}(V(x), \omega))i\omega + (\tilde{\mathbf{K}}_0 - \tilde{\mathbf{K}}_{ae}(V(x), \omega))]^{-1} \quad (2.41)$$

where

$$\begin{aligned} \tilde{\mathbf{K}}^{(ae)}(V(x), \omega) &= \int_L (\Phi^T(x) \mathbf{K}_{ae}(V(x), \omega) \Phi(x)) dx \\ \tilde{\mathbf{C}}^{(ae)}(V(x), \omega) &= \int_L (\Phi^T(x) \mathbf{C}_{ae}(V(x), \omega) \Phi(x)) dx \end{aligned} \quad (2.42)$$

The aerodynamic damping and stiffness matrices are defined as follows:

$$\mathbf{C}_{ae}(x, \omega) = \frac{\rho B^2}{2} \omega \begin{bmatrix} P_1^* & P_5^* & BP_2^* \\ H_5^* & H_1^* & BH_2^* \\ BA_5^* & BA_1^* & B^2 A_2^* \end{bmatrix}, \quad \mathbf{K}_{ae}(x, \omega) = \frac{\rho B^2}{2} \omega^2 \begin{bmatrix} P_4^* & P_6^* & BP_3^* \\ H_6^* & H_4^* & BH_3^* \\ BA_6^* & BA_4^* & B^2 A_3^* \end{bmatrix} \quad (2.43)$$

where $P_n^*, H_n^*, A_n^*, n \in \{1, 2, \dots, 6\}$ are the dimensionless aerodynamic derivatives which are functions of the reduced frequency, $K = B\omega/V(x)$. Since the reduced frequency is a function of the mean wind speed which is now potentially different at each point along the bridge, the frequency response matrix becomes dependent on the span-wise profile of mean wind speed.

2.4 Data handling and signal processing

The measurements, both the wind and acceleration data, need to be processed in order to be used in the calculation of the dynamic response.

2.4.1 Acceleration data

The acceleration data need to be processed to compare it with the calculated dynamic response. The measurement data contain the accelerations in three different directions, horizontal, vertical and longitudinal. The three different directions of interest when looking at the dynamic response is lateral, vertical and torsional. Some of the accelerometers are installed in pairs in the cross section. In the case of a pair of sensors, the acceleration in the horizontal and vertical direction is averaged. The torsional component needs two accelerometers in the same cross section to be calculated, and can be obtained as follows:

$$\theta(t) = \frac{z_2(t) - z_1(t)}{B} \quad (2.44)$$

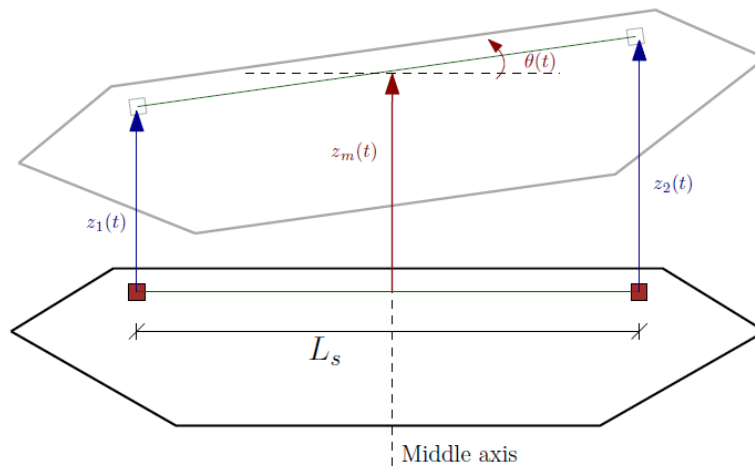


Figure 2.3: Transformation to torsional component

All data measured at the site is in unit g and needs to be multiplied with the gravitational acceleration, $9.81m/s^2$, to convert the data to acceleration. The spectral densities of the acceleration time series need to be obtained to calculate the response statistics. One method to obtain the spectral densities of the signal is Welch's method. Welch's method divides the signal into K different segments. Each segment is then Fourier transformed before each Fourier transform is merged into a final spectral density for the whole time series using a Hamming window. Each segment can overlap, and the

Hamming window is weighting the spectra when merging. For the analysis done in this report, the signal is divided into eight segments, and a Hamming window is used with 50% overlap between each segment.

The acceleration response can then be obtained by integrating the acceleration spectral response in the frequency domain. To calculate the displacement response, the acceleration spectra need to be transformed into displacement spectra by the following operation before integrating:

$$S_{rr}(\omega) = \frac{S_{\ddot{r}\ddot{r}}(\omega)}{\omega^4} \quad (2.45)$$

2.4.2 Wind data

The anemometers measure the wind in polar coordinates, where the different components are the angle indicating wind direction with respect to the bridge axis in the horizontal plane, magnitude of wind velocity in the horizontal plane and the vertical wind velocity. With a transformation as described below, it is possible to get the mean wind speed component in the mean wind direction, and the fluctuating components in three different directions in a new coordinate system with respect to the mean wind direction. Deviation from the mean wind direction can be obtained in radians as follows:

$$\phi(t) = (\theta(t) - \bar{\theta}) \frac{2\pi}{360} \quad (2.46)$$

where $\phi(t)$ is the angle between the velocity vector and the mean wind direction, $\theta(t)$ is the wind direction in the horizontal plane with respect to the bridge axis and $\bar{\theta}$ denotes the mean wind direction. The mean wind velocity component, U , in the horizontal plane, decomposed in the mean wind direction, can be calculated as follows:

$$R_u(t) = R_{uv}(t) \cos(\phi(t))$$

$$U = \frac{1}{N} \sum_{n=1}^N R_U(t_n) \quad (2.47)$$

where $R_{uv}(t)$ is the wind velocity vector in the horizontal plane before decomposition, $R_u(t)$ is the wind velocity vector decomposed in the mean wind direction and $\phi(t)$ is the angle between R_{uv} and the mean wind direction. The transformation to the mean wind component is graphically shown in Figure 2.4a. The fluctuating parts of the wind can be obtained in a new coordinate system with respect to the mean wind direction:

$$\begin{aligned}
 u(t) &= (R_{uv}(t) - \bar{R}_{uv})\cos(\phi(t)) \\
 v(t) &= (R_{uv}(t) - \bar{R}_{uv})\sin(\phi(t)), \quad \bar{R}_{uv} = \frac{1}{N} \sum_{n=1}^N R_{uv}(t_n) \\
 w(t) &= R_w(t)
 \end{aligned} \tag{2.48}$$

$R_w(t)$ is the vertical fluctuating component of wind velocity. In Figure 2.4b the transformation is shown. The x-axis corresponds to the bridge axis, and the mean wind direction $\bar{\theta}$ is shown for the mean wind component. The new coordinate system for the fluctuating components is shown with the red arrows. The global axis system is denoted with x , y and z , where x -axis is in the longitudinal direction of the bridge, y -axis is perpendicular and z -axis is vertical.

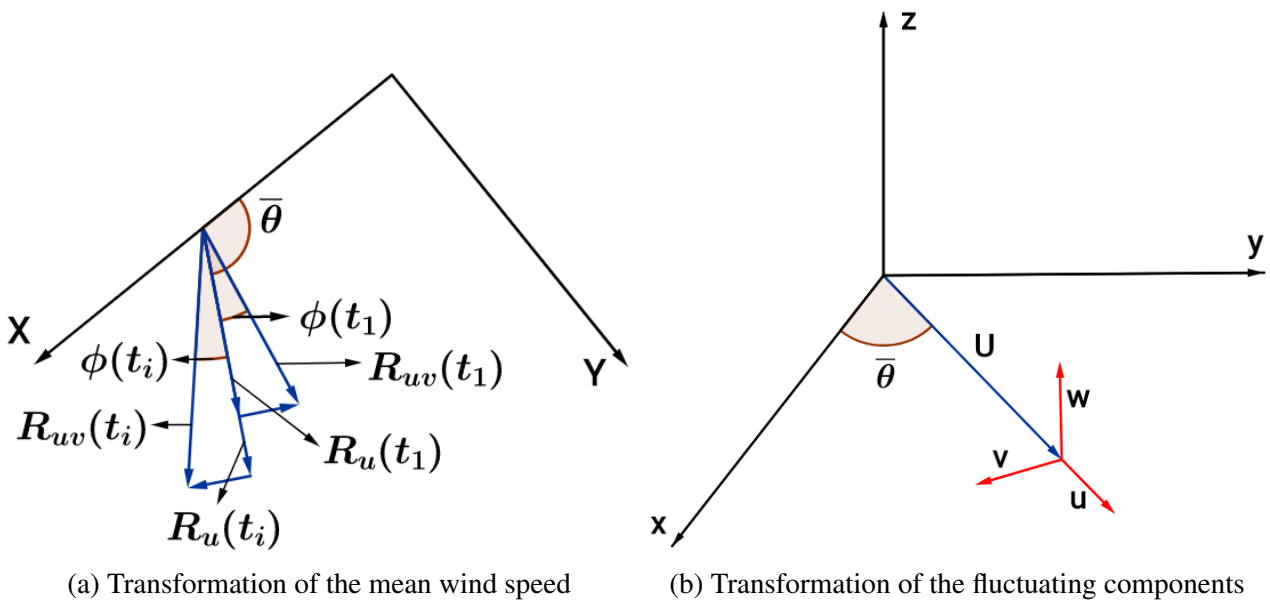


Figure 2.4: Transformation of the wind vectors

The Hardanger Bridge and monitoring system

3.1 Description of the Hardanger Bridge

The Hardanger Bridge is a suspension bridge opened for traffic in 2013 and is currently Norway's longest suspension bridge with a main span of 1 310 meters and a total length of 1 380 meters. The bridge is located in western Norway and crosses the Hardangerfjord (Figure 3.1), which is one of Norway's longest fjord. The bridge direction is perpendicular to the fjord and deviates approximately 25° to the west with respect to the north-south direction. The surroundings on both sides of the bridge consist of steep mountains over 1 000 meters high, where the highest has a height of 1 255 meters. A section of the map of Norway and the location of the bridge is shown in Figure 3.2, in addition to a local map with more details about the surroundings of the bridge. The vertical ship clearance height is 55 meters in the midspan, and the towers are 200 meters above sea level. The bridge was built to replace the ferry route across the fjord for one of the main roads between Bergen and Oslo, the two largest cities in Norway. It is built with only two traffic lanes and one pedestrian lane, which makes it unusually slender and susceptible to wind loading. The bridge deck is 18.3 m wide and 3.33 meters high, and the distance between the two main cables is only 14.5 meters.

The bridge is built with two main cables, which is connected to the bridge deck by vertical hangers in the main span. Each tower is built as two rectangular concrete columns which are connected with three cross beams, where the lowest cross beam works as bearing for the bridge deck. The bridge deck is a closed streamlined cross section made out of steel with cross bulkheads every 4 meters and guide vanes underneath to reduce vortex-induced vibrations. An illustration of the bridge deck cross section is shown in Figure 3.3. The main cables are deeply rooted into the mountain on each side.



Figure 3.1: The Hardanger Bridge. [16]

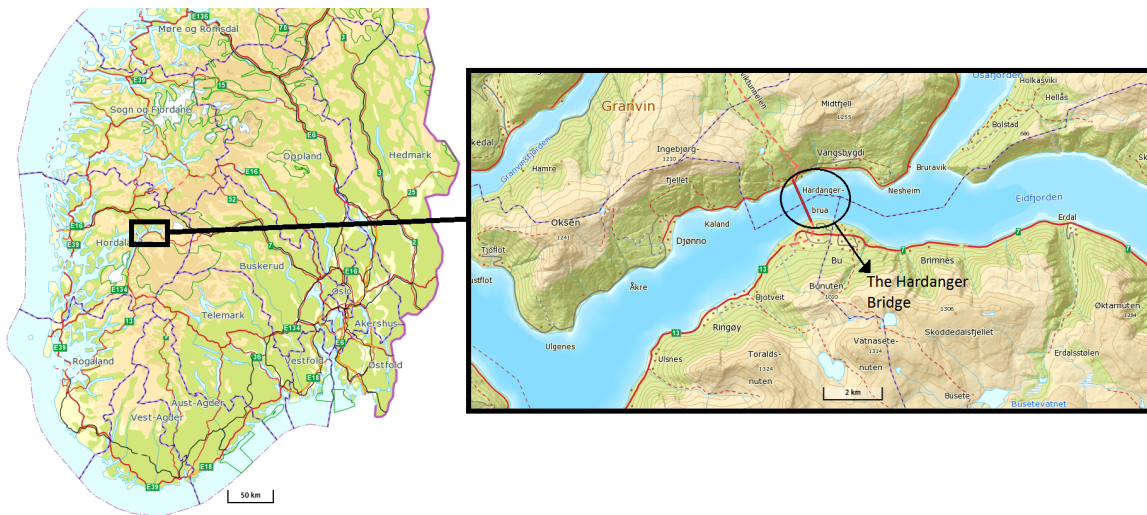


Figure 3.2: Location of the bridge and local map of the surroundings (map images from Kartverket).

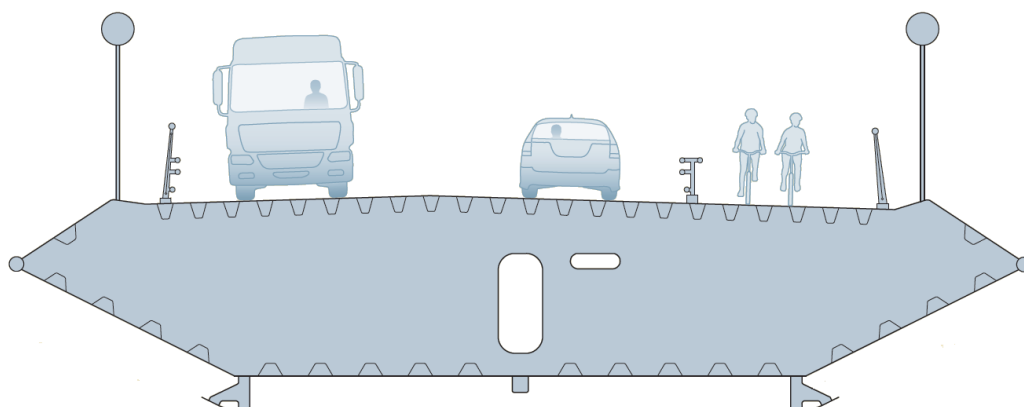


Figure 3.3: The cross-section of the bridge. [17]

3.2 Measurement system

After the completion of the bridge in 2013, a comprehensive measurement system was installed on the bridge, and the recordings started in December 2013. The measurement system consists of twenty accelerometers and nine anemometers measuring the wind speed, the wind direction and the acceleration of the bridge in several different locations. The locations of the sensors are shown in Figure 3.4. The coordinate system of the measurement system has its origin at the midspan of the bridge, and a positive axis toward the south. The three directions of the coordinate system are taken as x along the bridge, y crosswise and z vertical.

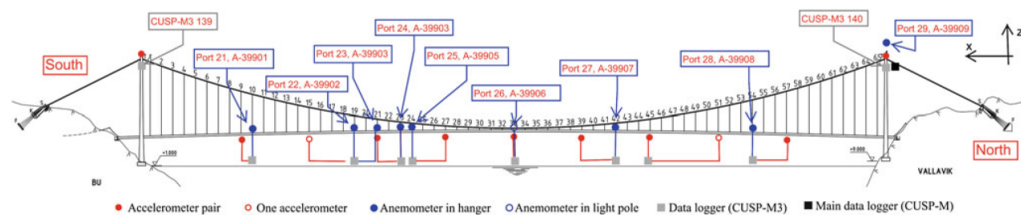


Figure 3.4: Illustration of the measurement system [18].

There are eight anemometers distributed along the main span of the bridge and one located at the top of the north tower. The anemometers measure horizontal wind speed, vertical wind speed and the direction of the horizontal wind, and it can measure wind gusts up to 65m/s . The wind sensors are installed asymmetrically about the midspan of the bridge span as seen in Figure 3.4, where the anemometers are indicated with blue dots. Four of the sensors are installed within a small area on the south side of the span.

A pair of accelerometers is installed at the top of each tower, and the remaining 16 are located inside the bridge deck on bulkheads. The accelerometers located in the bridge deck are distributed symmetrically around the midspan. 14 of them are placed as pairs in the same cross section, with one at each side, to get information about the torsional response. The two last accelerometers are single. The accelerometers measure the acceleration in 3 directions; perpendicular to the bridge (y), longitudinal (x) and vertical (z).

Each sensor is connected to a datalogger unit which sends the data to the main datalogger of the system located at the top of the north tower. The main datalogger is connected to an internet connection to transfer the data to the Norwegian University of Science and Technology (NTNU), where the data are stored. The measurement system is triggered automatically when a wind velocity threshold value of 15 m/s is exceeded in any of the wind sensors, but it can also be triggered manually. The accelerometers and anemometers record data for a duration of 30 minutes after the system is triggered. The sampling rates are 200 Hz for the accelerometers and 32 Hz for the anemometers, and the time series of acceleration and wind speed are later resampled to 20 Hz . The wind data is transformed to one mean component and three fluctuating components as described in Section 2.4.2.

Wind field characteristics

In this chapter, the characteristics of the wind field at the bridge site will be presented, with the use of 16 recordings, each lasting 30 minutes, measured at two different time spans (Jan 29 2016 and March 1-2 2016). The nine recordings from Jan 29 contain high mean wind speeds in the range of about 19-25 m/s, while the seven recordings from March 1-2 contain lower mean wind speeds of about 11-13 m/s. In the rest of the thesis, these two groups of recordings will be referred to as the high wind speed recordings and the low wind speed recordings. In this chapter, some of the high wind speed recordings and some of the low wind speed recordings will be chosen to show examples of span-wise profiles of mean wind speed and turbulence standard deviations, which are the profiles used in the wind spectra in Eq. (2.40) to calculate the dynamic response. In Table A.1 the wind characteristics from the recordings used in this report are summarised. Regarding the mean wind speed, only the 30-minute mean wind speed will be discussed in this report, because this is the measure of mean wind speed used in the response calculations in Chapter 7. The wind directions are defined relative to the bridge axis, which deviates approximately 25° to the west with respect to the north-south direction. This is shown in Figure 4.1. The influence of the horizontal angle of attack is not included when calculating bridge response in this report, since the wind directions are almost perpendicular to the bridge, and will not be discussed further in this chapter.

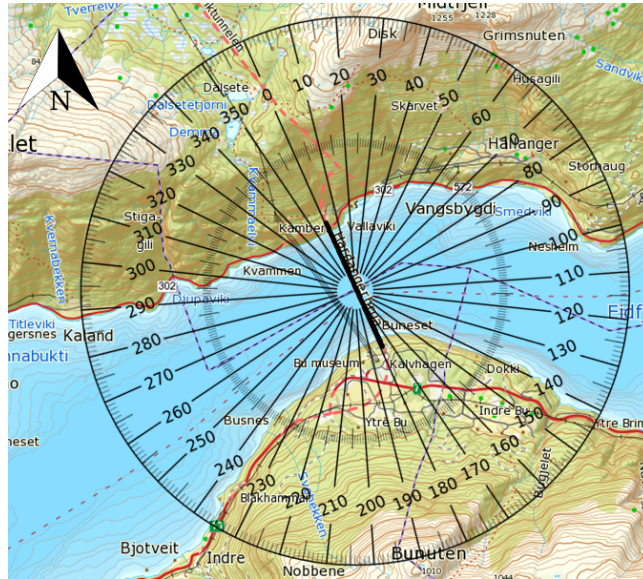


Figure 4.1: Orientation of the bridge and definition of wind direction angles.

4.1 Mean wind speeds

There are two main wind directions in the recordings, westerly wind direction for the low wind speed recordings on March 1-2 and easterly wind direction for the high wind speed recordings on Jan 29. Both are almost perpendicular to the bridge.

The two mean wind speed variables that will be compared when approximating the wind field as span-wise uniform in Chapter 7 are the midspan value and the span-wise mean value. In Table 4.1 the date, starting time, numbering, span-wise mean of mean wind speed, mean wind speed at the midspan and the mean wind direction of the 16 recordings are shown. The midspan value is taken from the sensor located 6 meters from the midspan. It can be seen that the difference between span-wise mean and midspan value is small and in some recordings they are the same. In Figure 4.2 the horizontal mean wind speed at the midspan for each recording is graphically shown. The numbers on the x-axis corresponds to the numbers in Table 4.1.

The mean vertical wind speed at the midspan vary between approximately 3% to 8% of the horizontal mean wind speed, but since the vertical mean wind speed component is not included in the dynamic response calculations, it will not be discussed any further in this thesis.

Table 4.1: The main wind characteristics in the horizontal plane for the recordings used.

	Date and starting time	Number	Span-wise mean wind speed [m/s]	30-minute mean wind speed at midspan [m/s]	Mean wind direction at midspan [°]
High wind speed	29-01-2016 13:00:00	1	21.1	20.7	101
	29-01-2016 13:30:00	2	21.3	21.3	102
	29-01-2016 14:00:00	3	19.9	19.8	104
	29-01-2016 15:30:00	4	21.3	21.2	102
	29-01-2016 17:30:00	5	24.8	24.7	102
	29-01-2016 19:30:00	6	25.5	24.6	103
	29-01-2016 20:00:00	7	23.2	22.9	98
	29-01-2016 20:30:00	8	20.5	20.6	101
	29-01-2016 21:00:00	9	18.9	18.9	101
Average			21.8	21.6	102
Low wind speed	01-03-2016 22:29:20	10	12.1	12.3	284
	02-03-2016 02:15:29	11	11.7	12.6	297
	02-03-2016 02:57:13	12	12.7	12.5	290
	02-03-2016 03:30:49	13	11.7	11.8	296
	02-03-2016 04:03:08	14	11.3	11.6	287
	02-03-2016 04:41:37	15	11.4	11.2	266
	02-03-2016 05:45:08	16	11.6	11.8	291
Average			11.8	12.0	287

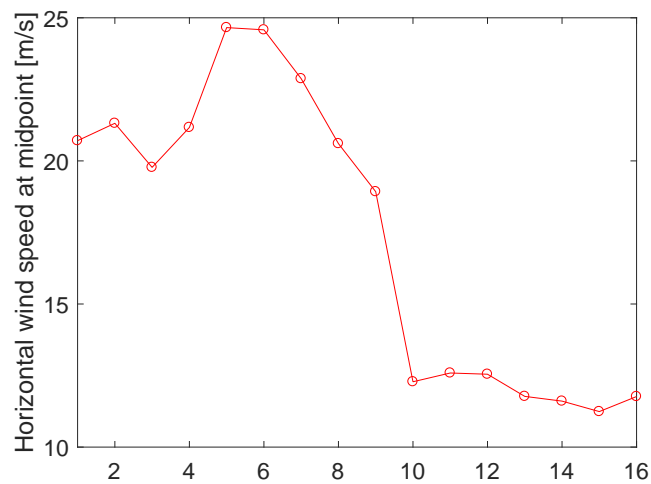


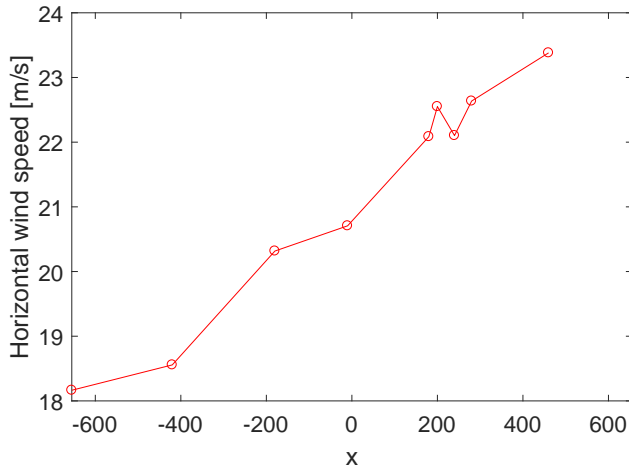
Figure 4.2: Variation of 30-minute mean wind speed at the midspan for all recordings.

In a paper by Fenerci et al. [19], the wind characteristics at the bridge site have been analysed using recordings from December 2013 to March 2016, corresponding to a total of 28 months. The measure

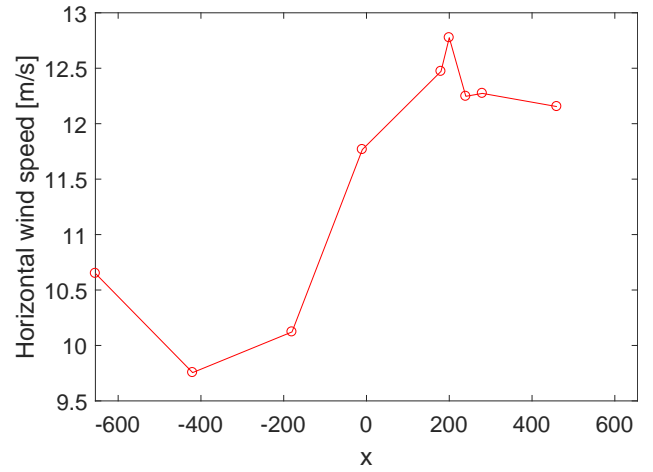
of mean wind speed considered in the paper is 10-minute mean wind speed, and the highest mean speeds observed were close to 30 m/s. This means that the recordings used in this thesis, which has 30-minute mean wind speeds spanning from about 10 to 28 m/s, cover a wide range of the wind speeds that can occur at the Hardanger Bridge site.

In Figure 4.3 the 30-minute horizontal mean wind speed at all sensor locations along the bridge is shown for one high wind speed recordings and three low wind speed recordings. The wind profiles from the high wind speed recordings all show the same approximately linear variation along the span, while the profiles from the low wind speed recordings are more different from each other. Therefore, wind profiles from three low wind speed recordings are shown to better cover the different span-wise variations. The circles in the plots indicate the measured values from the sensors, and linear interpolation has been used in between to obtain the mean wind speed profiles shown.

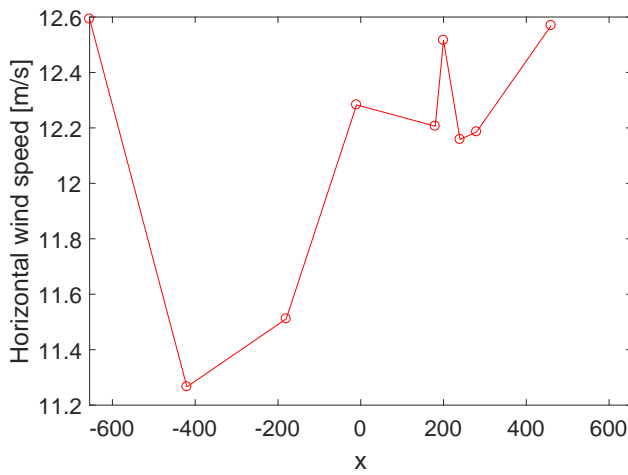
The wind profile in Figure 4.3a is from a high wind speed recording. In this profile, the mean wind speed varies almost linearly from about 18 to almost 24 m/s from one side of the bridge to the other, which is an increase of approximately 33%. The low wind speed recordings have variations from about 10 to 13 m/s, with relative increase from lowest to highest value of about 31% (Figure 4.3b), 12% (Figure 4.3c) and 21% (Figure 4.3d). The remaining twelve recordings considered in this thesis have relative increase from lowest to highest mean wind speed along the span ranging from 15 to 36%. While the high wind speed recordings show almost linear increase of mean wind speed from north to south side, the low wind speed recordings have maximum and minimum values at different points along the span. Still, the mean wind speeds are higher overall on the south side than on the north side for both the high wind speed and low wind speed recordings. One of the sensors is located at the top of the north tower, 140 meters above the other sensors, but in spite of this, the mean wind speeds observed here are not deviating much from the sensors along the bridge deck. Another minor observation is that the 30-minute mean wind speed measured at the fourth wind sensor from the right has slightly higher values than the nearby sensors, even if there are only 20 and 40 meters separating them. In Appendix A.1 all the wind profiles from the 16 recordings used are shown.



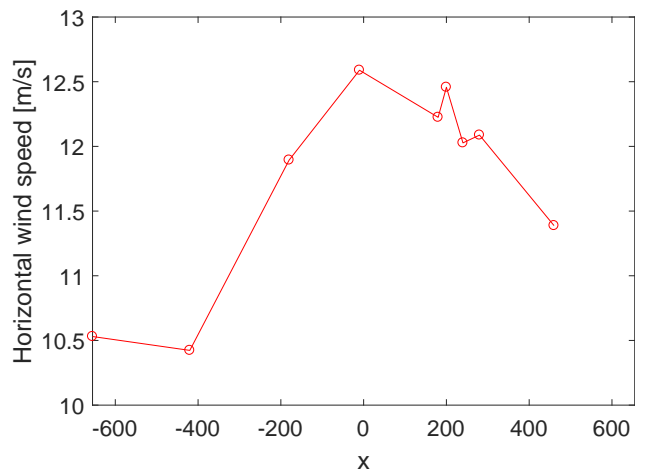
(a) 29-01-2016 13:00:00



(b) 02-03-2016 05:45:08



(c) 01-03-2016 22:29:20



(d) 02-03-2016 02:15:29

Figure 4.3: Variation of 30-minute horizontal mean wind speed along the bridge span.

4.2 Turbulence components

In Figure 4.4, the turbulence standard deviations at the midspan are shown both for the horizontal and the vertical component, for all 16 recordings. The numbers on the x-axis correspond to the numbers in Table 4.2, where the span-wise mean and midspan values of the turbulence standard deviations are shown. The turbulence standard deviation is obtained by taking the standard deviation of the fluctuating wind speed components in each direction. To obtain the fluctuating components, the method described in Section 2.4.2 is used. The standard deviation at the midspan ranges between 1.5 and almost 4 m/s in the horizontal direction, and between 0.6 and 1.3 m/s in the vertical direction. The relative difference between the span-wise mean and midspan values is larger for turbulence std than for mean wind speed, where the two values are almost the same for all recordings (Table 4.1).

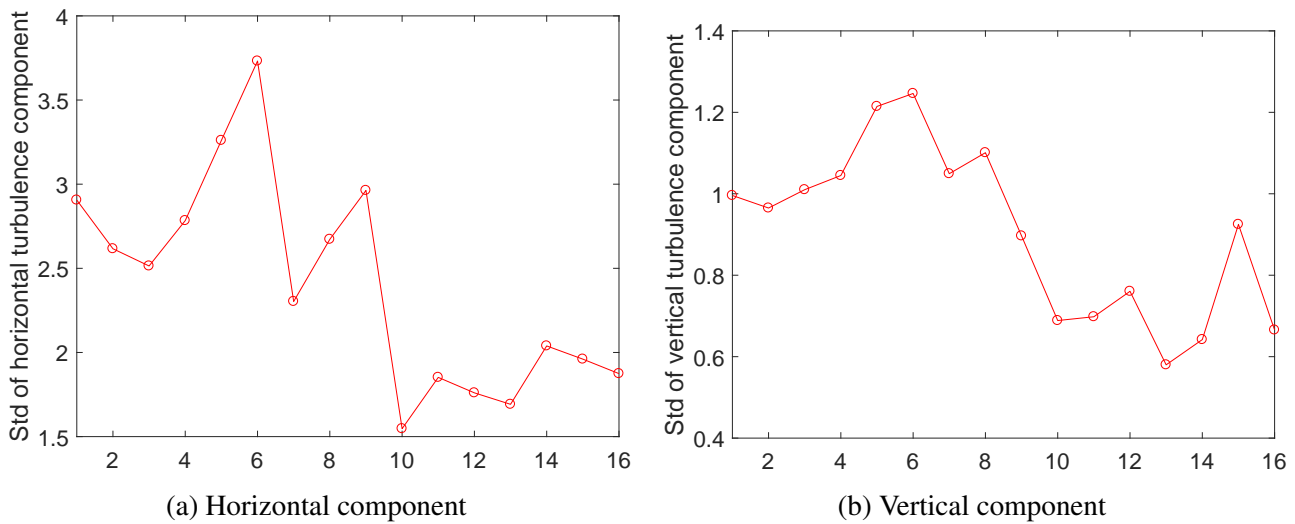
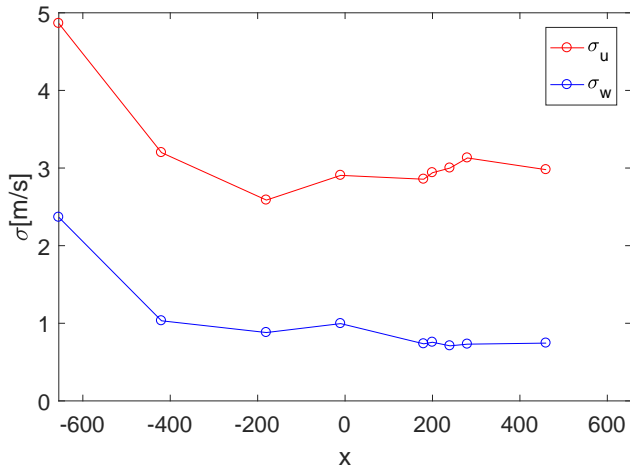


Figure 4.4: Variation of standard deviation of the turbulence components at the midspan for all recordings.

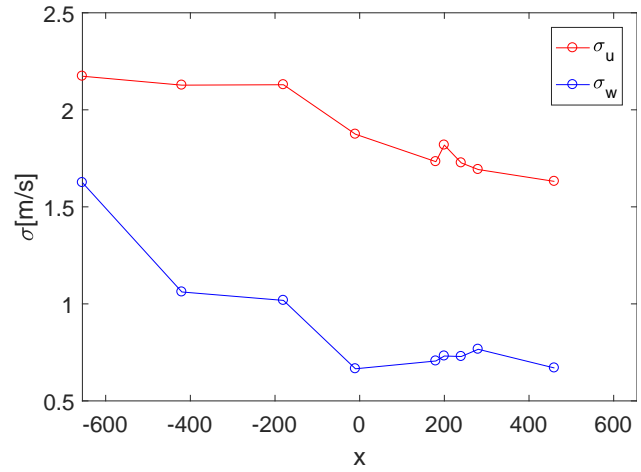
Table 4.2: Turbulence standard deviations for the recordings used.

	Date and starting time	Number	Turbulence std span-wise mean		Turbulence std midspan	
			σ_u [m/s]	σ_w [m/s]	σ_u [m/s]	σ_w [m/s]
High wind speed	29-01-2016 13:00:00	1	3.1622	0.9945	2.9056	0.9958
	29-01-2016 13:30:00	2	2.8216	0.9350	2.6164	0.9650
	29-01-2016 14:00:00	3	2.8633	0.9769	2.5139	1.0100
	29-01-2016 15:30:00	4	3.0658	1.0321	2.7835	1.0448
	29-01-2016 17:30:00	5	3.5481	1.1686	3.2600	1.2145
	29-01-2016 19:30:00	6	3.9037	1.1592	3.7318	1.2463
	29-01-2016 20:00:00	7	2.7777	1.0283	2.3031	1.0493
	29-01-2016 20:30:00	8	2.9507	1.0413	2.6723	1.1009
	29-01-2016 21:00:00	9	3.0840	0.9338	2.9628	0.8965
Average			3.1308	1.0300	2.8610	1.0581
Low wind speed	01-03-2016 22:29:20	10	1.5967	0.8950	1.5472	0.6887
	02-03-2016 02:15:29	11	1.9866	0.9601	1.8520	0.6981
	02-03-2016 02:57:13	12	1.8040	1.0056	1.7601	0.7605
	02-03-2016 03:30:49	13	1.6032	0.9020	1.6919	0.5800
	02-03-2016 04:03:08	14	1.8202	0.9030	2.0389	0.6419
	02-03-2016 04:41:37	15	1.9863	1.0567	1.9604	0.9248
	02-03-2016 05:45:08	16	1.8784	0.8857	1.8743	0.6655
Average			1.8108	0.9440	1.8178	0.7085

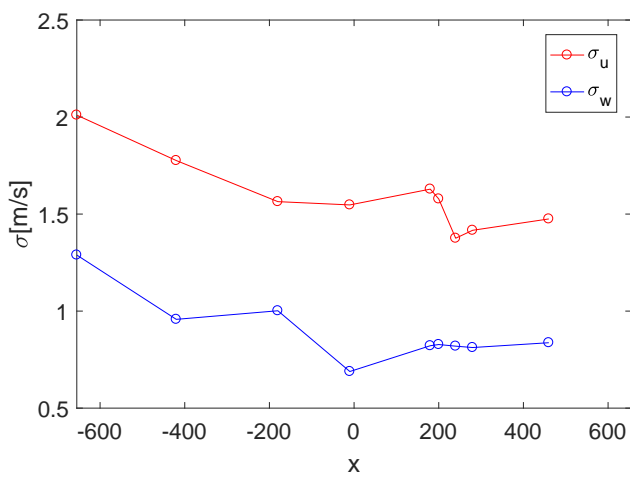
Also the span-wise profiles for the turbulence standard deviation indicate large non-uniformity. In Figure 4.5 the span-wise variation of the turbulence standard deviations in horizontal and vertical direction are shown for the same four recordings as in Figure 4.3. The horizontal component is represented by the red line, while the blue line indicates the vertical component. All the different turbulence std profiles are plotted and shown in Appendix A.2. The vertical component has the largest relative variations along the span. In percent, the difference between the lowest and the highest turbulence std along the span is ranging from 30 to 150% for the horizontal component for all recordings, while the difference spans from 30 to 250% for the vertical component. The turbulence std from the sensor at the top of the north tower has in general higher values than the other sensors for the high wind speed recordings.



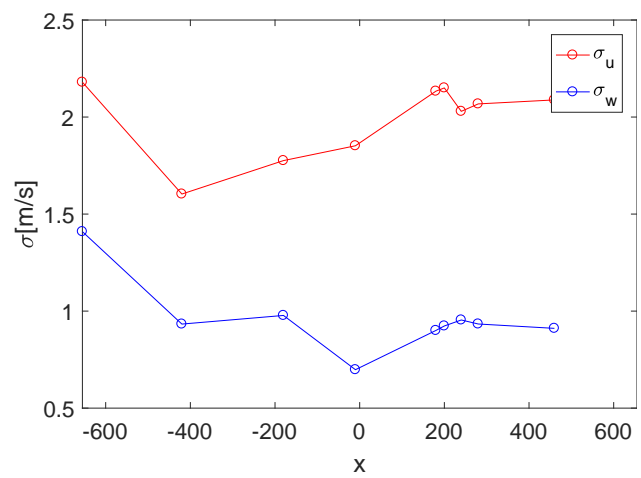
(a) 29-01-2016 13:00:00



(b) 02-03-2016 05:45:08



(c) 01-03-2016 22:29:20



(d) 02-03-2016 05:45:08

Figure 4.5: Standard deviation of the turbulence components.

Calculation basis

Here, the different methods and constants used in the calculations of the dynamic response of the Hardanger Bridge in this thesis will be presented. Most of the methods have been used in previous studies where the predicted response of the Hardanger Bridge was calculated. The response calculations has been carried out in Matlab.

5.1 Constants

In this section, the constants used for the dynamic response calculation will be presented. Inputs to the response analysis are air density $\rho = 1.25 \text{ kg/m}^3$, span length $L = 1\,310\text{m}$, and width and height of the girder is $B = 18.3$ and $D = 3.33\text{m}$. The frequency vector ranges from 0.0001rad/s to 4rad/s and has a resolution of 0.004rad/s .

The static force coefficients used in the buffeting load coefficient matrix (Eq. (2.28) and Eq. (2.37)) are taken from Hansen et al. [20]:

$$\begin{aligned}\bar{C}_D &= 0.7 & C'_D &= 0 \\ \bar{C}_L &= -0.25 & C'_L &= 2.4 \\ \bar{C}_M &= 0.01 & C'_M &= 0.74\end{aligned}\tag{5.1}$$

where D, L and M denotes drag, lift and moment, respectively, and \bar{C} and C' are the mean value and the derivative of the static force coefficients, respectively. They may also be used in calculating the aerodynamic derivatives from the quasi-steady-theory.

The aerodynamic admittance functions are characteristic for the specific cross section and are used

when calculating the buffeting load coefficient matrix in Equation (2.28). Their values (2.37) are taken as follows:

$$A_{mn} = 1 \quad m \in \{y, z, \theta\}, \quad n \in \{u, w\} \quad (5.2)$$

The decay coefficients C_u and C_w used in the cross-spectral densities in Eq. 2.39 have been set to 1.4 and 1, as assumed by Øiseth et al. [15]. A_u and A_w in the single point wind spectra (Eq. 2.40) have been given the values of 40.8 and 3.3 [21].

5.2 Modes

A finite element model of the Hardanger Bridge is made in the finite element method (FEM) program Abaqus. The model was used to carry out a frequency analysis on the bridge to obtain natural frequencies, mode shapes and structural properties in still air. A total of 13 vibration modes were extracted. The modes are used in the calculation of the dynamic response and consist of the first 5 horizontal, first 5 vertical and first 3 torsional modes. The mode shapes are plotted in Figure 5.1 and their natural frequencies listed in Table 5.1.

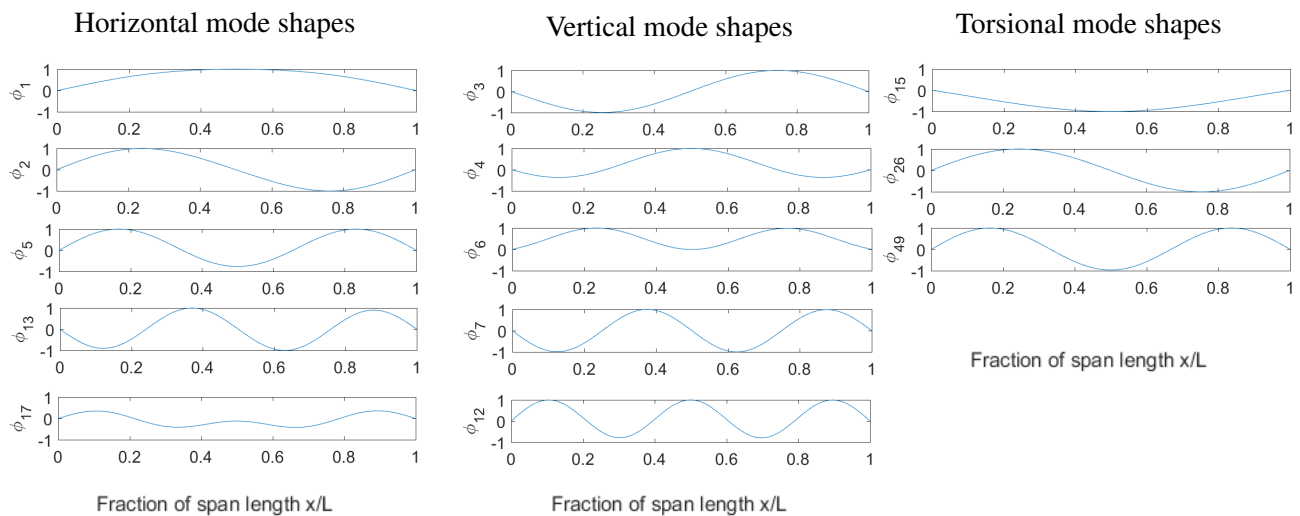


Figure 5.1: Still-air vibration modes for the Hardanger bridge.

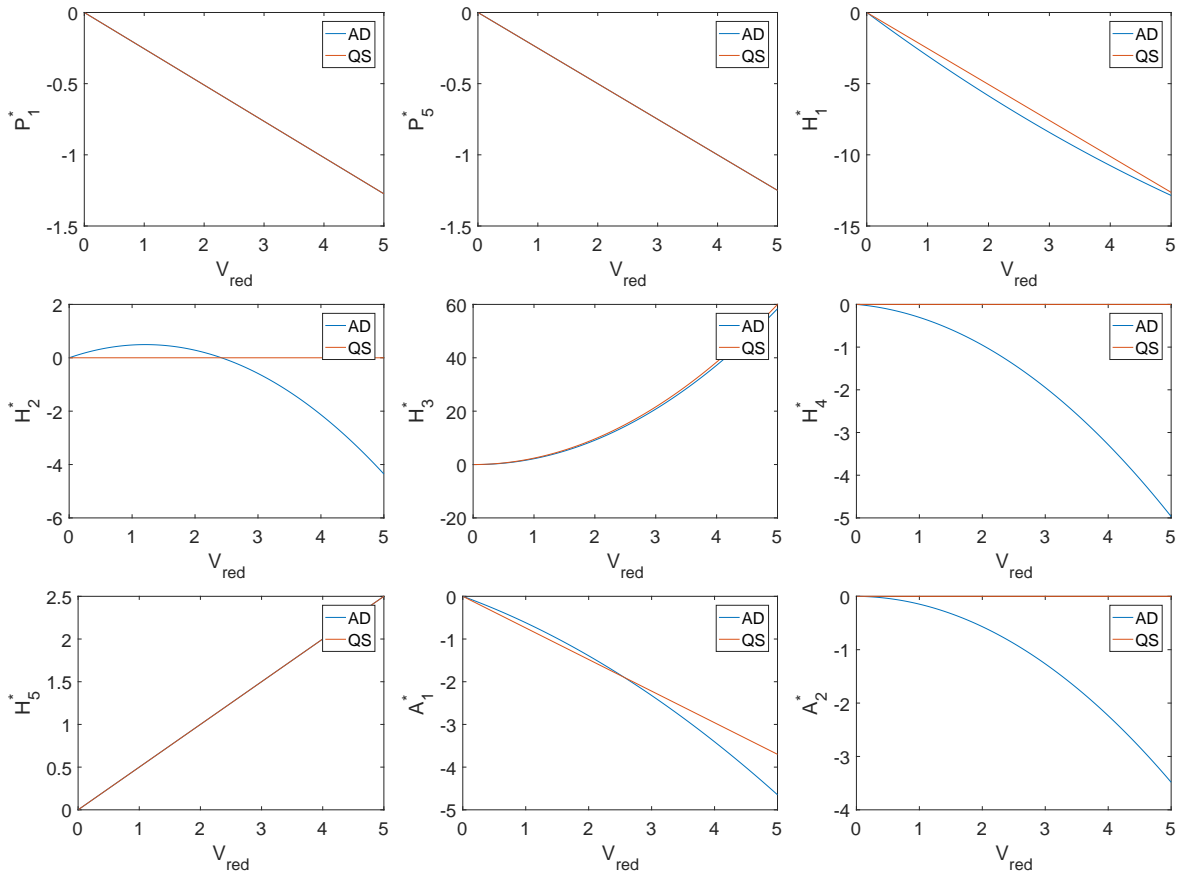
Table 5.1: Natural frequencies of the modes used in the analysis.

Mode number	Natural frequency ω [rad/s]	f [Hz]	Natural period T [s]	Mode type
1	0.31	0.05	20.27	Horizontal
2	0.62	0.10	10.13	Horizontal
3	0.69	0.11	9.11	Vertical
4	0.88	0.14	7.14	Vertical
5	1.06	0.17	5.93	Horizontal
6	1.24	0.20	5.07	Vertical
7	1.33	0.21	4.72	Vertical
12	1.71	0.27	3.67	Vertical
13	1.84	0.29	3.42	Horizontal
15	2.26	0.36	2.78	Torsional
17	2.46	0.39	2.55	Horizontal
26	3.29	0.52	1.91	Torsional
49	4.92	0.78	1.28	Torsional

5.3 Aerodynamic derivatives

The vertical and torsional aerodynamic derivatives, H_i^* and A_i^* where $i \in \{1, 2, 3, 4\}$, for the cross section of the Hardanger Bridge have been obtained through wind tunnel measurements. The aerodynamic derivatives related to the horizontal motion, P^* , H_5^* and A_5^* , have been obtained from quasi-steady theory as expressed in Equation (2.25), since experimental data are not available for these. These are the approaches used for obtaining the aerodynamic derivatives used in the calculations. A curve is fitted by a polynomial function to the experimentally obtained data points given by Hansen et al. [20]. In Figure 5.2 the different aerodynamic derivatives, except from those who are taken as zero, are plotted against reduced velocity, and compared with the quasi-steady theory. The derivatives which are taken as zero are P_i^* where $i \in \{2, 4, 6\}$, H_6^* and A_6^* . In addition, P_3^* is zero since the static force coefficient C'_D in the expression of P_3^* is zero. The aerodynamic derivatives P^* , H^* and A^* are related to the self-excited forces in the lateral, vertical and rotational direction, respectively. The reduced velocity is defined as the inverse of the reduced frequency and is expressed as

$$V_{red} = \frac{1}{K} = \frac{V}{B\omega} \quad (5.3)$$



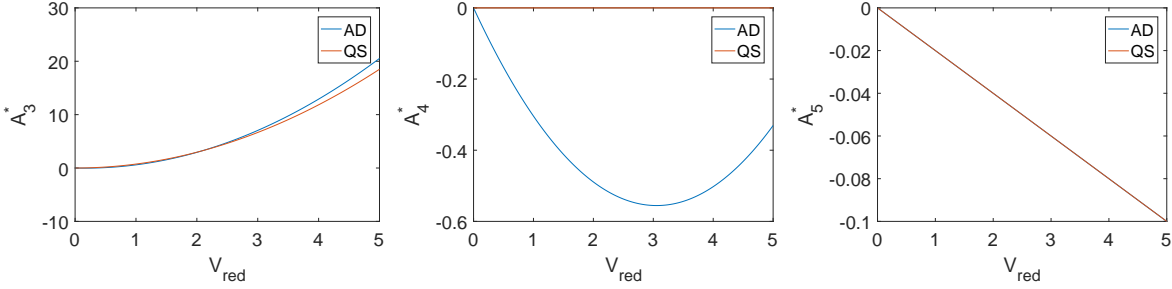


Figure 5.2: Fitted line to the aerodynamic derivatives compared with quasi-steady theory.

5.4 Wind profiles

In the numerical study in Chapter 6, several wind profiles with different shapes are compared to each other. To make the different wind fields comparable, they are all given the same span-wise mean of mean wind speed, meaning their integrated sum over the span is the same. Then their mean values can be increased correspondingly to compare their effect on dynamic response at different span-wise means of mean wind speed. For simplicity, when referring to a wind profile's span-wise mean of mean wind speed in the rest of this thesis, only the term mean wind speed will be used.

An illustration of different wind fields with the same mean wind speed is shown in Figure 5.3. All the wind profiles will be studied with mean wind speeds from 10 to 70 m/s, $V \in \{10, 20, 30, 40, 50, 60, 70\}$. They are all either symmetrical with maximum at the midspan or asymmetrical with maximum at one of the sides.

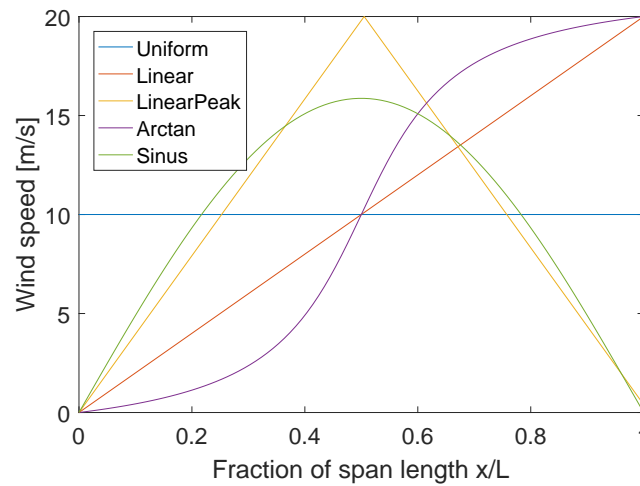


Figure 5.3: Example of different wind fields with span-wise mean wind speed of 10 m/s

The different wind profiles in Figure 5.3 can be modified to obtain a gradual transition from uniform to non-uniform profile. This is shown in Figure 5.4, where the wind profiles have been given different maximum values and slopes. The formulas which are used for defining the different wind profiles in Figure 5.4 will be given next. The constant c indicates which wind speed the profile has for $x = 0$. The factor a modifies the non-uniformity of the profile; for linear and linear peak it's the slope and for arctan and sinus the non-uniformity increases with the value of a .

$$\begin{aligned}
 \text{Linear} &= i(c + a * x) \quad x \in [0, 1] \\
 \text{where } c &\in \{0, 2, 4, 6, 8\} \quad \text{and} \quad a \in \{20, 16, 12, 8, 4\}
 \end{aligned} \tag{5.4}$$

$$\text{LinearPeak} = \begin{cases} i(c + a*x) & \text{if } x \in [0, 0.5] \\ i(a/2 - a*x) & \text{if } x \in [0.5, 1] \end{cases} \quad (5.5)$$

where $c \in \{0, 2, 4, 6, 8\}$ and $a \in \{40, 32, 24, 16, 8\}$

$$\text{Sinus} = i(c + a * \sin(x) / \text{mean}(\sin(x))) \quad x \in [0, \pi] \quad (5.6)$$

where $c \in \{0, 2, 4, 6, 8\}$ and $a \in \{10, 8, 6, 4, 2\}$

$$\text{Arctan} = i(10 + a * \arctan(4*x) / \arctan(4)) \quad x \in [-1, 1] \quad (5.7)$$

where $a \in \{2, 4, 6, 8, 10\}$

where $i \in \{1, 2, 3, 4, 5, 6, 7\}$ indicates the mean wind speed of the profile, $V = 10 * i$. The constant c and factor a change correspondingly. In Figure 5.4 the wind profiles are plotted for $i = 1$ and for different values of c and a . In Figure 5.6 the wind profiles are plotted for all i . In this figure, the a value that results in most non-uniform shape is used. The variations shown in both of these figures are used later in this thesis, in Chapter 6.

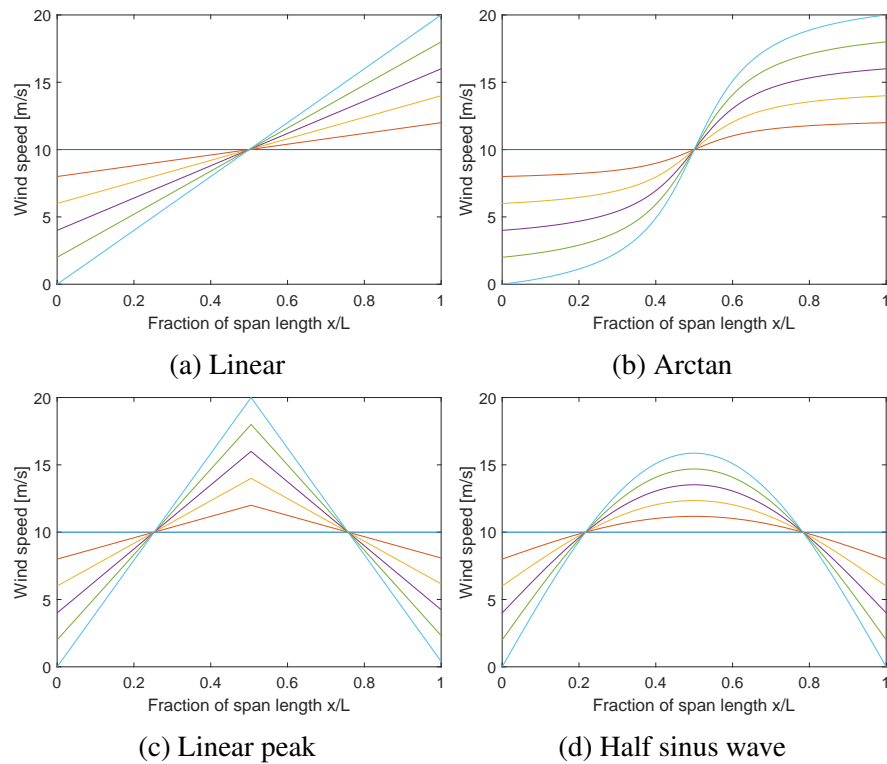


Figure 5.4: Wind profiles with mean wind of 10 m/s.

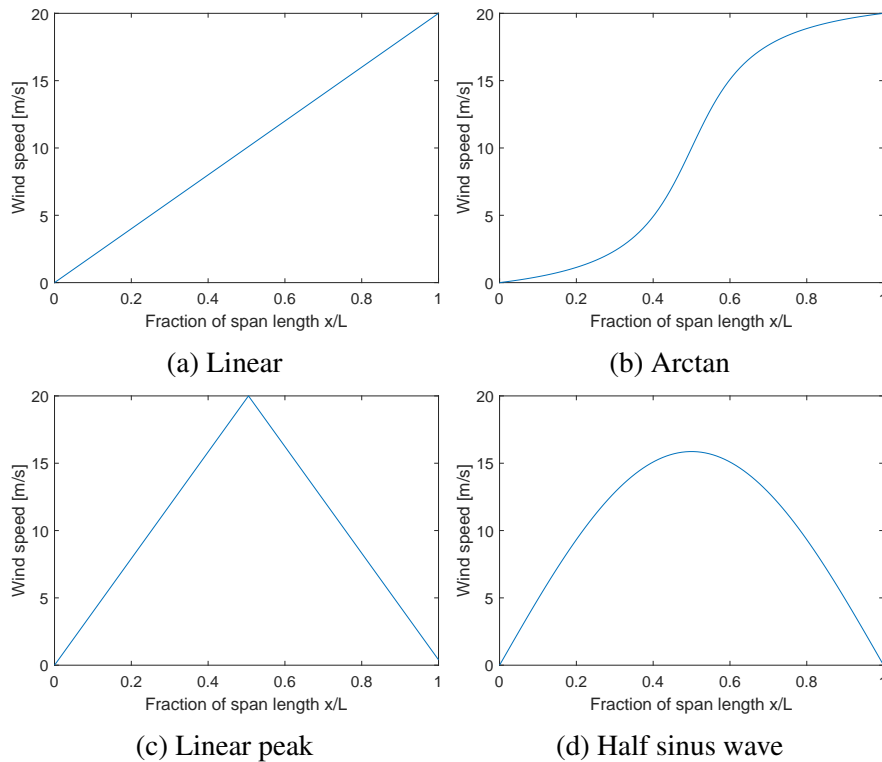


Figure 5.5: Wind profiles with mean wind of 10 m/s.

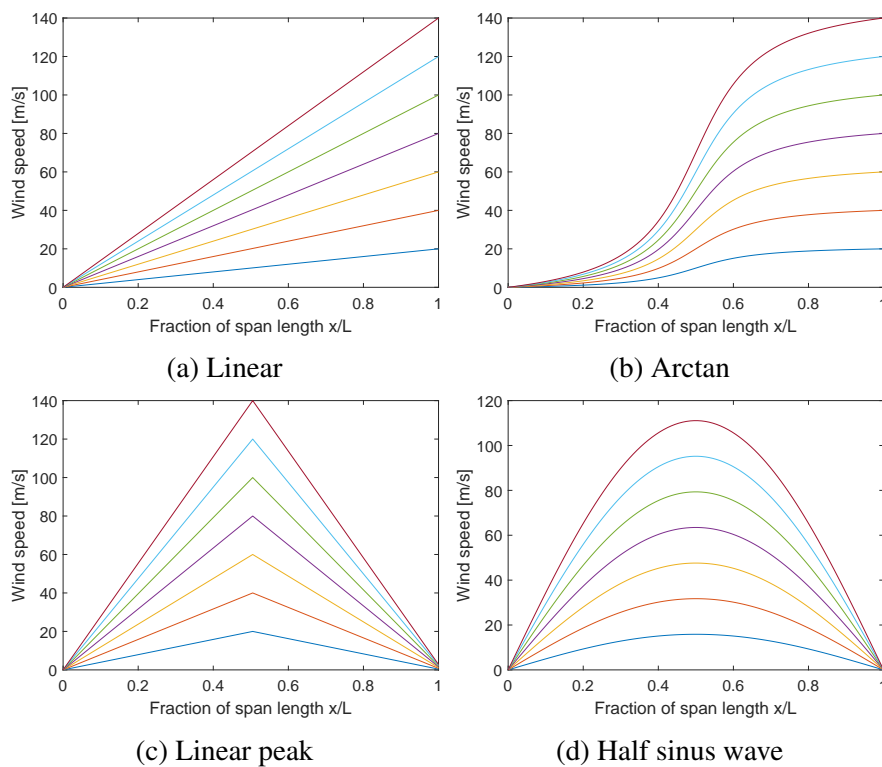


Figure 5.6: Wind profiles for all mean wind values.

Numerical study

In this chapter, the results from the numerical study will be presented. Several different wind profiles described by functions expressed in Section 5.4 have been analysed in order to investigate the effect of non-uniform wind fields on the dynamic bridge response. The different methods and procedures, constants and modes used in the dynamic calculations are presented in Chapter 5, in addition to the wind profiles in Section 5.4 that will be studied in this chapter. As mentioned earlier, the term mean wind speed refer to a wind profile's span-wise mean of mean wind speed, in other words, the integrated sum of the wind speeds along the span. When referring to the time average of wind speed, as in e.g 10-minute or 30-minute mean wind speed, only the term wind speed will be used. In this chapter, the term response is referring to displacement response and std is used as an abbreviation for standard deviation. This chapter is divided into three parts. The two first parts present the numerical study of how non-uniform wind speed and turbulence std profiles impact the dynamic response. The last part consists of including the non-uniform self-excited forces in the calculations. For the highest mean wind speeds, the wind profiles may have extreme values that are not realistic, but included to study how the response grows with increasing wind speed.

6.1 Influence of non-uniform wind speed profile

The effect of span-wise non-uniform horizontal wind speeds on the dynamic bridge response will be discussed in this section. Different wind speed profiles have been analysed, while keeping the standard deviation of turbulence and the self-excited forces constant along the span. The standard deviations of the vertical and horizontal turbulence components have been set to fairly realistic values of 10 and 20% of the mean wind speed of the different profiles. The self-excited forces are span-wise uniform and have been computed using the wind profiles' mean wind speed. The response along the span for the different wind profiles will be presented for mean wind speed 10m/s, because the response

for higher mean wind speeds shows similar behaviour compared to the response of a uniform wind profile.

In the following sections, the different wind profiles shown in Figure 5.4, with increasing degree of non-uniformity, will be compared to the uniform wind profile with respect to dynamic response.

Uniform compared to linear wind profile

The linear wind profile is the most simple way to make the wind non-uniform. In Figure 6.1, the different variations of the linear profile that will be considered in this section is presented for a mean wind speed of 10 m/s. The variations have different slopes a , as expressed in Eq. 5.4 and will be compared against the uniform wind profile with respect to the dynamic response. The linear profiles have been made with the same integrated sum of the wind speeds along the span.

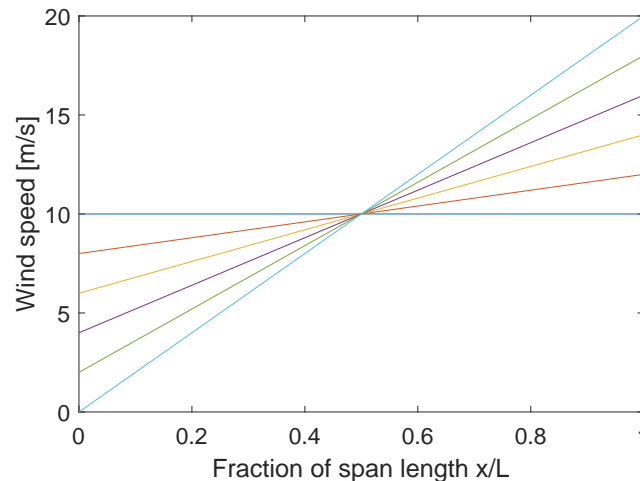


Figure 6.1: Comparison between linear wind profiles with different slopes and a uniform wind profile for mean wind speed 10m/s

It is interesting to investigate how the response along the span develops as the wind speed profile becomes more non-uniform. In Figure 6.2, the response along the span is shown for the linear wind profiles. The response curves correspond to the wind profiles with the same colour in Figure 6.1. As seen in these plots, it is the wind field with the largest slope that gives the largest response near the second quarter point, $x/L = 0.75$, for all three response variables. The lateral response in the first quarter point is almost the same for all the slopes, while the vertical and torsional response is almost the same near the midspan where all the response curves are crossing at the same point.

From the response plots along the span, it can be seen that there are higher wind speeds in the right side of the span. The response from the uniform wind profile is symmetrical along the span, while the response is shifted more to the right when the wind profile becomes more non-uniform. This is due to

higher wind speeds in the right side of the wind profile. In the point where the maximum response is found, the response increases almost linearly with the slope a . This is illustrated by Figure 6.3, where the response for certain mean wind speeds at the location where the response is largest, is plotted against the slope of the wind field. The mean wind speeds included are 10, 30, 50 and 70 m/s, and the response is normalised with respect to the response from the uniform wind profile, $a = 0$. As seen, the increase in the response depend almost linearly on the factor a . It is seen that increasing the slope has largest effect on the vertical response. The maximum vertical response is found for the steepest wind profile $a = 20$, and is about 40 to 55% higher than the uniform wind profile. The maximum normalised lateral and torsional responses are also found for $a = 20$ and are between 15 and 25% higher than the uniform wind profile. This indicates that the vertical response is more vulnerable to non-uniformity of linear wind profiles than the lateral and torsional response.

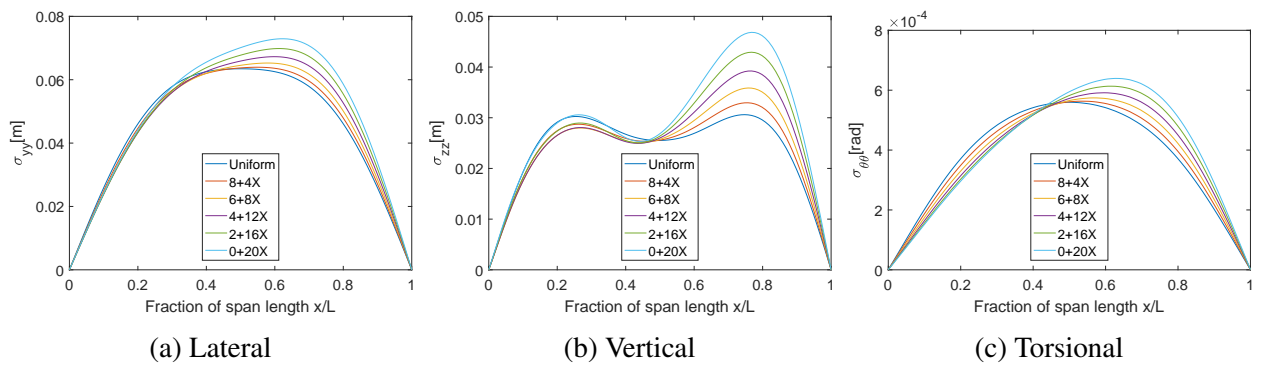


Figure 6.2: Response along the span for mean wind of 10 m/s for linear profiles

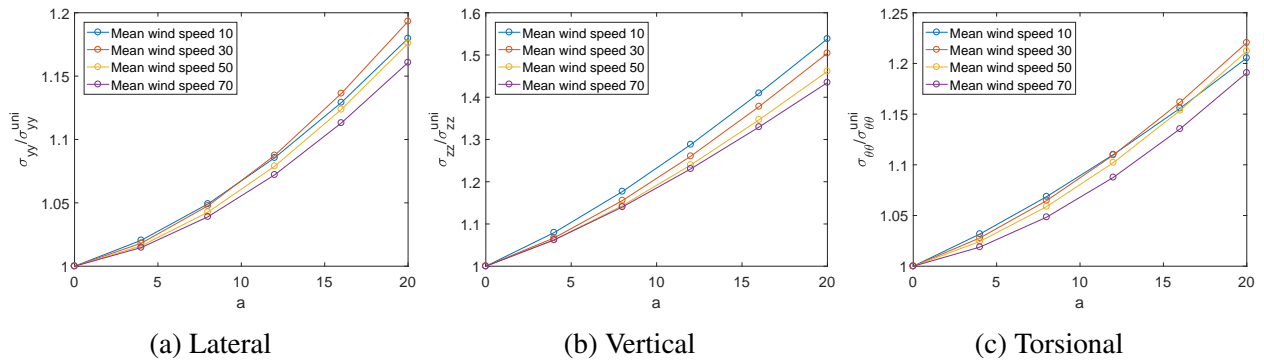


Figure 6.3: Maximum response along the span normalised with respect to the response from the uniform wind profile as a function of a for linear wind profiles, for different mean wind speeds

Uniform compared to arctan wind profile

The arctan profile is not very different from the linear profile, but it has lower wind speeds in the first half of the span and higher in the second half. Among the wind profiles tested in this chapter, the arctan profile has the most similar shape to the profiles obtained by interpolating the low wind speed

recordings presented in Chapter 4. The formula used to obtain the wind profile is shown in Equation (5.7). In Figure 6.4, the different arctan profiles and a uniform profile are shown for a mean wind speed of 10 m/s.

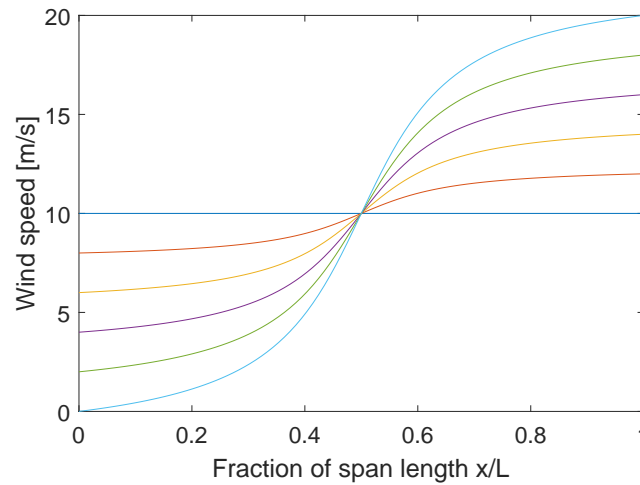


Figure 6.4: Comparison between arctan wind profiles with different shapes and a uniform wind profile for mean wind speed 10m/s

In Figure 6.5, the response is plotted along the span. Since the wind speed in the right side of the span is higher in the arctan wind profile than in the linear, the response shifts even more to this side compared to the linear profile. The shape of the lateral and torsional response is very similar to the response for the linear wind profiles, but the factor a has a larger impact on the response which makes the maximum response higher.

In the vertical direction, there is a bigger difference in the peak near the first quarter point than seen for the response from the linear wind profile. The arctan wind profile with the most abrupt transition, $a = 10$, gives the highest vertical response in both the first and second quarter point, even though this is the profile with lowest wind speed in the first quarter point. σ_{zz} is 0.03 m in the first quarter point for the uniform profile, and almost 0.04 m for the arctan profile, despite that the wind speed in that point is 10 m/s for the uniform profile and around 2 m/s for the arctan profile. In the second quarter point, the vertical response increases almost linearly with the factor a .

The response from different arctan profiles normalised with respect to the response from the uniform wind profile is plotted as a function of a in Figure 6.6. The response is plotted for the point where the maximum response is found. An approximately linear increase of normalised response with the factor a is seen, and the effect on vertical response is almost twice as large as for lateral and torsional response. Both effects are similar to what was seen for the linear wind profile.

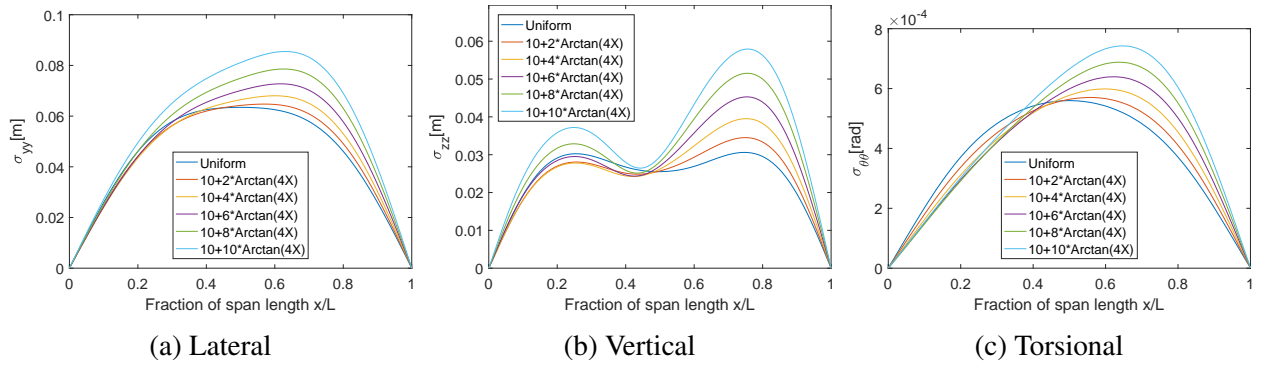


Figure 6.5: Response along the span for mean wind of 10 m/s for arctan profiles

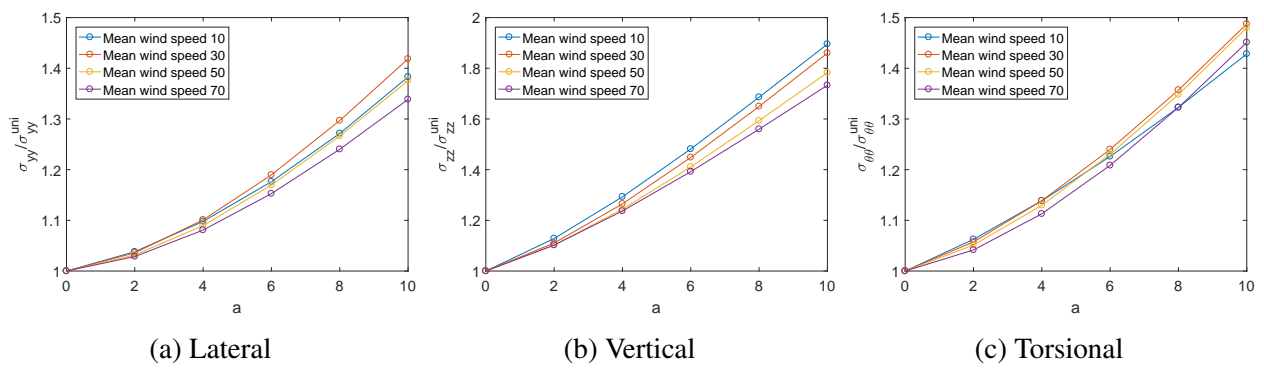


Figure 6.6: Normalised displacement where the response is largest for different mean wind speeds as a function of a for an arctan wind profile

Uniform compared to linear wind profile with a peak midspan

Until now, only asymmetric wind profiles have been studied. In this section, a symmetric wind profile that is linearly increasing towards the maximum wind speed at midspan will be considered. Five variations of this profile with different slopes are studied, as shown in Figure 6.7. The formula for the wind profile is described by Equation (5.5).

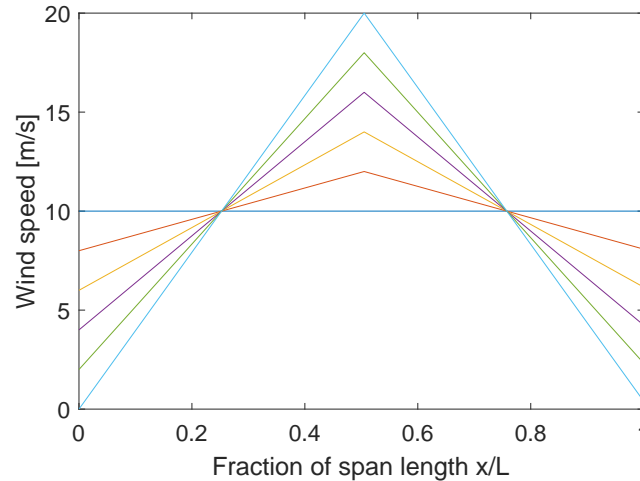


Figure 6.7: Comparison between linear wind profiles with a peak in the midspan and different slopes, and a uniform wind profile for mean wind speed 10m/s

In Figure 6.8 the response along the span is shown for linear wind profiles with a peak in the midspan with different slopes. The lateral and torsional responses in the midspan, where the maximum response is found, increase linearly with the factor a . This can also be seen in Figure 6.9, where the response for certain mean wind speeds, normalised with respect to the corresponding response for the uniform wind profile, is plotted against a . The response presented in the figure is taken from the point along the span that has the largest response of all profiles, which is the midspan. The uniform wind profile has the maximum vertical response in the quarter points, while the response for the linear profiles with a peak in the midspan has the maximum value at the midspan. The reason is that the second vertical mode gets more dominant when the wind profile has high wind speeds in the midspan. This is due to the mode shape which has three half sinus waves and a peak in the midspan. For a uniform profile, the first vertical mode contributes more than the second vertical mode, resulting in maximum response at the quarter points. The contributions from these two modes can be seen in Figure 6.10, where the vertical response spectra in the quarter point and the midspan are shown for a uniform profile and all the linear peak profiles. It can be seen that an increase of a has more impact on the second vertical mode than the first vertical mode, and consequently the second vertical mode gets dominant for the steepest linear peak profiles. Since the second vertical mode shape has close to zero value in the quarter points, the vertical response does not change much for increasing a values here. This is due to a larger increase in the wind speed in the midspan than the quarter points which has a constant wind speed for all these profiles.

The shape of the lateral and torsional response along the span does not change as much as the vertical response. The response only shifts upwards for increasing a values. The lateral response for all the different mean wind speeds increases almost linearly with approximately the same slope with respect to a . The same is seen for the torsional response, except from for 10 m/s mean wind speed where the response does not increase as much as for the other mean wind speeds.

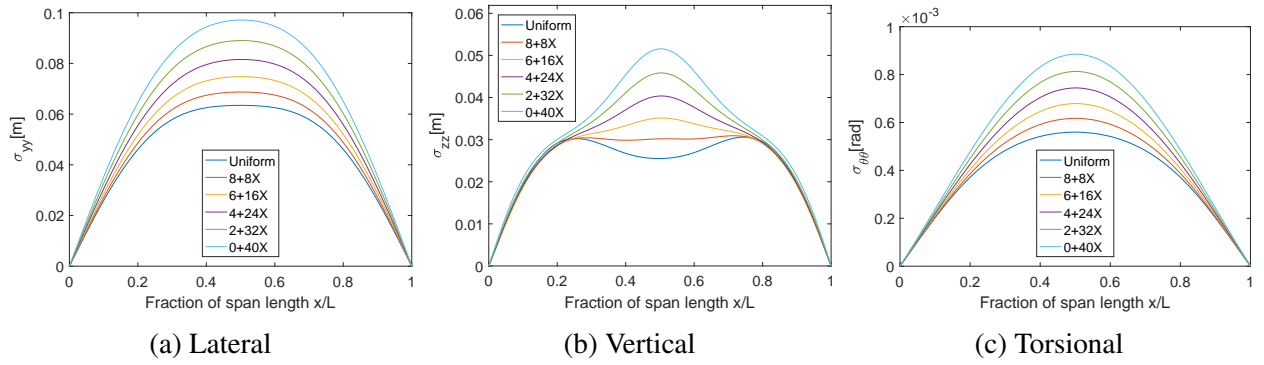


Figure 6.8: Standard deviation of the displacement along the span for span-wise mean of 10 m/s

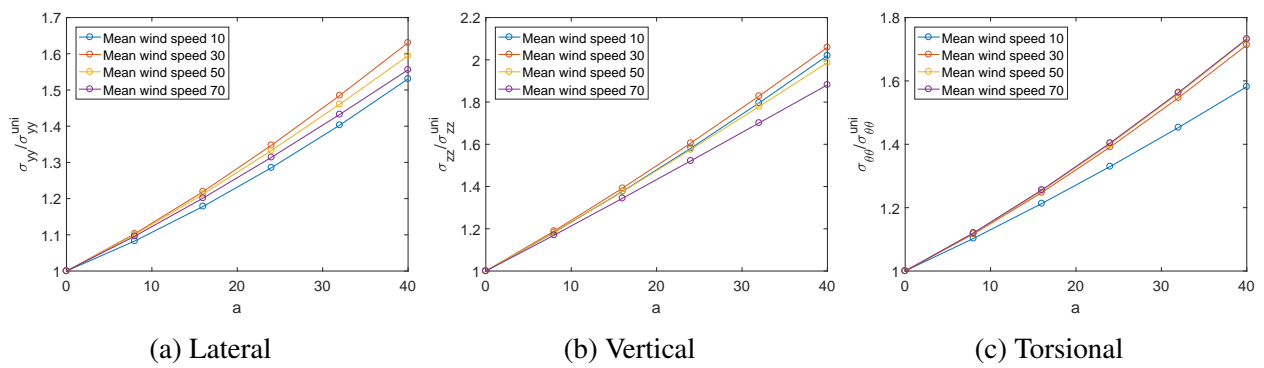


Figure 6.9: Displacement at midspan for different span-wise mean wind speeds, normalized with respect to the response to a uniform profile with corresponding mean wind speed, as a function of a for a linear profile with peak at midspan

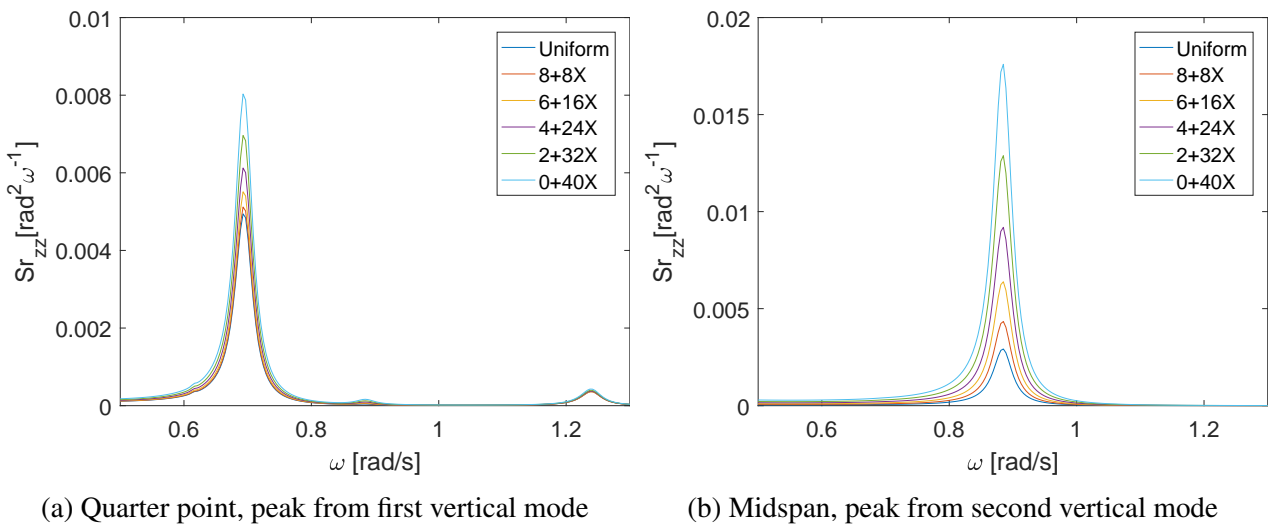


Figure 6.10: Vertical response spectra at mean wind speed of 10 m/s for uniform and different linear profiles with peak at the midspan.

Uniform compared to sinus wind profile

The wind profile using a half sinus wave is a more smooth wind profile compared to the linear with a peak in the middle and does not have the abrupt transition in the midspan. In Figure 6.11, the different sinus wind profiles are plotted together with the uniform wind profile. The formula of the sinus profiles is shown in Equation (5.6).

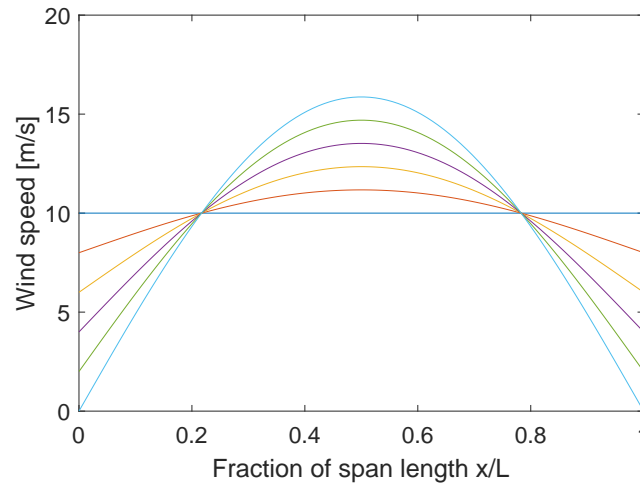


Figure 6.11: Comparison between sinus wind profiles with different shapes and a uniform wind profile for mean wind speed 10m/s

The same trend of the response along the span is seen for the sinus profiles, as for the linear profile with a peak in the midspan, which is seen in Figure 6.12. The lateral and torsional response shifts upwards for more non-uniform wind profiles of sinus. The maximum response is linearly increasing with the factor a , as shown in Figure 6.13. Since the differences in wind speed between each sinus profile are less than for the linear peak profiles, the differences in response are also less. The maximum normalised response among all three response variables about 75% for the most non-uniform sinus profile compared to the response from the uniform wind profile, and is seen for the vertical direction.

In Figure 6.14, the response spectra in the vertical direction at the quarter point and midspan are shown for mean wind speed of 10 m/s. As discussed in the section with the linear profile with peak in the midspan, the contribution from the second vertical mode becomes dominant with higher wind speeds at the midspan. The sinus profile does not have as high wind speed in the midspan as the linear profile with a peak, and therefore a smaller increase in the contribution from that mode is seen. In Figure 6.14 the two peaks correspond to the first and second vertical mode, and the distances between the spectra for each profile is larger for the second vertical mode than the first. This gives a larger difference in vertical response in the midspan compared to the quarter points. As for the linear wind profile with peak at the midspan, this is because the wind speed at midspan increases more with the factor a than the wind speeds at the quarterspan.

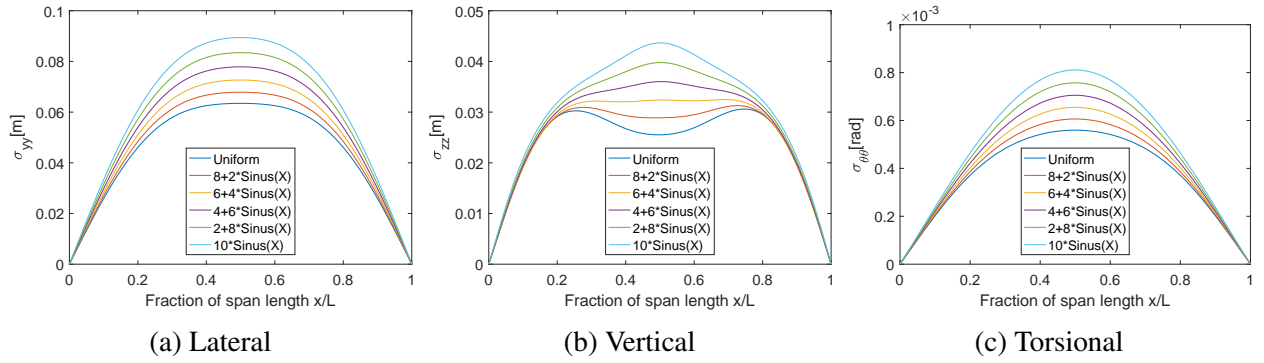


Figure 6.12: Standard deviation of the displacement along the span for span-wise mean of 10 m/s

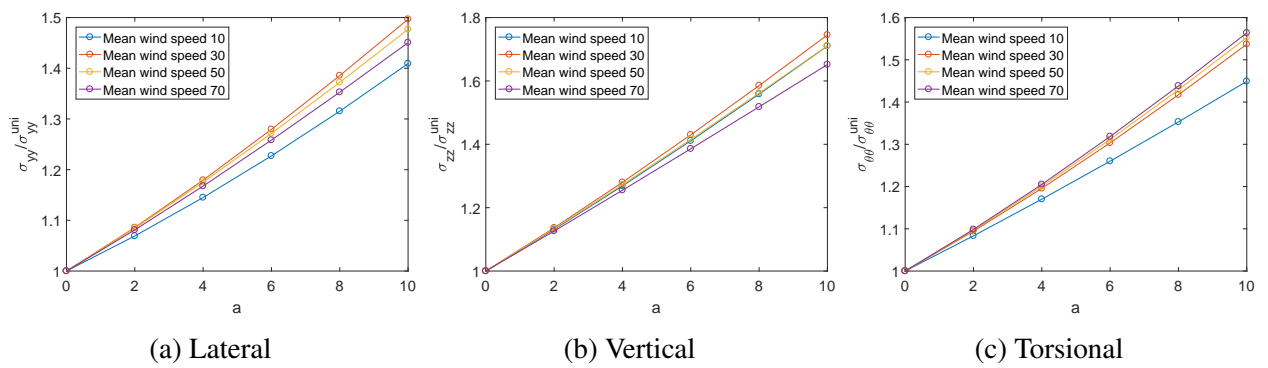


Figure 6.13: Displacement at midpoint for different mean wind speeds, normalised with respect to the response to a uniform wind profile with corresponding mean wind speed, as a function of a for a sinus wind profile

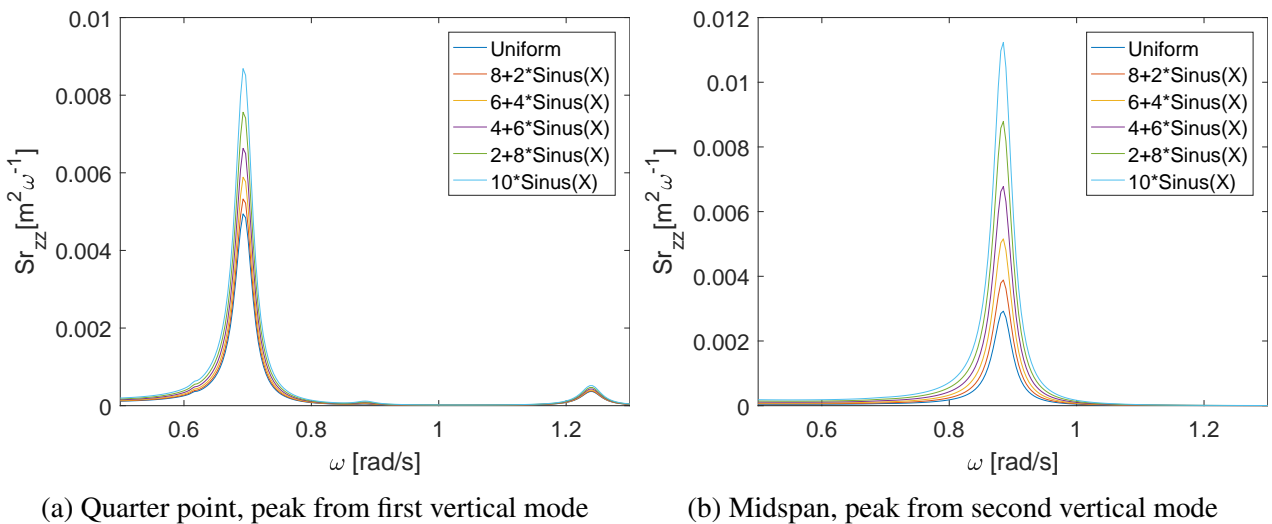


Figure 6.14: Vertical response spectra at mean wind speed of 10 m/s for uniform and different linear profiles with peak at the midspan.

Conclusion

As seen in this section, the maximum response increase for more non-uniform wind speed profiles. For all non-uniform wind profiles studied in this section, the maximum response along the span is always higher than the uniform wind profile and the response is increasing with the non-uniformity of the wind field. Therefore the profile with the highest value of a and the highest wind speeds, has the largest response along the span. This is due to higher values of the buffeting load coefficient matrix between points along the bridge which have high wind speeds. The cross-spectral densities of the velocity components also increase in average as the wind profile become non-uniform.

The asymmetric wind profiles cause a shift in the response along the span towards the side where the wind speeds are higher, as seen for the linear and arctan wind profiles. This is due to the buffeting load coefficient matrix and cross-spectral densities of the velocity components. These two have larger values where the wind speeds are high, which affects the modal response spectral matrix. In turn, this weighs the mode shape vectors in a way that makes the response higher in one side of the span.

In Table 6.1 the maximum response along the span and where it occurs, is shown for the most non-uniform wind profiles discussed in this section. Where the maximum response is found indicates which still-air vibration modes that give the most contribution to the response. Since the first mode in the lateral and torsional direction is symmetric with a shape of a half sinus wave and the linear peak wind profile has high wind speeds in the midspan, the linear peak wind profile gives the largest response in these two directions. The position of the largest lateral and torsional responses is near the midspan, where also the largest values of the first lateral and torsional mode shapes are found. The sinus wind profile is similar to the linear peak profile, but does not have as high wind speeds at the midspan. Therefore the sinus wind profile has mostly the same response characteristics as the linear peak wind profile, but with slightly lower response.

Regarding the vertical response, it is the arctan wind profile that has the maximum response. The first vertical mode shape has two half sinus waves, and has its largest values in the quarter points of the span. The arctan wind field has a wind speed of 18.3 m/s in the second quarter point, which results in a larger vertical response than the for the other wind profiles. The linear peak has its maximum vertical response in the midspan where the wind speed is 20 m/s, and gets most contribution from the second vertical mode.

Table 6.1: The maximum response along the span, the position and the difference compared to uniform wind profile for mean wind speed of 10 m/s.

Wind profile	Lateral direction			Vertical direction			Torsional direction		
	σ_{yy} [m]	Diff. %	x/L	σ_{zz} [m]	Diff. %	x/L	$\sigma_{\theta\theta}$ [10^{-3} rad]	Diff. %	x/L
Uniform	0.0635	-	0.51	0.0306	-	0.75	0.5598	-	0.50
Linear ($a = 20$)	0.0729	14.80	0.63	0.0468	52.94	0.77	0.6394	14.22	0.63
Arctan ($a = 10$)	0.0855	34.65	0.63	0.0579	89.22	0.76	0.7425	32.64	0.65
Linear peak ($a = 40$)	0.0971	52.91	0.51	0.0516	68.63	0.51	0.8855	58.18	0.51
Sinus ($a = 10$)	0.0894	40.79	0.51	0.0437	42.81	0.51	0.8111	44.89	0.50

Symmetric wind profiles with large wind speeds at the midspan excite the second vertical mode more than the first mode, and therefore have the largest response in the midspan. The asymmetric linear and arctan wind profiles excite the first vertical mode most, and maintain the shape of the response along the span with two peaks. So, the modes which is excited most, have mode shapes with large values where the wind speeds are high.

The vertical response is more vulnerable to the non-uniformity of the wind profiles than the lateral and torsional response. In the most extreme cases of non-uniformity, the increase in the vertical response from a non-uniform profile compared to the response from the uniform wind profile is almost 90% at most, while the increase in the lateral and torsional response is below 60%. The increase in the response with respect to non-uniformity of the wind speed has been studied through to the factor a . The normalised vertical response increases more with respect to the factor a than the two other response components for all the wind profiles studied in this section. The linear increase of response with respect to the factor a may be due to that each wind speed along the span has an increase or decrease that is also linear with respect to a .

6.2 Influence of non-uniform turbulence standard deviations

In this section, the influence of span-wise non-uniform turbulence standard deviations on the dynamic response will be presented. Three wind speed profiles have been analysed with different turbulence std profiles. The wind speed profiles used are the linear profile and the sinus profile shown in Figure 5.5a and 5.5d, in addition to a uniform wind speed profile. The three different turbulence std profiles shown in Figure 6.15 are studied. They all have the same integrated sum along the span to make them comparable. The two non-uniform turbulence std profiles chosen have the opposite shapes of the wind speed profiles used in this section, because this is often seen in the measurement data from the Hardanger Bridge. Both of these turbulence std profiles will be compared to uniform turbulence standard deviations, for all the three wind speed profiles. The horizontal turbulence std has a span-wise mean value of 20% of the wind profile's mean wind speed, and for the vertical component the corresponding value is 10%. The effect of turbulence std on the response is included in the calculations through the wind spectra, which have a quadratic dependency on the turbulence std, as shown in Eq. (2.40). The span-wise variation of wind speed is also included in the formula. Therefore, to study the effect of the turbulence std profiles isolated, the response using a uniform wind speed profile and different turbulence std profiles has been calculated. In addition comes the linear and sinus wind profiles, to study if the same turbulence std profiles have different effect on these than on the uniform wind speed profile. The calculated response will only be presented for wind profiles with the mean wind speed of 10 m/s, because the trends, the shape and differences of the response along the span are nearly the same for all mean wind speeds for the different wind speed profiles.

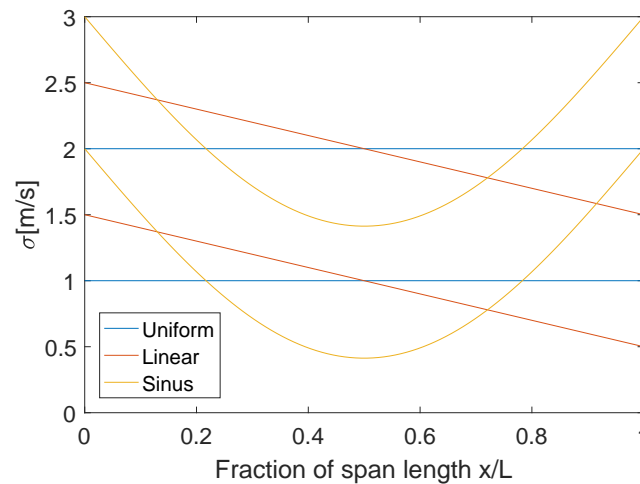


Figure 6.15: Several turbulence standard deviation profiles, both horizontal and vertical component.

Uniform wind profile

A uniform wind profile has been studied with the three different turbulence std profiles above. Since the wind profile is uniform, it is easier to see the influence of the non-uniform turbulence std along the span. In Figure 6.16 the response along the span is shown for mean wind speed 10 m/s. The legend indicates which turbulence standard deviation profiles are used, and the colours correspond to those in Figure 6.15. As seen in the plots below, the sinus turbulence std profile gives the lowest lateral and torsional response along the whole span. This is due to low turbulence std in the midspan, where the first lateral and torsional mode shapes have their highest values. For linear and uniform turbulence std profiles, the lateral and torsional response have almost the same maximum value, but the linear profile shifts the response slightly to the left side of the span.

In the vertical direction the maximum response is highest for the linear turbulence std profile. The sinus turbulence std profile has about 50% lower response in the midspan compared to the two others, because it's response is mostly dominated by the first vertical mode. The linear turbulence profile shifts the response to the left, since the turbulence standard deviations are higher there. It has maximum response around the first quarter point, while the response is lower than for the two other turbulence std profiles in the second quarter point.

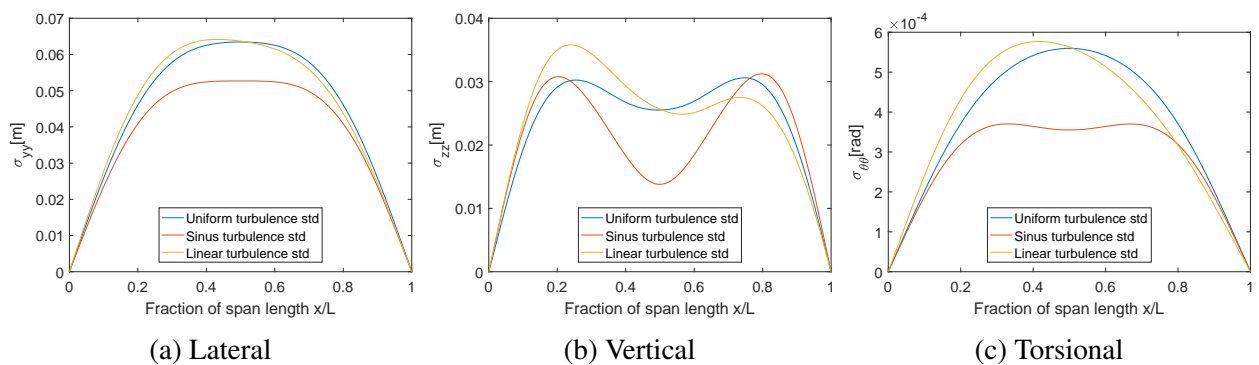


Figure 6.16: Response along the span for uniform wind speed profile with mean wind speed of 10 m/s and different turbulence std profiles.

Linear wind profile

The linear wind profile shown in Figure 5.5a has also been studied with different profiles of turbulence standard deviations. The wind profile is increasing between $x/L = 0$ and $x/L = 1$, while the linear turbulence std profile is decreasing, to simulate the behaviour seen in the measurement data. The response along the span for the different turbulence std profiles described above is shown in Figure 6.17 for all response components. The response is skewed to where the wind speeds are highest, even when using a linear turbulence std profile which has high values in the other side, but the linear turbulence std profile reduces this effect somewhat.

A uniform turbulence std profile gives the highest lateral and torsional response. In the vertical direction the response is highest using a sinus turbulence profile. This is due to both high wind speeds and high turbulence std in a range where the first vertical mode shape has high values.

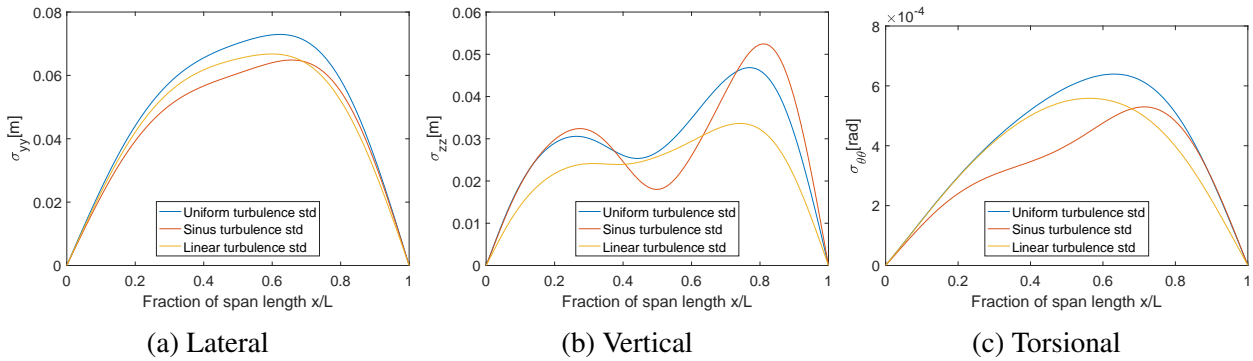


Figure 6.17: Response along the span for linear wind speed profile with mean wind speed of 10 m/s and different turbulence std profiles.

Sinus wind profile

In Figure 6.18 the response along the span is shown for a sinus wind profile (Figure 5.5d) with the same three different profiles of turbulence std as before. Using uniform and linear profiles for the turbulence standard deviations give almost the same horizontal and torsional response along the span, while a sinus turbulence std profile gives lower response. This is because of low turbulence standard deviations where the peaks in the first mode shapes are, and because high wind speed contributions to the single point wind spectra (Eq. 2.40) around the midspan is equalised by low turbulence std and high turbulence std towards the edges is equalised by low wind speeds.

The vertical response is clearly lowest for the sinus turbulence std profile, and has two maxima along the span because the contribution from the second vertical mode is reduced compared to the two other turbulence std profiles. The linear turbulence profile skews the response to the left and has a slightly higher response than the uniform turbulence profile, which has a symmetric shape with maximum response in the midspan.

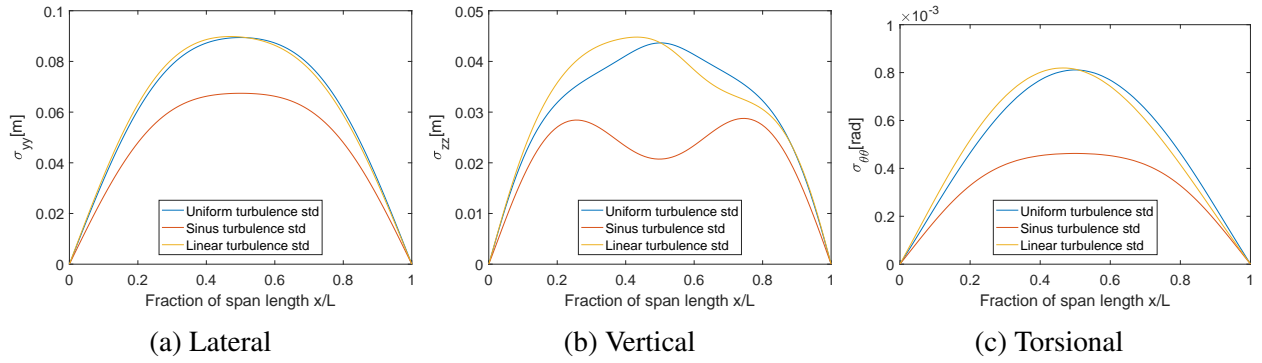


Figure 6.18: Response along the span for sinus wind speed profile with mean wind speed of 10 m/s and different turbulence std profiles.

Conclusion

After studying the response from several wind profiles with different turbulence standard deviation profiles, it can be seen that the response along the span is affected by the shape of the turbulence std profile. Low turbulence std in ranges where the first mode shapes have high values, gives a lower response in the corresponding response component. When the turbulence std profile is taken as the opposite shape of the wind profile, a lower maximum response is seen in general.

A symmetric turbulence std and wind profile gives a symmetric response along the span, while an asymmetric turbulence profile shifts the response to where the turbulence std is higher. This is seen for the response using a uniform wind profile and linear turbulence std profile. This is due to the cross-spectral densities of the velocity components where the span-wise variations of turbulence standard deviation is included, as seen in Equation 2.40. In the previous section, it was mentioned that the response was shifted to where the wind speeds were higher. In this section, combinations where the turbulence std is high when the wind speed is low and opposite have been studied, for instance linear decreasing turbulence std profile and linear increasing wind profile. The result of this is that the wind speed is dominating and shifts the response more than the turbulence std, for this particular combination of wind speed profile and turbulence std profile. It should be noted that the linear wind speed profile has a higher degree of non-uniformity than the linear turbulence std profiles in this case. The wind speed increases from 0 to 20 m/s along the span, while the standard deviations of the turbulence decreases from 2.5 to 1.5 m/s for the horizontal component and from 1.5 to 0.5 m/s for the vertical component. So a statement saying that non-uniform wind speeds shifts the response more than non-uniform turbulence cannot be made on a general basis, only for this particular case.

6.3 Influence of non-uniform self-excited forces

To study the influence of span-wise non-uniform self-excited forces on the dynamic response, several wind speed profiles have been numerically tested with both uniform and non-uniform self-excited forces. The non-uniform self-excited forces are caused by the non-uniform wind profile. The response is predicted with uniform self-excited forces where the aerodynamic properties are dependent on the mean wind speed of the wind profile, and with non-uniform self-excited forces where the aerodynamic properties vary along the span with the wind speed. Then the bridge response in both cases are compared. The wind profiles tested are presented in Figure 5.5. As in section 6.1, the standard deviations of turbulence components are span-wise uniform, such that the influence of the non-uniform self-excited forces are investigated separately. The horizontal and vertical turbulence standard deviations have been set to 20 and 10%, respectively, of the horizontal mean wind speed. The results are presented in the following tables as the ratio between response when non-uniform and uniform self-excited forces are used in the calculations,

$$\frac{\sigma_i^{non-uniform}}{\sigma_i^{uniform}}, \quad i \in \{y, z, \theta\} \quad (6.1)$$

The ratios are shown for three different locations along the bridge span, $x/L \in \{0.25, 0.50, 0.75\}$, and for six different mean wind speed values, $\{10, 20, 30, 40, 50, 60\}$. Plots of the response along the span for the two cases will also be shown, in addition to response spectra where it is needed.

Linear wind profile

This first wind profile is a linear profile that starts at 0 m/s at one side and has its maximum wind speed at the other side, shown in Figure 5.5a. Table 6.2 shows the ratios explained in the introduction of this chapter (Eq. 6.1).

The non-uniformity of self-excited forces has almost no effect on the lateral response for the linear wind profile. A very slight decrease in lateral response is seen, less than 1% in the worst case, which is at the quarter point for the highest mean wind speed. While the lateral response decrease for non-uniform compared to uniform self-excited forces, the vertical and torsional responses increase. In the vertical case, the ratio is largest in the maximum points of the first vertical mode shape; the two quarter points where the response has increased with around 18%. The most affected response variable is the torsional displacement, where the largest ratio is found at $x/L = 0.75$. The ratio for torsional response increases almost linearly between the quarter points, like the wind speed. At the first quarter point, the ratio decreases with mean wind speed up to 40 m/s, and increases with mean wind speed in the midspan and the second quarter point. At mean wind speed of 60 m/s, the torsional

ratio increases significantly at the midspan and the second quarter span.

Table 6.2: Ratios between the standard deviations of displacements when using non-uniform and uniform self-excited forces for the linear wind profile.

Wind speed		Lateral direction			Vertical direction			Torsional direction		
Mean	Max	x/L			x/L			x/L		
[m/s]	[m/s]	1/4	1/2	3/4	1/4	1/2	3/4	1/4	1/2	3/4
10	20	1.0000	1.0000	1.0000	1.0042	0.9998	1.0026	0.9977	1.0015	1.0049
20	40	0.9999	0.9999	0.9998	1.0181	0.9991	1.0115	0.9903	1.0073	1.0209
30	60	0.9997	0.9997	0.9996	1.0406	0.9982	1.0274	0.9808	1.0210	1.0524
40	80	0.9992	0.9994	0.9991	1.0734	0.9973	1.0538	0.9727	1.0474	1.1074
50	100	0.9976	0.9986	0.9980	1.1207	0.9977	1.0985	0.9729	1.0983	1.2029
60	120	0.9940	0.9967	0.9955	1.1923	1.0061	1.1791	1.0173	1.2273	1.4009

In Figure 6.19 and 6.20 the span-wise response is shown for the wind speeds where the largest effects of including non-uniform self-excited forces are seen; span-wise mean of 50 and 60 m/s. Between these two wind speeds, it is seen that the span-wise shape of the response is somewhat maintained and that the effect of including non-uniform self-excited forces increases most for the torsional response. The torsional response also gets even more skewed to the right when including non-uniform self-excited forces compared to using uniform self-excited forces.

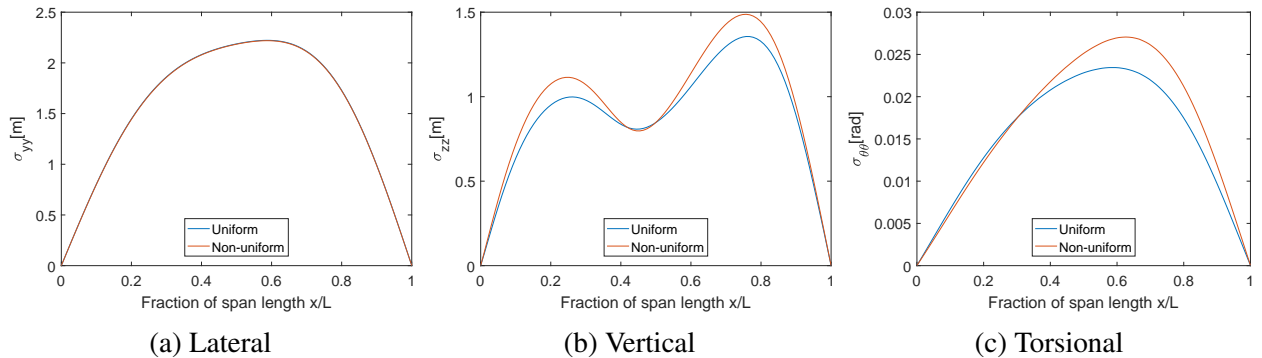


Figure 6.19: Comparison of response when using non-uniform self-excited forces and uniform self-excited forces at mean wind speed 50 m/s.

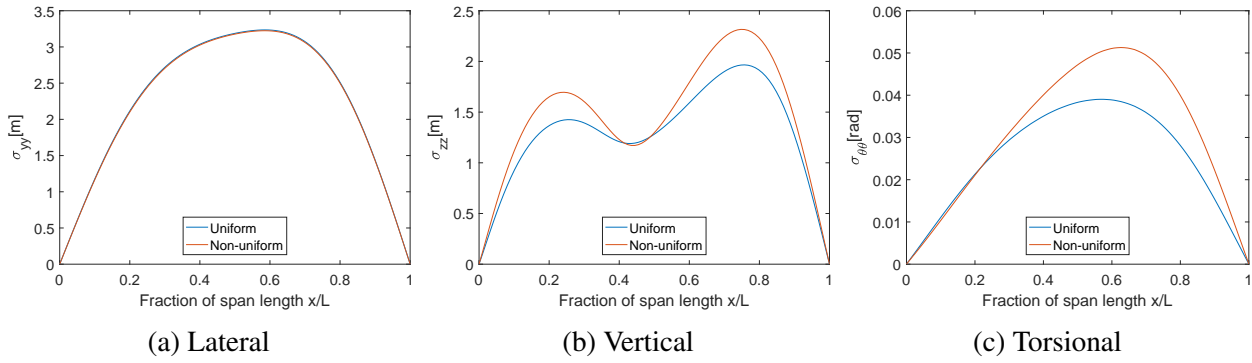


Figure 6.20: Comparison of response when using non-uniform self-excited forces and uniform self-excited forces at mean wind speed 60 m/s.

Linear wind profile with a peak at the midspan

Below, the effect of including the non-uniformity of self-excited forces on a linear profile with peak at the midspan is shown. The wind profile studied here is shown in Figure 5.5c. The maximum wind speed is the same for this profile as for the linear wind profile, but is found at the midspan instead of on the outer edge of the span. Therefore, the response using non-uniform self-excited forces deviates most from the response using uniform self-excited forces in the midspan, as seen in Table 6.3. While including non-uniform self-excited forces had almost no effect on the lateral response for the linear wind profile in the previous section, a decrease of lateral response from about 3% for mean wind speed 10 m/s to about 11% for mean wind speed 60 m/s is seen for the linear profile with peak at the midspan. It's the lateral response that is most affected for span-wise means 10-30 m/s, while the vertical and torsional response gets more affected for the highest mean wind speeds. For mean wind of 40-60 m/s, it is torsional response at the midspan that has the highest ratios; 1.19 for 40 m/s, 1.58 for 50 m/s and 1.70 for 60 m/s. The vertical response is also greatly affected for mean wind speed of 50 and 60m/s, with ratios of 1.21 and 1.44, respectively. Both torsional and vertical response ratios are below 1 for the low mean wind speeds, and increase as the mean wind speed gets higher.

Table 6.3: Ratios between the standard deviations of displacements when using non-uniform and uniform self-excited forces for the linear wind profile with peak at the midspan.

Wind speed		Lateral direction			Vertical direction			Torsional direction		
Mean	Max	x/L			x/L			x/L		
[m/s]	[m/s]	1/4	1/2	3/4	1/4	1/2	3/4	1/4	1/2	3/4
10	20	0.9736	0.9726	0.9739	0.9966	0.9490	0.9977	0.9961	0.9997	0.9969
20	40	0.9464	0.9446	0.9468	0.9961	0.9451	0.9977	0.9904	1.0054	0.9937
30	60	0.9324	0.9300	0.9328	0.9972	0.9705	0.9995	1.0152	1.0521	1.0223
40	80	0.9237	0.9208	0.9241	1.0014	1.0339	1.0058	1.1104	1.1868	1.1238
50	100	0.9154	0.9122	0.9159	1.0292	1.2065	1.0450	1.4286	1.5828	1.4545
60	120	0.8997	0.8959	0.9003	1.1252	1.4424	1.1566	1.4659	1.7000	1.5042

In Figure 6.21 and 6.22, the response along the span is shown for the mean wind speeds where the differences between non-uniform and uniform self-excited forces are largest; 50-60 m/s. As seen, it is a large difference in the midpoint for the vertical and the torsional response. The non-uniform self-excited forces affects the torsional response greatly already at mean wind speed of 50 m/s, and is large for 60 m/s. The lateral response has only 2 pp more difference for the mean wind speed of 60m/s than 50m/s.

The vertical and torsional response spectra at the second quarter point for mean wind speeds of 50 and 60m/s are shown in Figure 6.23, both for uniform and non-uniform self-excited forces. From the peaks in the frequency range around 1.45-1.50 rad/s, it can be seen that some of the contribution to the increased vertical and torsional response in the non-uniform case probably comes from a coupling between the first torsional mode ($\omega_n = 2.26\text{rad/s}$) and two or three of the vertical modes 3-5 ($\omega_n = 1.24\text{rad/s}$, $\omega_n = 1.33\text{rad/s}$ and $\omega_n = 1.71\text{rad/s}$).

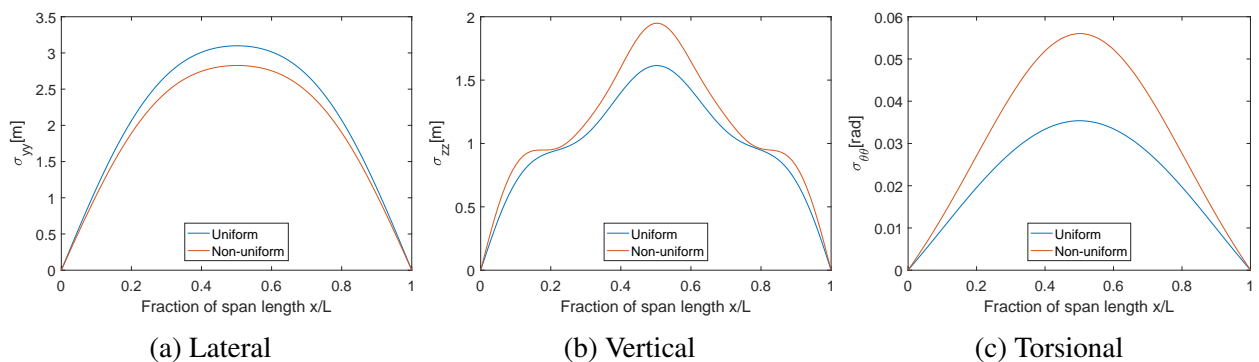


Figure 6.21: Comparison of response when using non-uniform self-excited forces and uniform self-excited forces at span-wise mean 50 m/s.

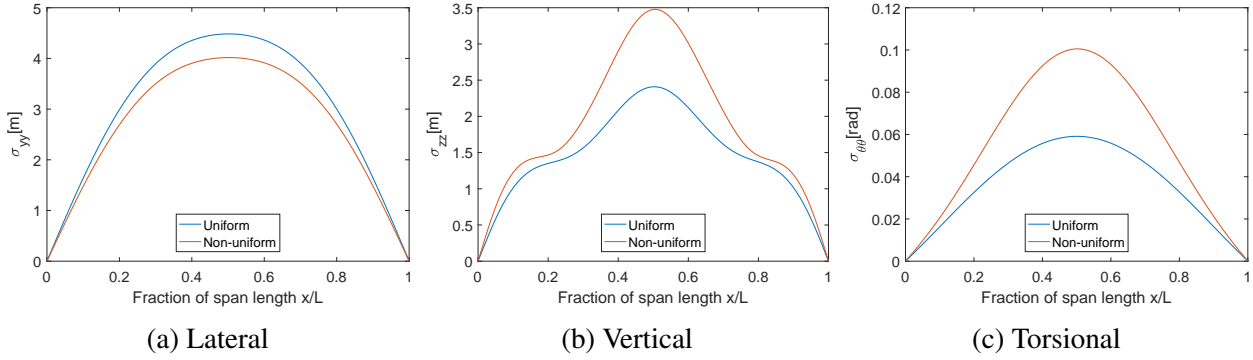


Figure 6.22: Comparison of response when using non-uniform self-excited forces and uniform self-excited forces at span-wise mean 60 m/s.

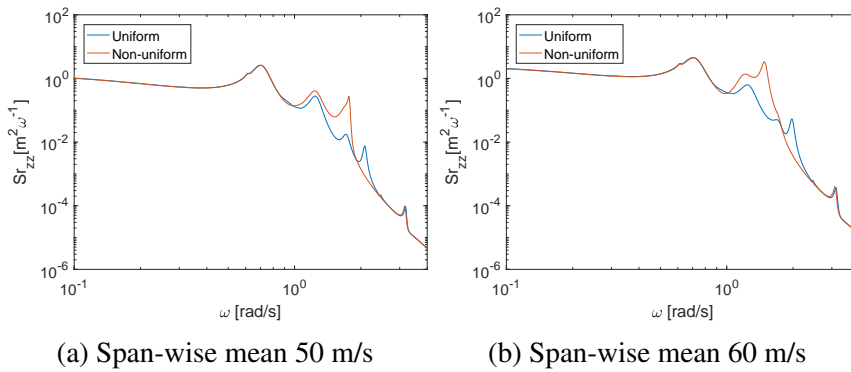


Figure 6.23: Comparison of vertical response spectra at the quarter point when using non-uniform and uniform self-excited forces.

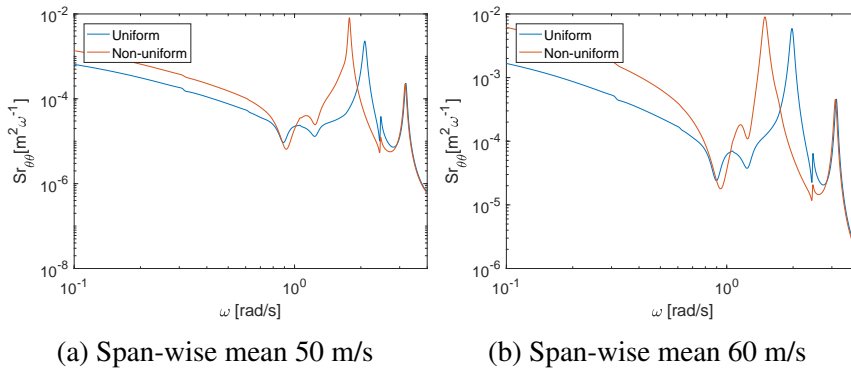


Figure 6.24: Comparison of torsional response spectra when using non-uniform self-excited forces and uniform self-excited forces.

Sinus wind profile

The half sinus wave wind profile is similar to the linear profile with peak in the midspan in the sense that they both have maximum wind speed at the midspan. But in the sinus wind profile the wind

speeds are more evenly distributed along the span and the maximum wind speed is lower, as seen in Figure 5.5d. As found for the linear wind profiles, the ratio between using non-uniform and uniform self-excited forces in vertical and torsional increases rapidly for mean wind speed around 50m/s. Also for mean wind speed 40m/s (max wind 63.46m/s) the ratio for torsional response is considerable, with 1.1165.

At a mean wind speed of 60m/s, the sinus profile differs from the rest of the wind profiles with both larger vertical and torsional response ratio and different span-wise shape of the vertical response. The vertical displacements at the quarter points for mean wind speed of 60m/s are more than doubled using non-uniform compared to uniform self-excited forces, and the torsional response is over five times higher at both midspan and quarter points. And as seen in 6.26, the span-wise shape of the vertical response at mean wind speed of 60m/s is unlike any response shape of the other wind profiles. The response spectra for the quarter point at mean wind speed of 60m/s in the Figures 6.27 and 6.28 reveal a dominating peak around $\omega = 1.6\text{rad/s}$ for both vertical and torsional response, which is not seen in any of the other spectra shown. It is believed that the fifth vertical mode gets more excited in this case, because of the similarity seen between the mode shape and the span-wise shape of vertical response. The peak at about $\omega = 1.6\text{rad/s}$ is also seen in the lateral response spectrum, and in all the response spectra at the midspan.

Table 6.4: Ratios between the standard deviations of displacements when using non-uniform and uniform self-excited forces for the sinus wind field.

Mean wind speed		Lateral direction			Vertical direction			Torsional direction		
Mean	Max	x/L			x/L			x/L		
[m/s]	[m/s]	1/4	1/2	3/4	1/4	1/2	3/4	1/4	1/2	3/4
10	15.8660	0.9800	0.9787	0.9800	0.9874	0.9648	0.9881	0.9981	1.0000	0.9982
20	31.7319	0.9569	0.9545	0.9567	0.9837	0.9609	0.9846	0.9952	1.0036	0.9957
30	47.5979	0.9442	0.9413	0.9441	0.9833	0.9780	0.9845	1.0116	1.0337	1.0130
40	63.4639	0.9365	0.9331	0.9363	0.9861	1.0198	0.9879	1.0698	1.1165	1.0727
50	79.3298	0.9302	0.9265	0.9300	0.9969	1.1106	1.0007	1.2333	1.3247	1.2392
60	95.1958	0.9214	0.9193	0.9212	2.0515	1.6784	2.1538	5.5113	6.1692	5.5562

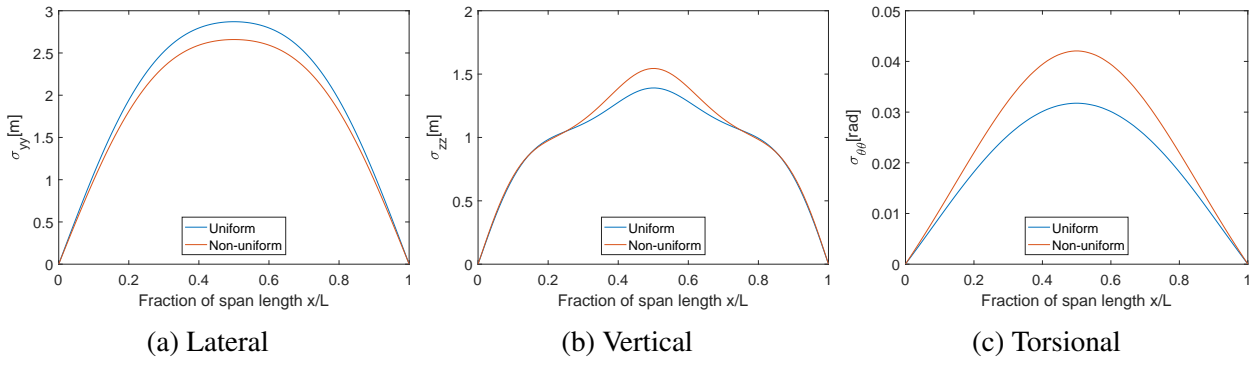


Figure 6.25: Comparison of response when using non-uniform self-excited forces and uniform self-excited forces at mean wind speed 50 m/s.

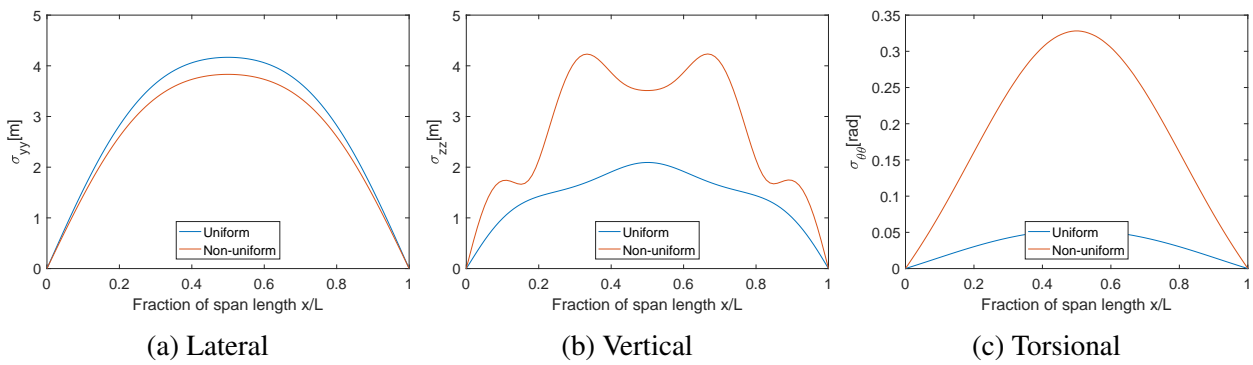


Figure 6.26: Comparison of response when using non-uniform self-excited forces and uniform self-excited forces at mean wind speed 60 m/s.

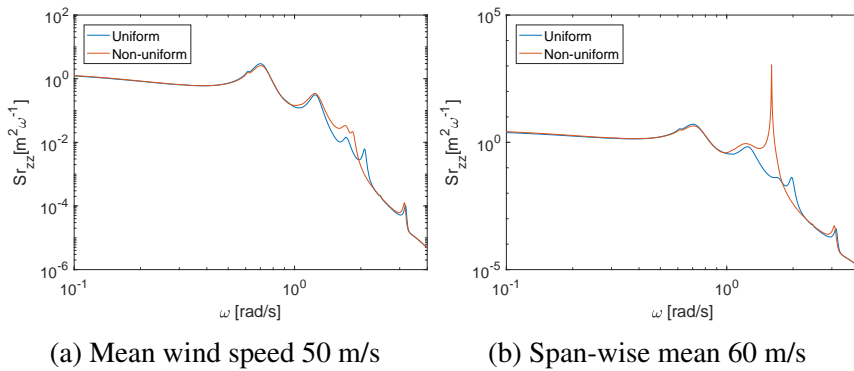


Figure 6.27: Comparison of vertical response spectra when using non-uniform self-excited forces and uniform self-excited forces at the quarter point.

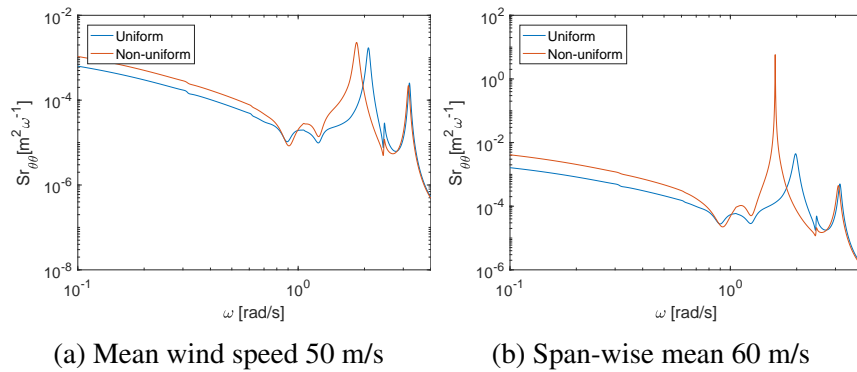


Figure 6.28: Comparison of torsional response spectra when using non-uniform self-excited forces and uniform self-excited forces at the quarter point.

Arctan wind profile

The arctan wind profile has most of the high wind speeds concentrated on one side of the span, similar to the linear profile, and the effect of including non-uniform self-excited forces is also similar, but for the highest mean wind speeds the effect is larger for the arctan profile than for the linear profile. The arctan wind profile is shown in Figure 5.5b. Table 6.5 shows that the ratio between the responses when including non-uniform and using uniform self-excited forces is largest around $x/L = 0.75$. The vertical and torsional response ratio is highest for mean wind speed of 60 m/s, as for the other wind profiles. For this mean wind speed, the torsional response at the second quarter point is 3.5 times higher when using non-uniform self-excited forces compared to uniform self-excited forces.

The plots of torsional response along the span in Figure 6.29 indicate a further shift of the response towards the side of the span where the wind speeds are higher when the self-excited forces are non-uniform. Since more of the high wind speeds are located at one side of the span for the arctan profile compared to linear profile, the response along the span is shifted more to the right for the arctan wind profile compared to the linear wind profile.

Table 6.5: Ratios between the standard deviations of displacements when using non-uniform and uniform self-excited forces for the arctan wind field.

Wind speed		Lateral direction			Vertical direction			Torsional direction		
Mean	Max	x/L			x/L			x/L		
[m/s]	[m/s]	1/4	1/2	3/4	1/4	1/2	3/4	1/4	1/2	3/4
10	20	0.9999	0.9999	0.9999	1.0113	1.0003	1.0059	0.9953	1.0033	1.0087
20	40	0.9998	0.9997	0.9996	1.0405	1.0008	1.0238	0.9805	1.0159	1.0371
30	60	0.9992	0.9993	0.9990	1.0846	1.0016	1.0545	0.9683	1.0499	1.0989
40	80	0.9972	0.9982	0.9975	1.1472	1.0049	1.1057	0.9717	1.1256	1.2227
50	100	0.9915	0.9952	0.9935	1.2411	1.0177	1.2005	1.0369	1.3207	1.5009
60	120	0.9768	0.9856	0.9835	1.4543	1.1643	1.5934	2.0918	3.0573	3.5218

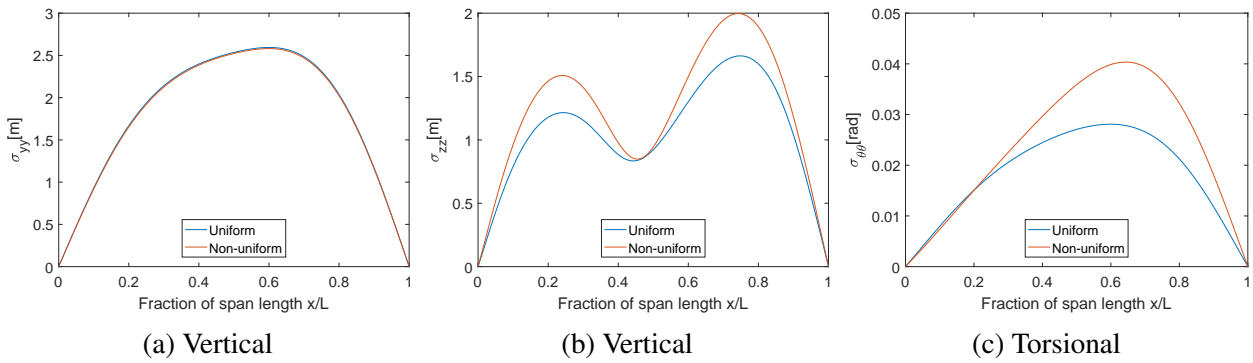


Figure 6.29: Comparison of response when using non-uniform self-excited forces and uniform self-excited forces at mean wind speed 50 m/s.

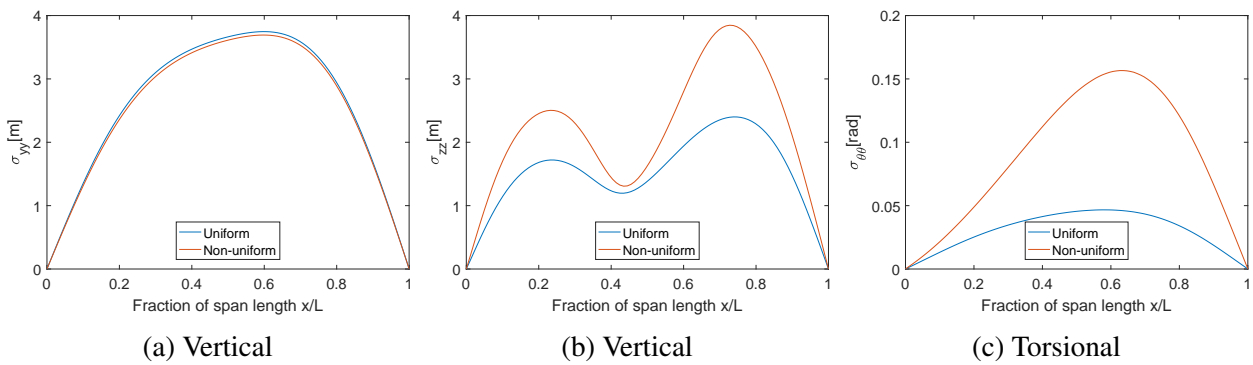


Figure 6.30: Comparison of response when using non-uniform self-excited forces and uniform self-excited forces at mean wind speed 60 m/s.

Conclusion

As can be seen from the above tables, the differences between the response for non-uniform and uniform self-excited forces are most prominent for vertical and torsional response at high mean wind speeds. By taking account for the non-uniform wind speed when calculating the self-excited forces, some parts of the bridge will approach the critical flutter limit earlier than when only the wind profile's mean wind speed is used to calculate them. This is assumed to be one of the reasons for the differences. When using non-uniform self-excited forces in the calculations, the torsional response seems to get an unstable development at a mean wind speed of 50-60 m/s which may be due to that the critical flutter speed has been reached. The critical flutter speed for the Hardanger Bridge, when the wind profile is uniform, was estimated to be 78 m/s by Øiseth [15]. That the critical flutter speed is lower for the non-uniform wind profiles tested in this section is in agreement with the findings of Arena et al. [10], who found that the non-uniform wind profiles they tested on a Runyang Suspension Bridge model led to lower critical flutter speeds than an energy equivalent uniform wind profile.

The ratio between lateral response when non-uniform and uniform self-excited forces are considered, is decreasing with mean wind speed for all the different wind profiles, but the decrease is small compared to the differences seen for the vertical and torsional response. The decrease in the ratio is below 3% for the asymmetric wind profiles and about 11% for the symmetric wind profiles. The ratios for torsional and vertical response increase as the mean wind speed increases, and the highest ratio is found in the point where the highest wind speeds are found. If the torsional response was shifted to one side with uniform self-excited forces, the non-uniform self-excited forces shift the response even more for the particular wind profile.

If wind speeds at a more realistic level are considered, the effect of including non-uniform self-excited forces are small. The Hardanger Bridge is designed for a mean wind speed with a return period of 50 years, which is about 38-39 m/s at the bridge deck height (60 meters) [21]. For the wind profiles with the maximum wind speed of 40 m/s, the largest ratio between response when using non-uniform and uniform self-excited forces is 1.0371 for the torsional response (Table 6.5) and the lowest ratio is 0.9446 for the lateral direction (Table 6.3).

The aerodynamic derivatives that have been used in this thesis have been discussed previously in Section 5.3. The different P^* are related to the lateral aerodynamic damping and stiffness, which can be seen in the aerodynamic damping and stiffness matrices in Section 2.3, and $P_i^* = 0$ where $i \in \{2, 3, 4, 6\}$. The contribution to the aerodynamic stiffness in the lateral direction is zero because all the aerodynamic derivatives related to the lateral stiffness are zero. In other words, the displacement components and the rotational velocity of the bridge have no influence on the self-excited forces in the lateral direction. This is the main reason that the influence of including the non-uniform self-excited forces is small for lateral response. The two aerodynamic derivatives that contribute to the aerodynamic damping in the lateral direction is P_1^* and P_5^* which has been taken as linear functions from the quasi-steady theory and are negative for all values of the reduced velocity. This implies that

the total lateral damping increases. It is seen that the total lateral damping increases more for non-uniform compared to uniform self-excited forces, and this is responsible for the decrease in lateral response observed.

For the aerodynamic derivatives related to the vertical and rotational direction, only H_6^* and A_6^* are taken as zero. This means that the contribution from the lateral displacement is not taken into account for the self-excited forces in the vertical and rotational directions, while the other displacement components and all velocity components contribute. The aerodynamic derivatives H_i^* and A_i^* where $i \in \{1, 2, 3, 4\}$, are expressed by second order functions of the reduced velocity. The vertical and torsional response increase when the non-uniform self-excited forces are included, especially for high wind speeds, which means that the total damping and stiffness to the structure decrease in these two directions. This may be due to the aerodynamic derivatives H_3^* and A_3^* , which are positive and rapidly increasing with reduced velocity. This will give a negative contribution to the stiffness of the structure. Also H_5^* , which increases linearly with reduced velocity and is positive, gives a negative contribution to the damping.

6.4 Conclusion

In this chapter, the results from the numerical study have been presented for different profiles of both mean wind speed and turbulence standard deviations. The effect of including the non-uniform self-excited forces has also been investigated.

The main findings about how the non-uniform wind profiles effect the response is shown in Table 6.1, where the increase of response in the point of maximum response is shown. The increase in response for all wind profiles studied is almost linear with respect to the factor a . The vertical response is found to be most affected by the factor a , which implies that the vertical response is most vulnerable to the non-uniformity of wind speed. The reason for the linear increase in the response with respect to a , may be due to that the wind speeds along the span also have a linear dependency on a . The linear profile with a peak in the midspan and the sinus profile, which has high wind speeds in the midspan, gets more contribution from the second vertical mode, and the vertical response along the span changes its shape as the factor a increases for these two profiles. All non-uniform wind speed profiles studied has larger response compared to the uniform wind speed profile. The more non-uniform the wind speed profile becomes, the larger the maximum response gets. The higher response is due to the buffeting load coefficient matrix and the cross-spectral densities of the turbulence components which are dependent on the non-uniform wind profile. The two matrices get high values when two points with high wind speeds are considered.

The influence of the non-uniform turbulence standard deviation has connection to the shape of the wind speeds along the span. As discussed previously, the response shifts to where the wind speeds is largest. The same can be said about the turbulence std. It was seen that the wind is dominating and shifts the response more than the turbulence std, for this particular shapes and ratio between the mean wind speed and standard deviation of the turbulence components. The horizontal shift in the response due to the non-uniform turbulence std comes from the cross-spectral densities of the turbulence components which is high when two points with large turbulence std are considered.

The effect of including the non-uniform self-excited forces on the response increase with the mean wind speed of the wind profile. The difference between the response using non-uniform and uniform self-excited forces are largest for the highest mean wind speeds studied. The lateral response using non-uniform self-excited forces deviates less from the response using uniform self-excited forces compared to the vertical and torsional response. This is due to the aerodynamic derivatives which has been taken as zero. The reason for the large ratios in the vertical and torsional direction is the aerodynamic derivatives that reduce the total damping and stiffness of the structure as mentioned. For lower mean wind speeds, 10-20m/s, the difference is below 10% for all response components.

Comparison with measured response

In this chapter, wind data from the bridge site will be used to estimate the dynamic response. Values of 30-minute mean wind speed and standard deviation of turbulence will be picked in different ways from these measured wind data, and the resulting predicted response will be compared to the measured response from the same time period. The goal is then to decide which of the wind profile approximations that estimates the response most accurately. Three different ways of picking wind values from the data to obtain a span-wise horizontal wind profile will be compared; using the mean value of all wind sensors (uniform profile), midspan value (uniform profile) and values from all nine wind sensors (non-uniform profile). This will be done for both the 30-minute mean wind speed and standard deviation of the turbulence components. Then, at last, the effect of including span-wise non-uniform self-excited forces will be evaluated. The different inputs and methods of the calculations of the response are presented in Chapter 5.

16 different recordings from the site are used in this thesis, and one should keep in mind that the findings will only be valid for these. By considering a larger amount of recordings, the findings could be treated as valid for the Hardanger Bridge. The recordings used are divided into two groups, high and low wind speeds. Therefore, the results will be presented in groups. The wind speeds are taken to attack perpendicular to the bridge, as the horizontal direction of the wind speed is close to perpendicular at each sensor in all of the recordings. The wind direction at the midspan is shown for all recordings in Table 4.1, and it varies between 98° and 103° from the east and 266° and 297° from the west. The largest deviation from the perpendicular direction is 27° .

Similar to Chapter 6, the mean value of the 30-minute mean wind speed from each sensor is referred to as the wind profile's mean wind speed. This will not technically give the true mean, since there are only nine sensors and that the sensors are distributed asymmetrically along the span, but the term will still be used for simplicity. 30-minute mean wind speed at the midspan is referred to as midspan wind speed. The response discussed will be displacement, with units of meters and radians, and std is

used as an abbreviation for standard deviation. When discussing some of the figures in this chapter, there's a need to compare different percentage values, and in this case the term percentage points will be used and abbreviated to pp.

The analysis will be done in a step-wise manner starting with uniform profiles for the wind speed and the turbulence standard deviations and ending up with non-uniform profiles with span-wise non-uniform self-excited forces. The influence of each step will be assessed, with the goal of determining which of the wind approximations that has the most accurate response prediction with respect to the measured response. The steps are as follows:

Uniform steps:

1. Study which value, mean or midspan wind speed, that should be taken for the uniform wind speed profile to predict the response most accurately with respect to the measured response
2. Study which value, mean or midspan, that should be taken for the uniform turbulence standard deviation profiles to predict the response most accurately with respect to the measured response

Non-uniform steps:

3. Non-uniformity of the wind speed is included in the calculations. The predictions are compared with the most accurate response from the uniform steps.
4. Non-uniformity of both the wind speed and the turbulence standard deviations is included in the calculations. The predictions are compared with the most accurate response from the uniform steps.
5. Study if the predicted response with non-uniform self-excited forces is more accurate than with uniform self-excited forces.

Since the estimated response has units of displacement, the measured accelerations are transformed to displacements in the frequency domain as expressed in Equation (2.45). Then the standard deviations of the displacements are obtained by $\sigma = \sqrt{\int_{0.12}^4 S_r d\omega}$. The integration starts at 0.12 rad/s because the accelerometers are not capable of measuring very low frequencies, and stops at 4 rad/s because the contribution from modes with higher natural frequencies is negligible. The lowest natural frequency of the bridge is 0.31 rad/s, which means that contributions from all the first still-air vibration modes are included. The results will be presented as plots of the average ratio between the predicted and measured response at the accelerometer locations, for each recording group separately. If the ratio is one, the predicted and measured response is the same. Ratios below one underestimate and above one overestimate the predicted response with respect to the measured response. The predicted and measured response will also be shown for single recordings to better compare the response shapes.

7.1 Uniform profiles

In this section, the mean and midspan values of wind speed and turbulence standard deviations will be considered. The predicted response using these two values in uniform profiles will be compared to the measured response, to study which values that give the most accurate predictions. The self-excited forces are uniform in this part, meaning the aerodynamic properties are calculated using the mean wind speed.

7.1.1 Step 1: Wind speed

First, the mean and midspan values of wind speed are compared with respect to the accuracy of response prediction. Both values have been used for a uniform wind profile, and the response has been predicted. The profiles of turbulence standard deviations are taken as uniform where the mean value has been used. The mean and midspan values from all recordings are shown in Table 4.1.

In Figure 7.1, the average ratio between predicted and measured response at the accelerometer locations are shown for the high wind speed recordings. As seen, the predicted response is slightly higher when using the mean value than when using the midspan value, but the difference is only about 1 pp. The response is predicted in the range of 62 to 70% of the measured response in the lateral direction and in the range of 70 to 85% in the vertical direction. The torsional response is predicted well for the five accelerometers closest to the midspan with a maximum deviation of 5% with respect to the measured response.

Plots of the average ratio between the predicted and measured response for the low wind speed recordings are shown in Figure 7.2. Here, the midspan wind speed gives higher predicted response than the mean wind speed, but the difference is small. The torsional response is overestimated by 50-75% in six of the seven locations. The lateral response is underestimated by 30-50% for both mean and midspan wind speed, and the vertical response is predicted well in the quarter points. The difference between the mean and midspan wind speed is only about 1 pp also for the low wind speeds.

Comparing the accuracy of the response predictions for the high and low wind speeds, it is seen that the vertical response is predicted more accurately for low wind speeds, while the torsional response is predicted more accurately for high wind speeds. In the lateral direction, the low wind speeds underestimate the response more than the high wind speeds. For both groups of wind speeds, the lateral response is predicted most accurately near the midspan, and the vertical response is predicted best near the quarter points.

As can be seen from the plots, the difference in estimated response between using mean and midspan values for the wind speed in a uniform wind profile is small. This is due to a small difference between

these two values. The largest difference between the mean and midspan wind speed for all the 16 recordings is 0.9 m/s.

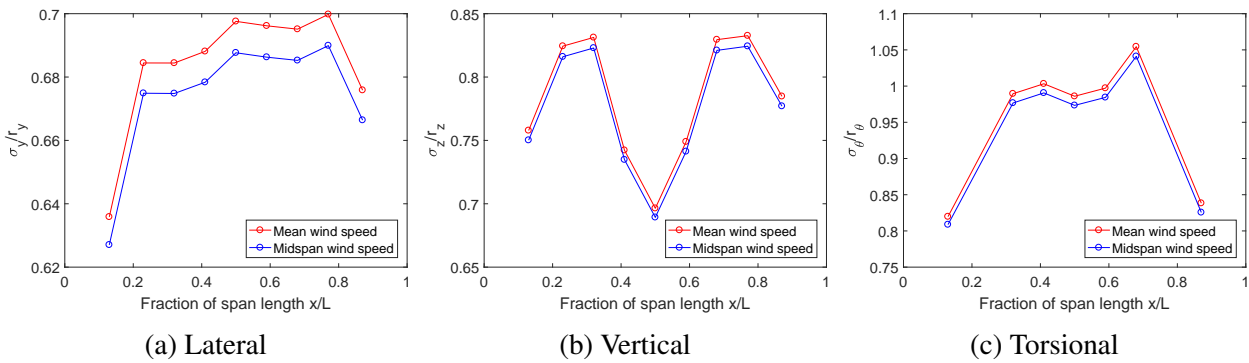


Figure 7.1: Ratio between predicted and measured response in the location of the accelerometers for the recordings with high wind speeds.

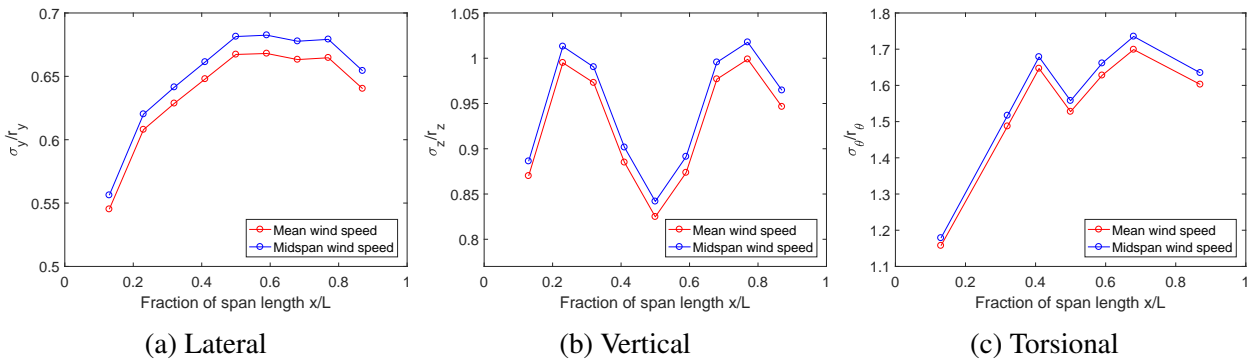


Figure 7.2: Ratio between predicted and measured response in the location of the accelerometers for the recordings with low wind speeds.

In Figure 7.3, 7.4 and 7.5, the predicted span-wise response is shown for one high and one low wind speed recording together with the measured response. The two recordings chosen are the ones with the largest difference between mean and midspan wind speed. The response plots to the left are for the high wind speed recording, with mean wind speed 25.5 m/s and midspan wind speed 24.6 m/s. The response plots to the right are for the low wind speed recording, where mean wind speed is 11.7 m/s and midspan wind speed is 12.6m/s. The measured response is represented as dots in the location of the accelerometers.

As seen, the wind values do not differ much, and as expected, neither do the predicted responses. Overall, the predicted response is better and more consistent between the response components for the high wind speed recording, and the mean wind speed is slightly better than midspan wind speed in this case. For the recording with low wind speeds, the response prediction is not consistent between the response components and a decision between mean and midspan wind speed is harder to make in this case. Because uniform wind profiles are used in this section, the wind profile which has the

highest wind speed predicts the highest response. This is seen in these plots, where the mean wind speed is highest to the left and midspan wind speed is highest to the right. For high wind speed, the torsional response is predicted most accurately, while the vertical response is predicted most accurately for low wind speed.

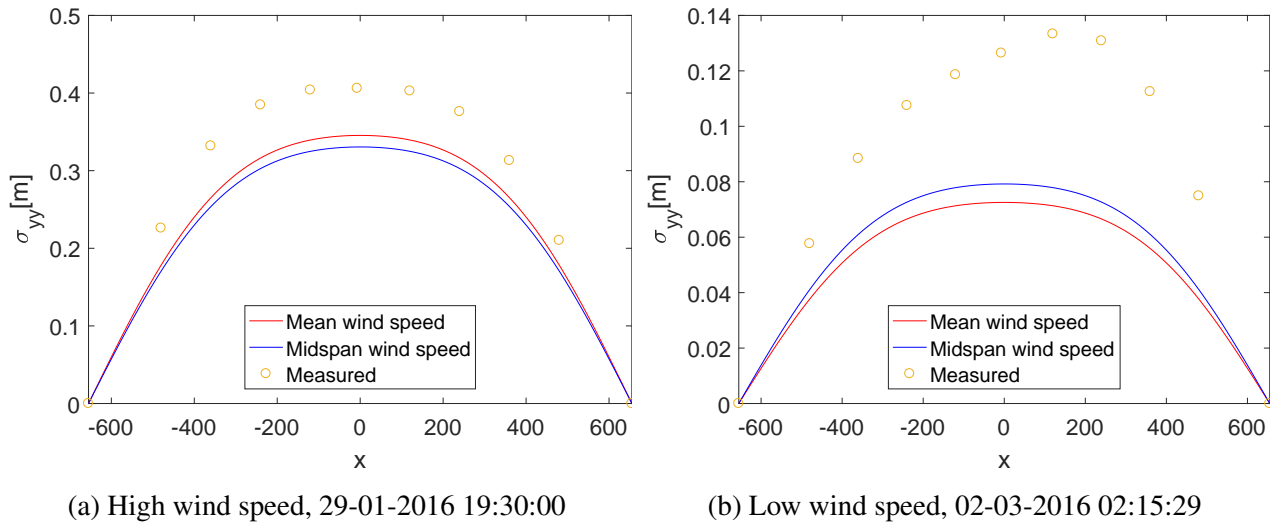


Figure 7.3: Standard deviation of lateral displacement along the bridge using uniform wind profile.

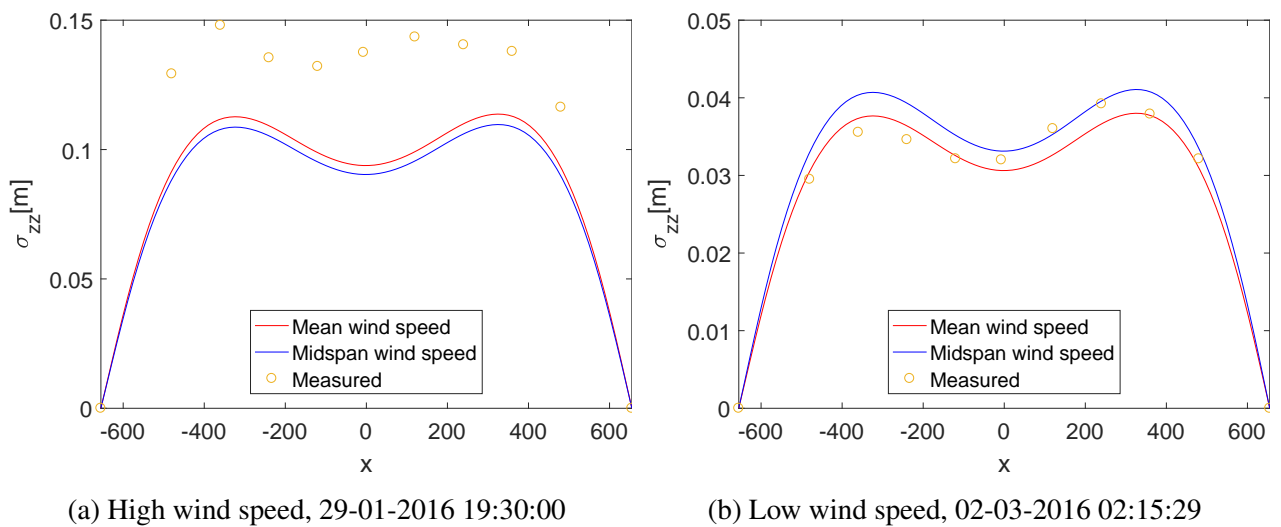


Figure 7.4: Standard deviation of vertical displacement along the bridge using uniform wind profile.

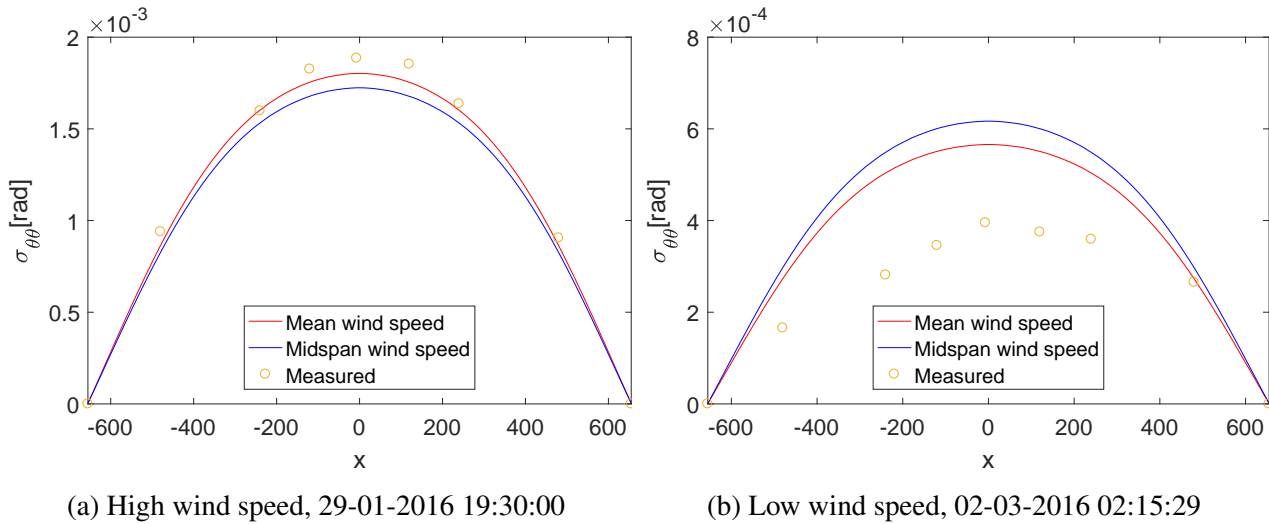


Figure 7.5: Standard deviation of rotation along the bridge using uniform wind profile.

7.1.2 Step 2: Standard deviation of turbulence components

In this section, the mean and midspan values of the turbulence standard deviations are compared with respect to the accuracy of the response prediction. Both values have been used for a uniform turbulence std profile, for both the horizontal and vertical turbulence standard deviation components. The response has been predicted using these profiles and compared with the measured response. The wind speed profiles are taken as uniform with the value of mean wind speed. The mean and midspan values of the turbulence standard deviations from all recordings are shown in Table 4.2.

In Figure 7.6, the average ratio between predicted and measured response at the accelerometer locations are shown for the high wind speed recordings. The difference in the response predictions using mean or midspan turbulence std is small for the vertical and torsional response. For the lateral response, the mean value of turbulence std estimates the response in average 4-6 pp more accurately than the midspan turbulence std, but still only in the range of 64 to 70% of the measured response. Like for mean value of turbulence std as seen in step 1, also the midspan value gives the most accurate prediction of vertical response near the quarter points and the torsional response in the five points closest to the midspan.

Plots of the average ratio between the predicted and measured response for the low wind speed recordings are shown in Figure 7.7. It can be seen that the response is higher when using mean than when using midspan turbulence std, for all response components. For the lateral and vertical response, the mean turbulence std predicts the response most accurate; 55 to 70% of measured response in the lateral direction and 80 to 100% of measured response in the vertical direction. For torsion, both the mean and midspan values of turbulence std overestimates the response, and the midspan value is more accurate in this case.

Comparing the two groups of recordings with respect to the accuracy of response prediction, it is seen that the lateral response is slightly better predicted for high wind speeds than for low wind speeds. Also the torsional response is better predicted for the high wind speed recordings, especially at the five accelerometer locations closest to the midspan. The vertical response predictions depend more on the choice of mean and midpoint values. For high wind speeds, the vertical response is almost the same for mean and midspan turbulence std, while for low wind speeds there's 20 pp difference between the two. This is due to the larger difference between the mean and midspan values of vertical turbulence std for the low wind speed recordings than the high wind speed recordings, as seen in Table 4.2.

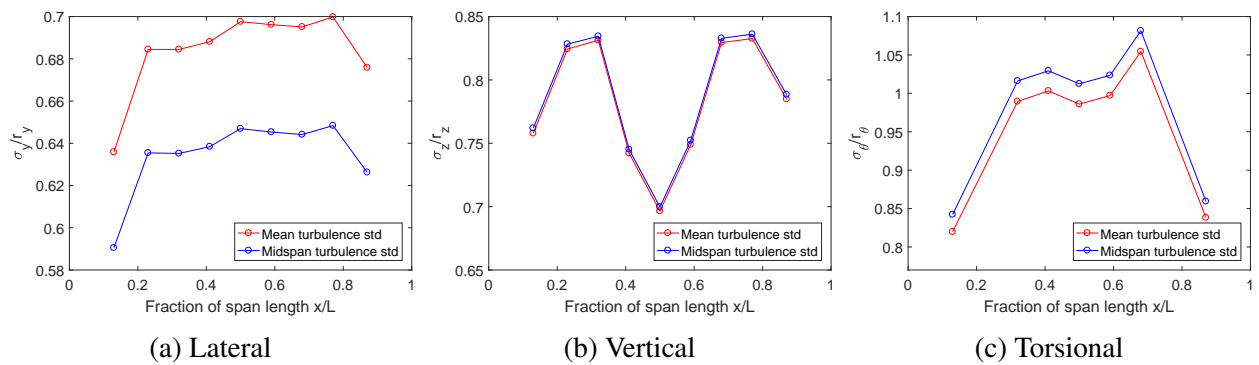


Figure 7.6: Ratio between predicted and measured response in the location of the accelerometers for the recordings with high wind speeds.

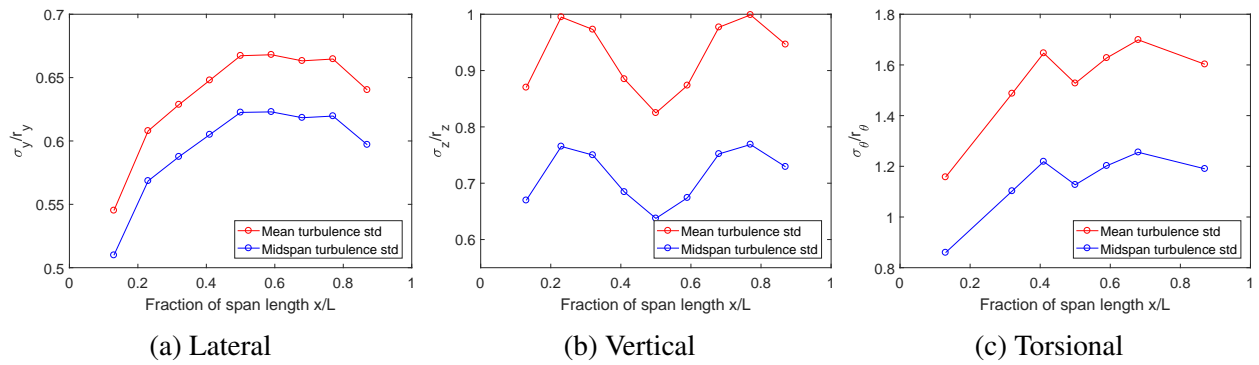


Figure 7.7: Ratio between predicted and measured response in the location of the accelerometers for the recordings with low wind speeds.

In Figure 7.8, 7.9 and 7.10, the predicted span-wise response is shown for one high and one low wind speed recording together with the measured response. The two recordings chosen to show the response along the span are the ones with the largest difference between mean and midspan value of horizontal turbulence standard deviation. These are chosen to show the differences in the response prediction in the worst case. The response plots to the left are for a high wind speed recording, and the ones to the right are for a low wind speed recording. The values of turbulence std for these two recordings can be seen in Table 4.2.

For the high wind speed recording, the difference between mean and midspan is largest for the lateral response, and for the vertical and torsional response, there's almost no difference. The opposite is seen for the low wind speed recording; almost no difference between mean and midspan for the lateral response, but larger differences in vertical and torsional response predictions.

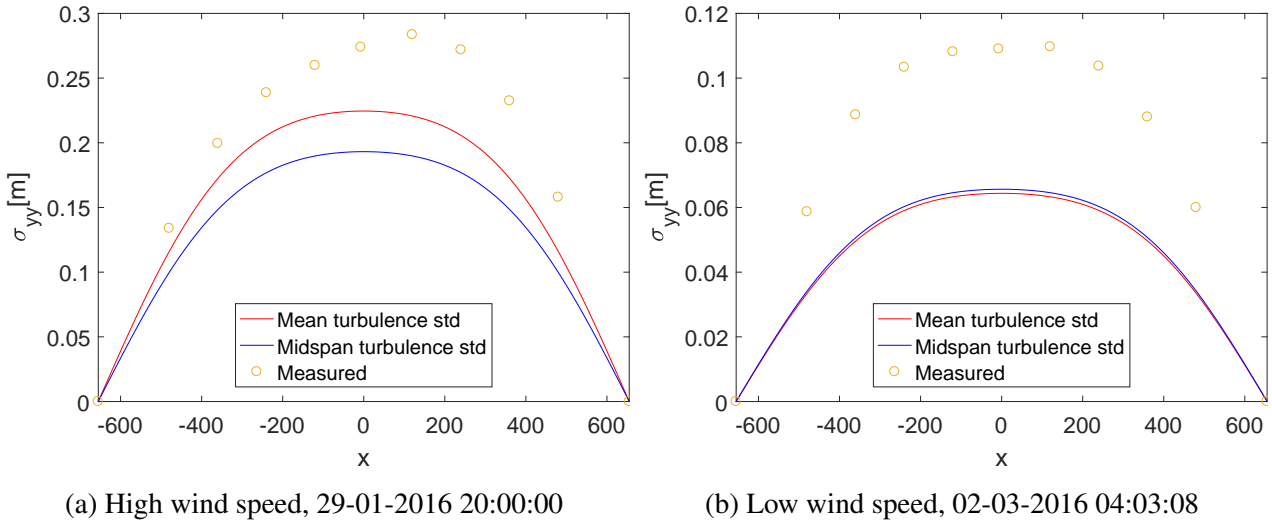


Figure 7.8: Standard deviation of lateral displacement along the bridge.

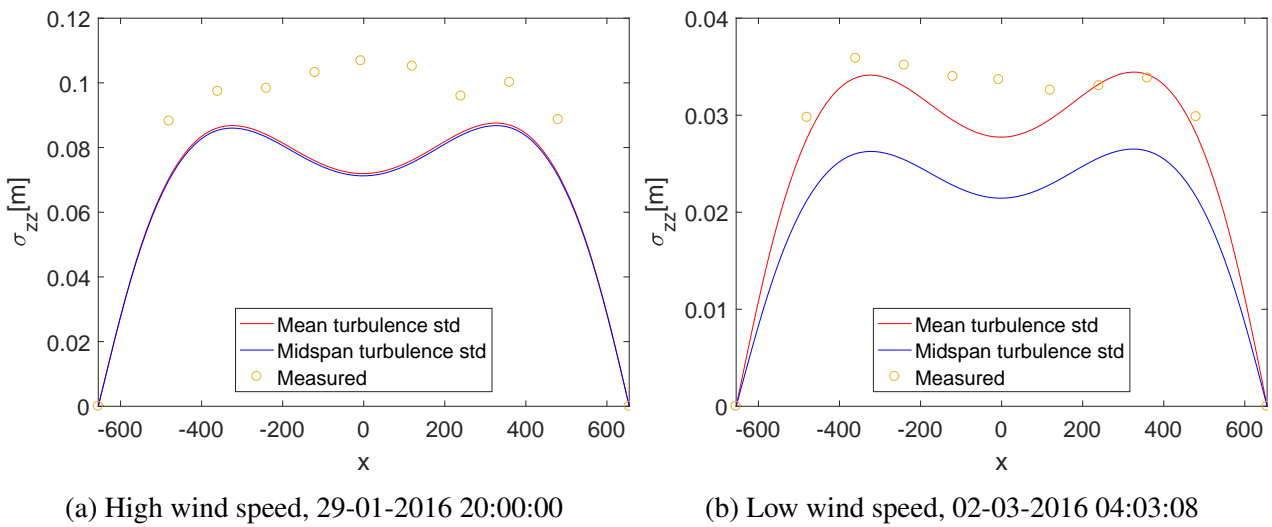


Figure 7.9: Standard deviation of vertical displacement along the bridge.

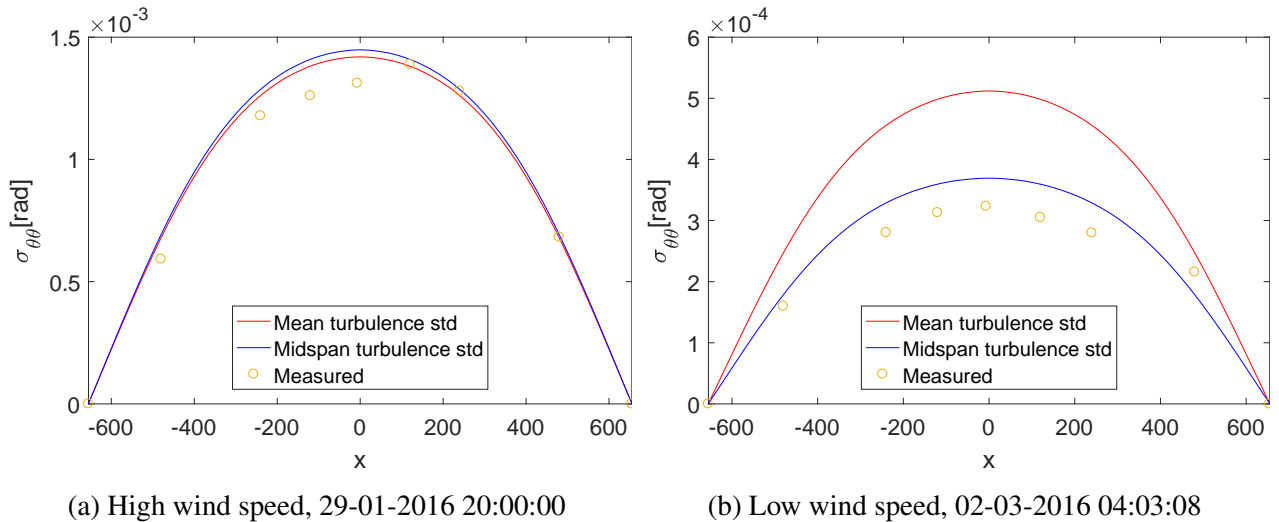


Figure 7.10: Standard deviation of rotation along the bridge.

Conclusion

In Table 7.1 and 7.2 a summary of the findings in this section is presented for high and low wind speed recordings, respectively. The average of the maximum response along the span is shown for the different combinations of wind speed and turbulence standard deviation. The difference between the measured and the calculated response is included in percent. The tables indicate which values that have been used for the uniform profiles. Using these tables and the figures with average ratio between predicted and measured response, it should be possible to suggest if the mean or midspan value should be taken for the uniform profiles to predict the response most accurately.

It is seen in step 1 that there is almost no difference in response prediction between using the mean value and the midspan value of wind speed in a uniform wind speed profile. This is due to small difference in these two wind speed values. Regarding the turbulence standard deviations, a common feature of the high wind speed and the low wind speed recordings is that the mean value predicts the lateral response about 5 pp better than the midspan value. Still, the predicted responses are only 55-70% of the measured response. For the high wind speed recordings there's almost no difference in the predictions of vertical and torsional response. But for the low wind speed recordings, vertical response is predicted about 20-25 pp better with mean turbulence std and torsional response is predicted about 40 pp better with midspan turbulence std.

Overall, it seems that the vertical response can be predicted more accurately in low wind speeds, if the mean value of turbulence std is used. On the other hand, torsional response is predicted more accurately for high wind speeds, where the average error is 3-8% for the five points closest to the midspan and 15-20% in underestimation for the outermost points. For the lateral response, neither the mean nor midspan values are able to do a good response prediction and both give underestimations

of 50-70% of measured response for both high wind speeds and low wind speeds.

Table 7.1: Average of the maximum response for recordings with high wind speeds.

Wind speed		Turbulence std		Lateral		Vertical		Torsional	
Mean	Midspan	Mean	Midspan	σ_{yy} [m]	Diff. %	σ_{zz} [m]	Diff. %	$\sigma_{\theta\theta}$ [10^{-3} rad]	Diff. %
Measured response									
-	-	-	-	0.3439	-	0.1061	-	1.4255	-
Predicted response									
x	-	x	-	0.2343	-31.87	0.0850	-19.89	1.3349	-6.36
-	x	x	-	0.2310	-32.83	0.0841	-20.74	1.3164	-7.65
-	x	-	x	0.2178	-36.67	0.0857	-19.23	1.3744	-3.58

Table 7.2: Average of the maximum response for recordings with low wind speeds.

Wind speed		Turbulence std		Lateral		Vertical		Torsional	
Mean	Midspan	Mean	Midspan	σ_{yy} [m]	Diff. %	σ_{zz} [m]	Diff. %	$\sigma_{\theta\theta}$ [10^{-3} rad]	Diff. %
Measured response									
-	-	-	-	0.1154	-	0.0396	-	0.3793	-
Predicted response									
x	-	x	-	0.0683	-40.81	0.0374	-5.56	0.5614	48.01
-	x	x	-	0.0697	-39.60	0.0381	-3.79	0.5720	50.80
-	x	-	x	0.0637	-44.80	0.0291	-26.52	0.4207	10.91

The results in this chapter, indicates that it is almost no difference in the response when using the mean or the midspan value for the uniform wind speed profile. So, using the mean or the midspan wind speed does not change the accuracy in the methods for the Hardanger Bridge. Regarding the value for the uniform turbulence std profile, the difference between taking the mean or the midspan value is larger. The midspan value predicts the torsional response for the low wind recordings better than the mean turbulence std, while a worse prediction for the vertical response for the same group of recordings.

The conclusion from this section is that the mean and midpoint values are not interesting and has almost the same accuracy of the response predictions compared to the measured response. Therefore it is chosen to take the mean value for the uniform wind and turbulence standard deviation profiles in the following sections.

7.2 Non-uniform profiles

In this section, the uniform profiles for wind speed and turbulence standard deviations that predicted the dynamic response most accurately are compared with non-uniform profiles for wind speed and turbulence std. This will be done step-wise in two separate sections. The mean value was found to give slightly better predictions of response overall than the midpoint value, and therefore the uniform profiles in this section will use the mean value for both wind speed and turbulence standard deviations.

7.2.1 Step 3: Wind speed

First, the wind speed profile will be made non-uniform. The profile has been obtained by using each anemometer along the span of the Hardanger Bridge and interpolating linearly in between. The response from the non-uniform wind speed profiles will be compared with the response from the uniform profile, with regard to accuracy of response prediction. The different wind speed profiles from the recordings are shown in Appendix A.1. The aerodynamic properties responsible for self-excited forces are kept constant along the span and dependent on the mean wind speed.

In Figure 7.11, the average ratio between the predicted and measured response at the accelerometer locations are shown for the high wind speed recordings. The lateral and torsional response is predicted about 1-5 pp better in average for the non-uniform wind profiles compared to the uniform. In the vertical direction, the non-uniform wind profiles are more accurate in the left part of the span and has a smaller decrease in response near the midspan than the uniform profiles, while near the second quarter point the uniform profiles are more accurate. Overall, the non-uniform profiles predict a higher response than the uniform ones.

Plots of the average ratio between the predicted and measured response for the low wind speed recordings are shown in Figure 7.2. The difference between the response using uniform and a non-uniform wind profiles is small for these low wind speeds, but the non-uniform wind profiles predict the response slightly higher in all directions as for the high wind speeds.

If the effects of using non-uniform profiles on each group of wind speeds are compared, the lateral and torsional responses are predicted better for the high wind speed than the low wind speed recordings. However, the lateral response is still only about 60-75% of the measured response. The vertical response is predicted more accurately for the low wind speeds, but the difference in prediction between uniform and a non-uniform wind profiles is same for high and low wind speeds.

The difference between the uniform and the non-uniform wind speed profile is not big. Based on the discussed figures, it can be said that the non-uniform wind speed profiles do not predict the response any better than the uniform profiles. In some points the non-uniform profiles are slightly closer the

measured response, and in other points the uniform profiles are slightly closer.

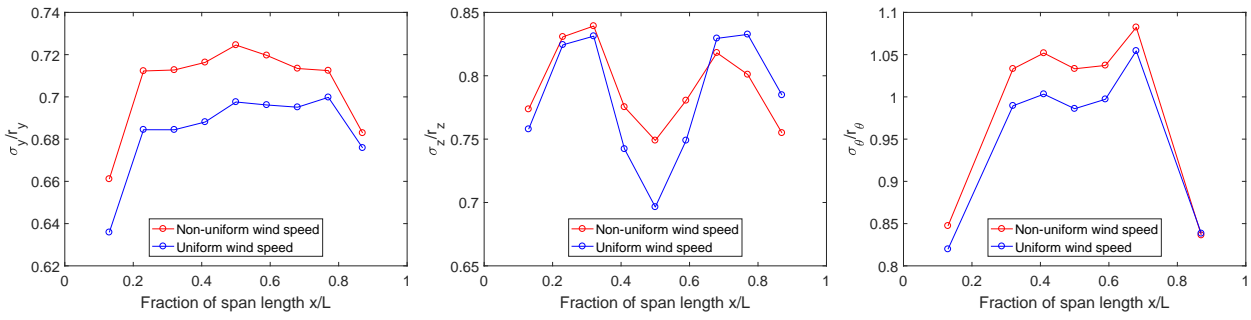


Figure 7.11: Ratio between predicted and measured response in the location of the accelerometers for the recordings with high wind speeds.

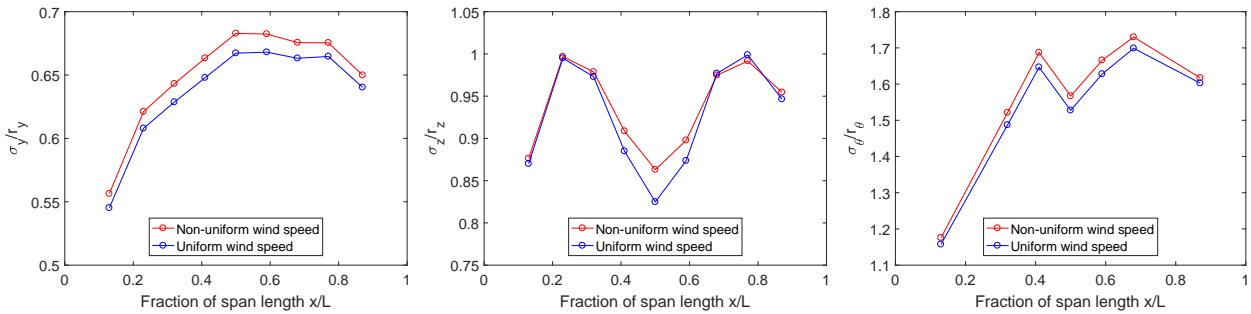


Figure 7.12: Ratio between predicted and measured response in the location of the accelerometers for the recordings with low wind speeds.

Figure 7.14, 7.15 and 7.16 show the response along the span when using a uniform and a non-uniform wind speed profile, for one high wind speed and one low wind speed recording. The non-uniform wind profiles that correspond to the response plots are shown in Figure 7.13. The two wind profiles have around 30% difference between the highest and lowest wind speed. The plots to the left are for the high wind speeds, while the plots to the right are for the low wind speeds.

The non-uniform wind speed profile and the uniform profile predict the response with approximately the same accuracy, and have almost identical shapes. Since the uniform wind profile is symmetric its response is symmetric, but for the non-uniform wind profile the response may shift towards the side with highest wind speeds. This can be seen in the vertical response for the high wind speeds, where the response is almost the same in the first quarter point, but lower in the second quarter point.

In the numerical study in Section 6.1, the responses to a uniform and several non-uniform wind profiles were studied. It was seen that all response components increased for the non-uniform wind profiles compared to a uniform profile when the turbulence standard deviations were kept uniform. This is in agreement with the response shown in the figures below where the maximum predicted response increases slightly for the non-uniform wind profile.

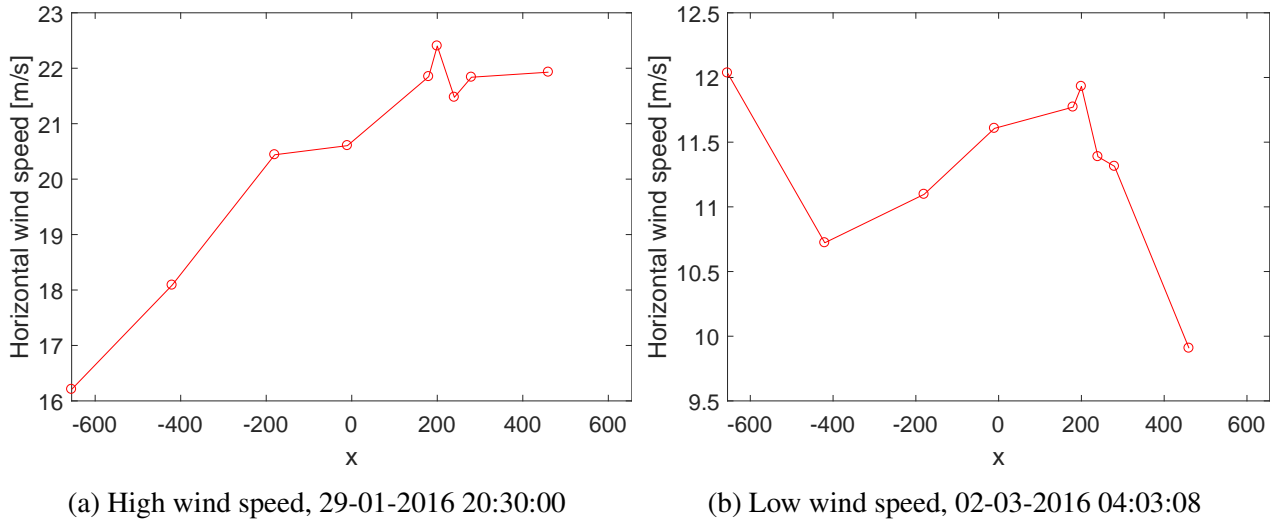


Figure 7.13: Non-uniform wind profile.

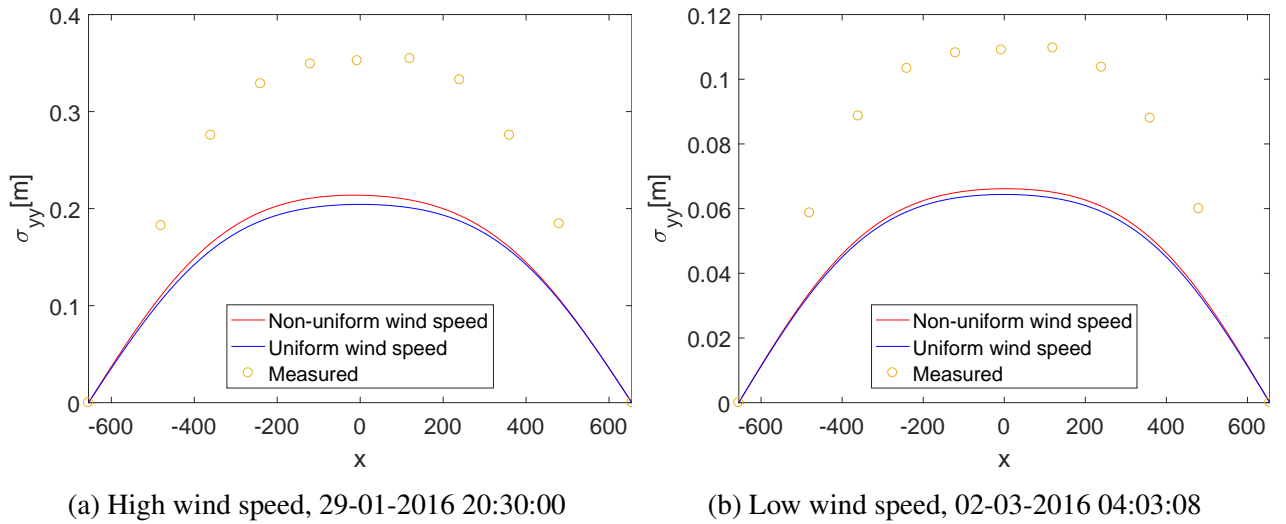


Figure 7.14: Standard deviation of lateral displacement along the bridge using uniform and non-uniform wind profile.

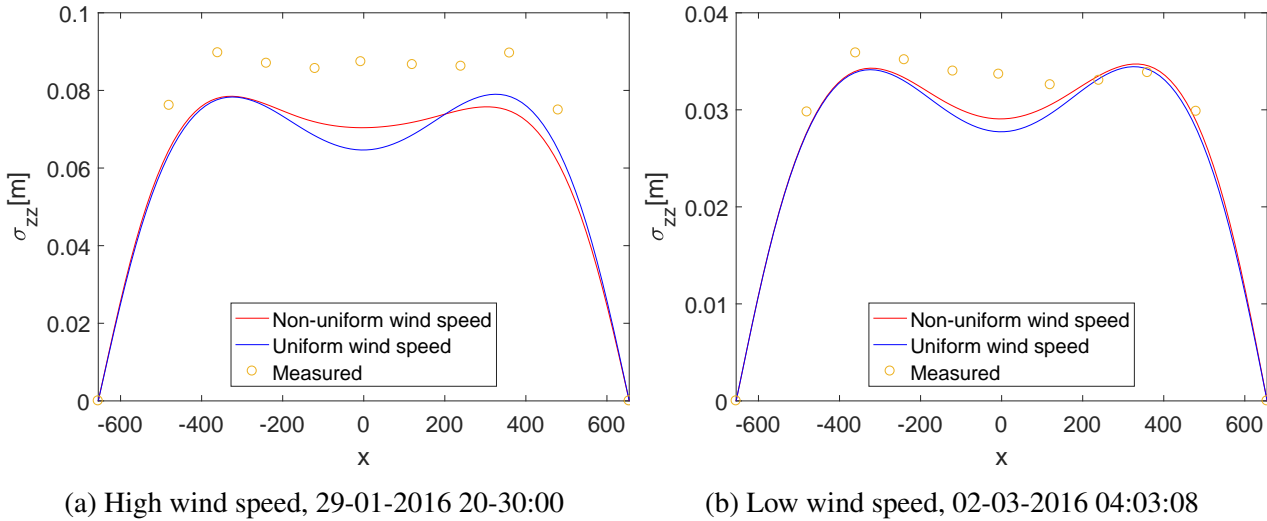


Figure 7.15: Standard deviation of vertical displacement along the bridge using uniform and non-uniform wind profile.

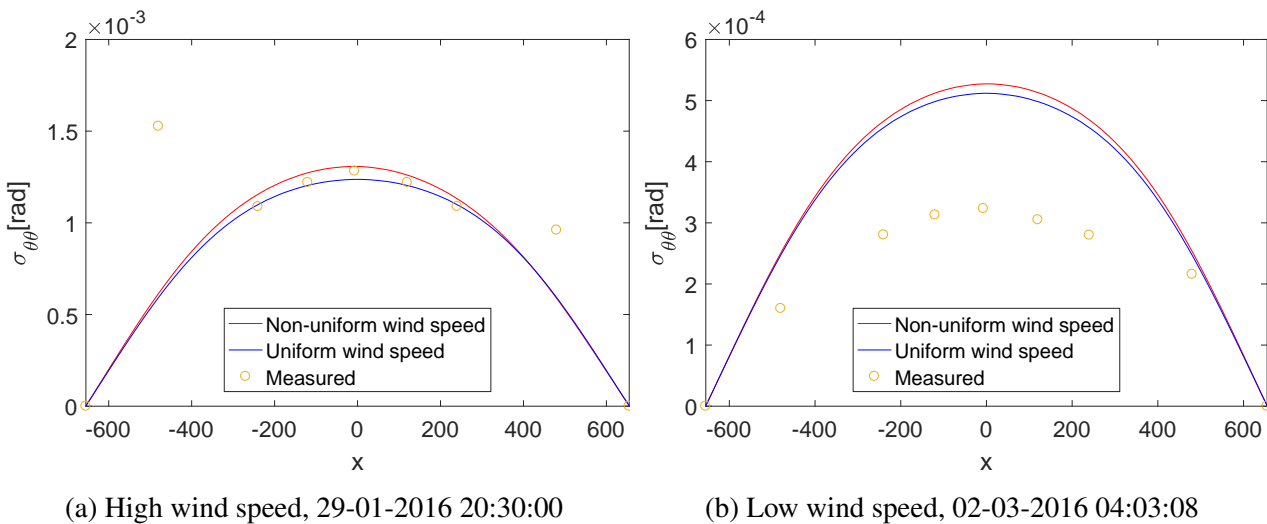


Figure 7.16: Standard deviation of torsional response along the bridge using uniform and non-uniform wind profile.

7.2.2 Step 4: Standard deviation of turbulence components

The turbulence standard deviations will now be made span-wise non-uniform, by including the measured values of turbulence standard deviations at the locations of each anemometer and interpolating linearly in between. The response is calculated with both the wind speed and turbulence std as non-uniform, and compared with the response from the uniform profiles where the mean value is used for both wind speed and turbulence std. The predictions will be compared with the measured response to study if non-uniform profiles can predict the response more accurately. The aerodynamic proper-

ties that the self-excited forces are calculated from are kept span-wise uniform and dependent on the mean wind speed. In Appendix A.2 the horizontal and vertical turbulence standard deviations from all recordings are plotted at the locations of the anemometers.

In Figure 7.6, the average ratio between predicted and measured response at the accelerometer locations are shown for the high wind speed recordings. All response components are predicted higher when using the uniform profiles; 6-7 pp higher lateral response and about 10-15 pp higher vertical and torsional response. The uniform profiles also give more accurate predictions.

The plots of average ratio between predicted and measured response for the low wind speed recordings are shown in Figure 7.7. Again it is seen that for all response components the uniform profiles give higher predictions than the non-uniform profiles. For the low speed recordings, the difference between the two curves becomes larger to the right. The torsional response is overestimated for low wind speeds, which is the only case where the non-uniform profiles predict the response more accurately than the uniform profiles.

All in all it is seen that the response predictions get worse when the non-uniformity of turbulence standard deviations is taken into account in the response calculations, both compared to the fully uniform profiles and to step 3 when only the wind speed was taken as non-uniform. This is the case for both the high wind speed and the low wind speed recordings.

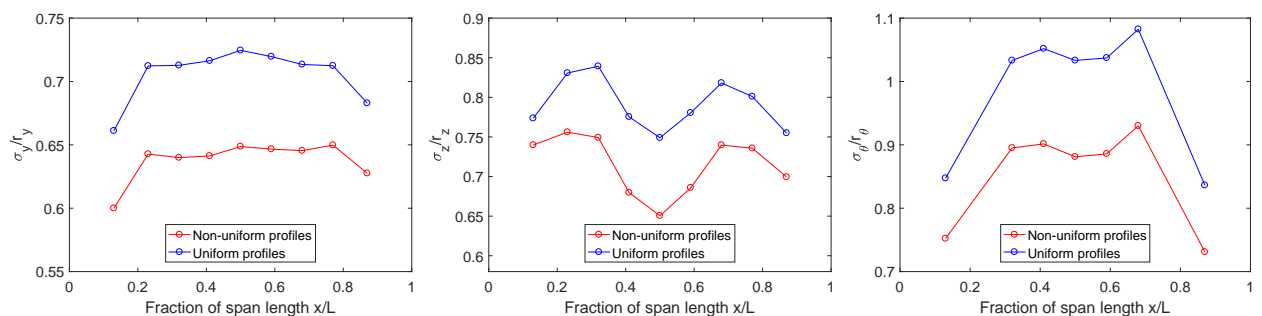


Figure 7.17: Ratio between predicted and measured response in the location of the accelerometers for the recordings with high wind speeds.

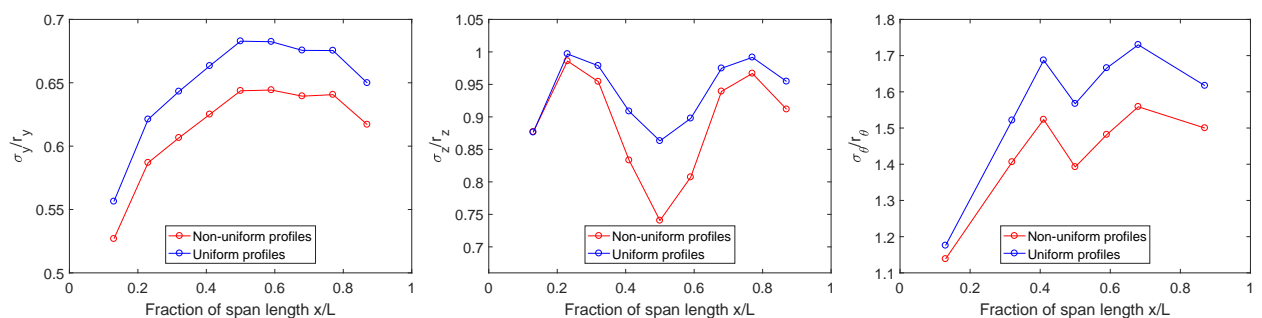


Figure 7.18: Ratio between predicted and measured response in the location of the accelerometers for the recordings with low wind speeds.

In Figure 7.20, 7.21 and 7.22 the response along the span are shown when the turbulence standard deviation profiles shown in Figure 7.19 and the wind profiles shown in Figure 7.13 are used in the response predictions. The plots to the left show the response for the high wind speeds and the plots to the right show the response for the low wind speeds. The measured and predicted responses along the bridge using non-uniform wind speed and turbulence std profiles can be seen for all recordings in Appendix B.2.

The uniform profiles give slightly higher response in all off the figures 7.20, 7.21 and 7.22, except for vertical response in a part of the span for the low wind speed recording. In the lateral direction, the response predictions are only about half of the measured response. The vertical response shapes are somewhat skewed towards the left side where the turbulence std are higher. This is effect is slightly higher for the low wind speed recording, which has larger difference in vertical turbulence std between the left and right side than the high wind speed recording. A small skew in the torsional response can be seen also for the torsional response for the low wind speed recording.

The influence of non-uniform turbulence std profiles was investigated for different wind profiles in the numerical study in Section 6.2. When the non-uniform turbulence profile was used to predict the response and had the opposite shape as the wind speed profile, the response decreased compared to the response with a uniform turbulence profile. The measured data often show a similar correlation between the wind speed and turbulence std, which can be seen to some extent in Figure 7.13 and 7.19 for the recordings used in step 3 and 4. This is especially true for the high wind speed recording, where the wind speed is at its highest where the turbulence standard deviations are at their lowest, and the other way around. The results in step 4 show a decrease in predicted response when both wind speed and turbulence std are non-uniform compared to when only the wind speed is non-uniform, which is in agreement with the findings in Section 6.2.

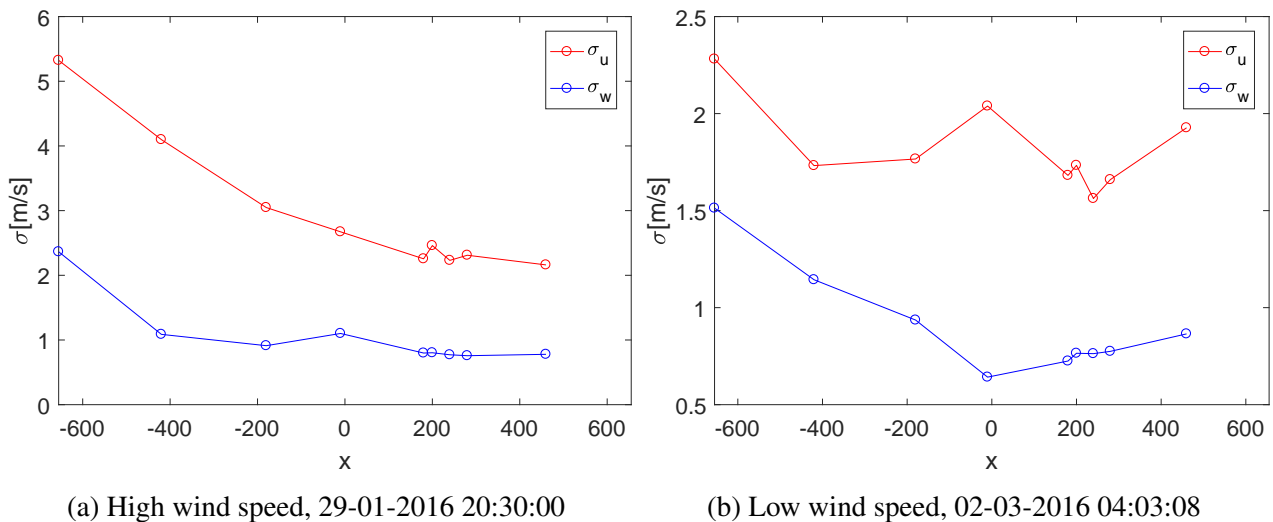


Figure 7.19: Turbulence standard deviation profiles.

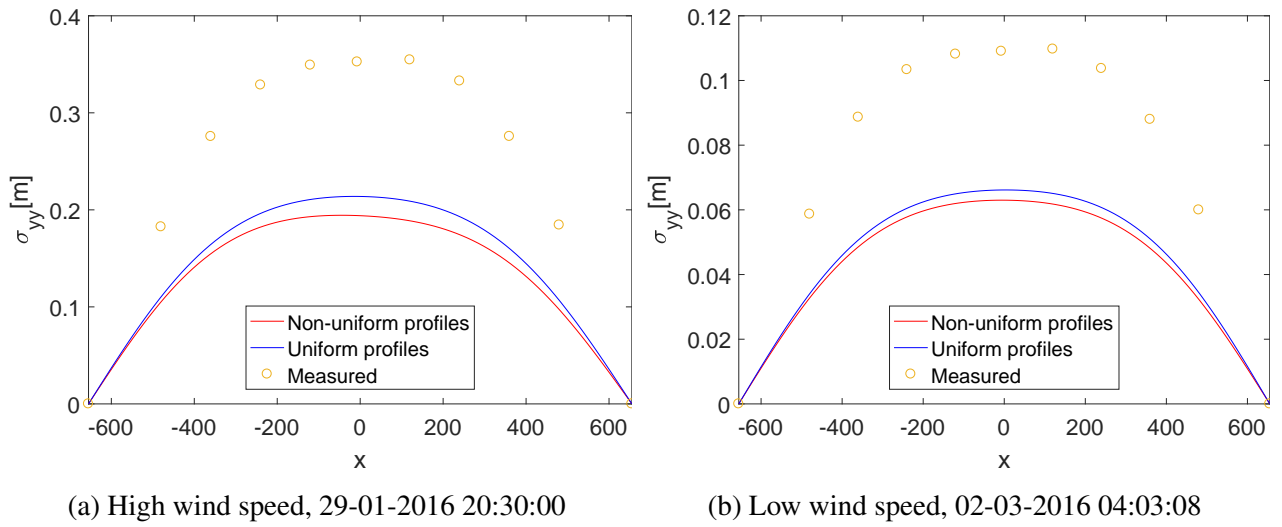


Figure 7.20: Standard deviation of lateral displacement along the bridge using uniform and non-uniform profiles for turbulence standard deviations.

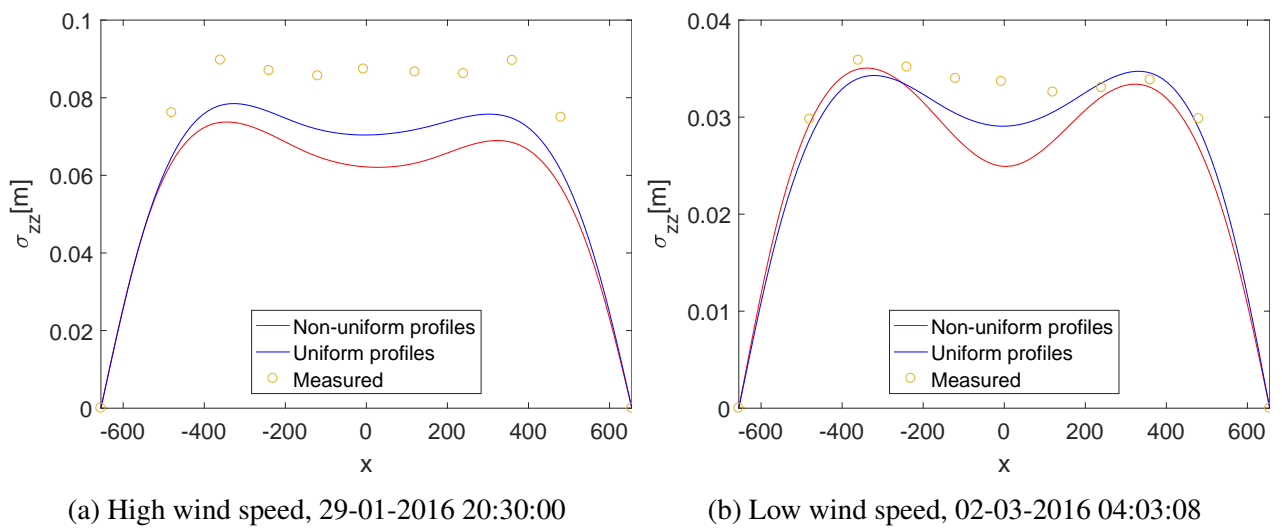


Figure 7.21: Standard deviation of vertical displacement along the bridge using uniform and non-uniform profiles for turbulence standard deviations.

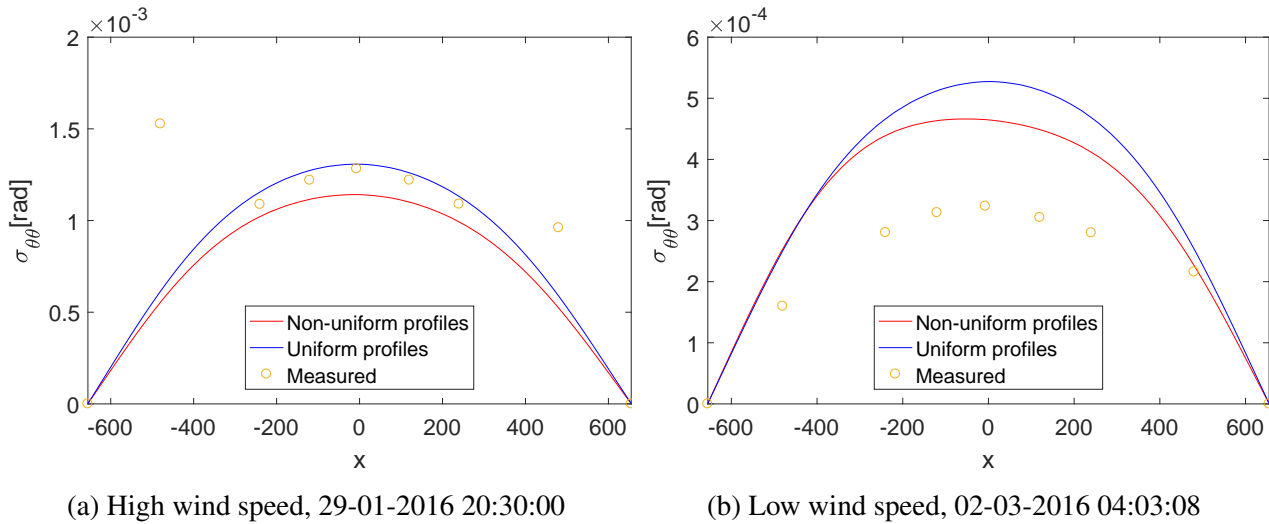


Figure 7.22: Standard deviation of torsional response along the bridge using uniform and non-uniform profiles for turbulence standard deviations.

7.2.3 Step 5: Self-excited forces

The influence of non-uniform self-excited forces on the predicted response when using measured wind data is studied in this section. Both wind speed and turbulence standard deviations are non-uniform in this part, and the non-uniform self-excited forces are caused by the non-uniform wind profile. The response is predicted with uniform self-excited forces where the aerodynamic properties are dependent on the mean wind speed, and with non-uniform self-excited forces where the aerodynamic properties vary with the wind speed along the span. The predicted responses are compared in plots with the measured response to study if the response prediction gets better by including the non-uniform self-excited forces.

In Figure 7.23, 7.24 and 7.25, the predicted and measured response along the span is shown. The predicted response is calculated with non-uniform and uniform self-excited forces for the wind speed profiles shown in Figure 7.13 and turbulence std profiles shown in Figure 7.19. It is seen that including non-uniform self-excited forces results in almost no difference in the response prediction. None of the 16 recordings used in this thesis result in a difference of more than 1% in any point along the span between using uniform and non-uniform self-excited forces.

Among the wind profiles from Chapter 6, the linear profile is the one that is most similar in span-wise shape to the profiles obtained from the high wind speed recordings. Profiles from the low wind speed recordings show similarities to both the linear and the arctan profile (see Appendix A.1). The effect of including span-wise non-uniform self-excited forces for these profiles was shown for different mean wind speeds in Table 6.2 and 6.5. For the mean wind speeds closest to the recordings with high and low wind speeds (20 m/s and 10 m/s, respectively), the effect of including span-wise non-uniform

self-excited forces was shown to be small, consistent with the result from this chapter.

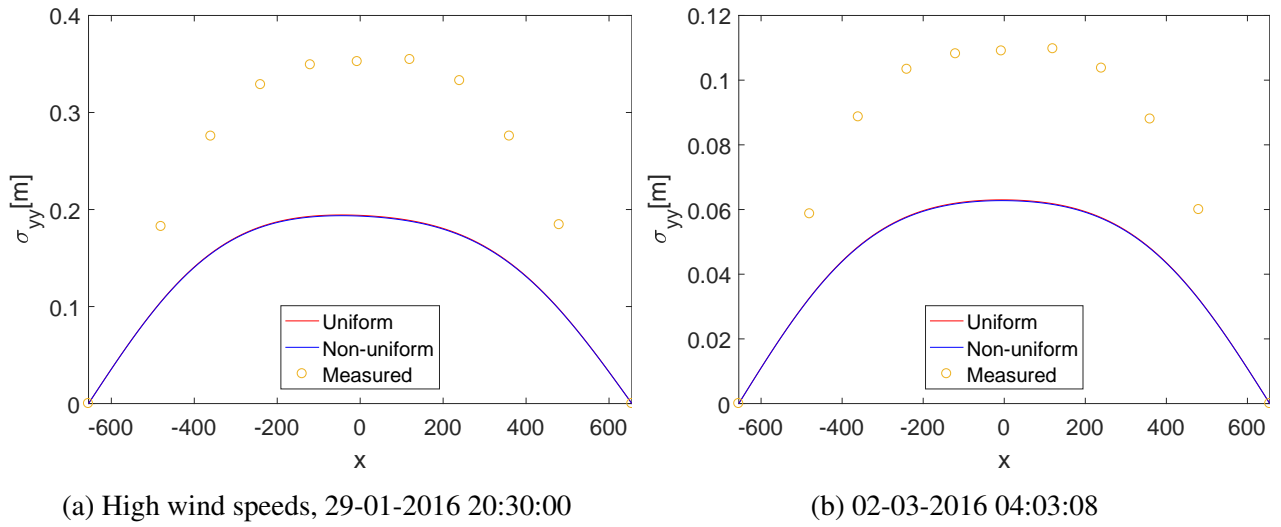


Figure 7.23: Standard deviation of horizontal displacement along the bridge using non-uniform and uniform self-excited forces.

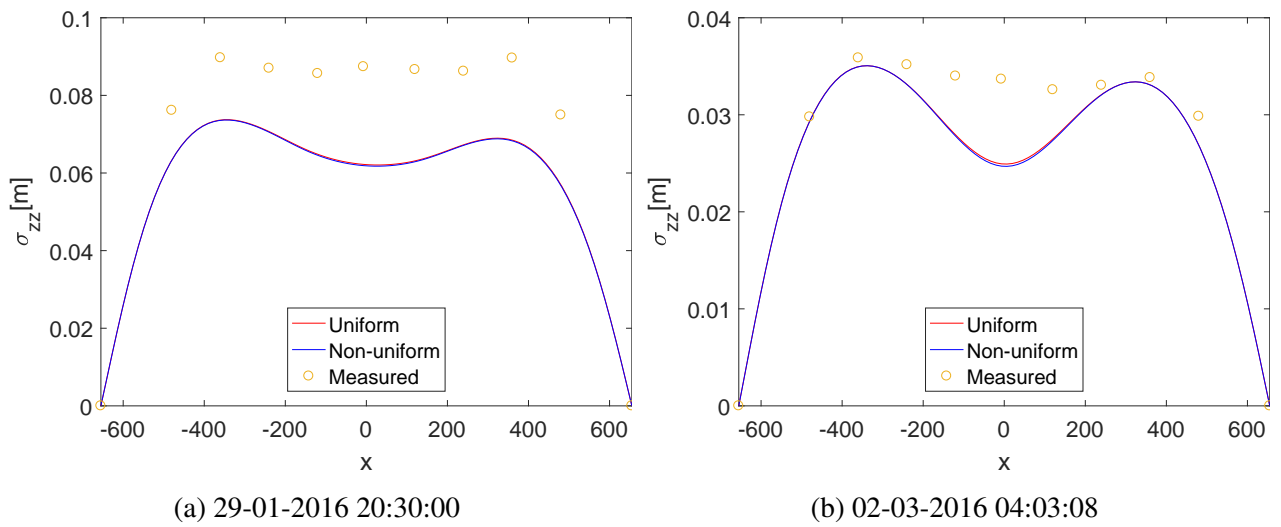


Figure 7.24: Standard deviation of vertical displacement along the bridge using non-uniform and uniform self-excited forces.

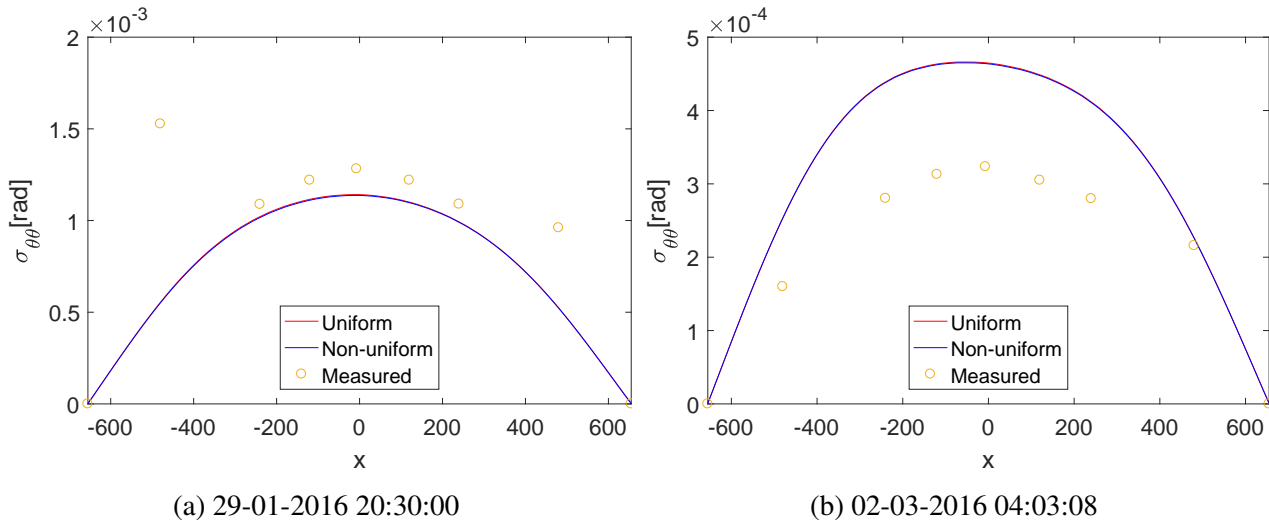


Figure 7.25: Standard deviation of torsional displacement along the bridge using non-uniform and uniform self-excited forces.

Conclusion

In this section the influence of including non-uniform wind speed and turbulence standard deviation profiles obtained from measured wind data has been studied. The predicted responses have been compared with measured bridge response to investigate if a non-uniform profile for the wind or turbulence std can improve the response predictions. The non-uniform self-excited forces have also been studied.

In Table 7.3, the average maximum predicted responses for the high wind speed recordings are shown and compared with the average maximum measured response. The table indicates a small difference between the non-uniform wind speed profiles and the uniform ones. By introducing the non-uniform wind speed profiles for the high wind speed recordings, the predictions of average maximum lateral and torsional response are improved by approximately 2 pp and 5 pp, respectively, while the vertical maximum response prediction is almost unaffected. In the next step, when also the turbulence std profiles are non-uniform, the predictions of average maximum response get 7 pp worse for lateral and vertical, and 15 pp worse for torsional response.

The average maximum response using the low wind speed recordings are shown and compared with the measured response in Table 7.4. The maximum response predictions are almost unaffected by introducing non-uniform wind speed profiles. Including non-uniform turbulence profiles results in only a small change of maximum lateral and vertical response, while the torsional response prediction is improved by about 30%.

Table 7.3: Mean of the maximum response for recordings with high wind speeds.

Wind speed		Turbulence std		Lateral		Vertical		Torsional	
Uniform	Non-uniform	Uniform	Non-uniform	σ_{yy} [m]	Diff. %	σ_{zz} [m]	Diff. %	$\sigma_{\theta\theta}$ [10^{-3} rad]	Diff. %
Measured response									
-	-	-	-	0.3439	-	0.1062	-	1.4255	-
Predicted response									
x	-	x	-	0.2343	-31.87	0.0850	-19.96	1.3349	-6.36
-	x	x	-	0.2436	-29.17	0.0847	-20.24	1.3993	-1.84
-	x	-	x	0.2183	-36.52	0.0769	-27.59	1.1945	-16.20

Table 7.4: Mean of the maximum response for recordings with low wind speeds.

Wind speed		Turbulence std		Lateral		Vertical		Torsional	
Uniform	Non-uniform	Uniform	Non-uniform	σ_{yy} [m]	Diff. %	σ_{zz} [m]	Diff. %	$\sigma_{\theta\theta}$ [10^{-3} rad]	Diff. %
Measured response									
-	-	-	-	0.1154	-	0.0396	-	0.3793	-
Predicted response									
x	-	x	-	0.0683	-40.81	0.0374	-5.56	0.5614	48.01
-	x	x	-	0.0698	-39.51	0.0375	-5.30	0.5749	51.57
-	x	-	x	0.0660	-42.81	0.0369	-6.82	0.5155	35.91

Including the non-uniform wind speed profile has been found to improve the predictions slightly in some cases, but the accuracy is still not good in general. Including non-uniform profiles of turbulence standard deviations has been shown to have larger effect, but results in lower and less accurate predictions compared to using uniform turbulence std profiles where the span-wise mean values are used. Overall the predictions are not accurate and including the non-uniformity of the wind field does not improve the accuracy.

The changes in response prediction when including the non-uniform self-excited forces are negligible, and result in less than 1% difference in every point along the span in all recordings compared to uniform self-excited forces. This was as expected since the results from the numerical study showed small differences between the response with non-uniform and uniform self-excited forces for low wind speeds, and the wind profiles used in that part were more non-uniform than the wind profiles obtained from the measured wind data.

In this section, the response predictions was mainly presented in the two groups of wind speeds. Through the work, it has been noticed that the response prediction is accurate for some recordings

and bad for others. In some recordings it was seen that the wind and turbulence std was almost the same, but the measured response was higher for one of the recordings than the other, which resulted in one accurate prediction and one bad. This may be due to that the wind field is not stationary and varies with time over the 30-minute recording.

Response prediction of suspension bridges involves uncertainties, like for instance modelling of structural damping, admittance functions and cable forces. In addition, non-stationarity of the wind field might have effects on the response that are not included in the response calculation methods used in this thesis. The uncertainties and deficiencies in the methods used seem to have larger impact on the response prediction than whether or not the non-uniform profiles for wind speed and turbulence standard deviations are used in the calculations. And because the effect of including the non-uniform profiles, in addition to being small, led to worse predictions of bridge response in some cases, it is concluded that uniform profiles can predict the bridge response just as good as or better than non-uniform profiles, for the recordings used from the Hardanger Bridge site in this thesis.

Summary and Recommendations for Further Work

A summary of the main findings will be given in this chapter. Conclusions will be made based on the results in Chapter 7 together with the numerical study in Chapter 6. At last, some recommendations for further work will be suggested.

8.1 Summary and Conclusions

The objective of this thesis was to study if non-uniform profiles should be included in the response calculations to predict the response more accurately. Several different span-wise profiles of wind speed and turbulence standard deviations, both uniform and non-uniform, have been used to predict the bridge response. Measured wind data from the Hardanger Bridge have been used to define the wind load acting on the bridge, and the predictions have been compared to measured response. A total number of sixteen recordings with both wind and acceleration data have been evaluated.

Numerical study

It was shown in a numerical study that the non-uniform profiles of wind speed and turbulence standard deviations had influence on the predicted response along the span. The main findings were that the response increased when a non-uniform wind speed profile was introduced in the calculations compared to a uniform profile with the same span-wise mean. By introducing a non-uniform turbulence standard deviation profile with the opposite shape of the non-uniform wind speed profile, the

maximum response along the span decreased. Also the influence of including non-uniformity of self-excited forces was studied, which was shown to be small for low span-wise mean wind speeds, but increased when the response got unstable for very high mean wind speeds.

Comparison with measured data

The response was also predicted using measured wind data from the Hardanger Bridge, and the calculated response was compared with the measured response of the bridge deck. Different values of the uniform wind speed profiles were studied, and it was concluded that using the span-wise mean and midspan values of wind speed resulted in the same accuracy of response prediction. The difference between using the same two values for the uniform turbulence standard deviation profiles gave more difference in the response predictions. The span-wise mean of the measured turbulence standard deviations predicted the response more accurately than the midspan value. When using the uniform profiles that were most accurate overall, the lateral response predictions were still underestimated by 30-50% in average, while the vertical response for low wind speeds and torsional response for high wind speeds were predicted better with average errors of 0-20%. The torsional response for low wind speeds was consistently overestimated by 50-70% at most points along the bridge.

Including the non-uniform wind speed profile in the response prediction increased all response components slightly compared to the uniform profile, but the average error was still over 25% in the lateral direction at all points considered along the bridge. The response decreased with 0-20% when non-uniform turbulence standard deviation profiles were introduced compared to uniform turbulence std profiles. This led to a worse response prediction for both high wind speed and low wind speed recordings, except from the torsional response for low wind speeds.

Regarding the non-uniform self-excited forces the influence was negligible, and the maximum difference in response between using non-uniform and uniform self-excited forces was below 1% among all points along the span and all recordings considered in this thesis.

The uncertainties in the prediction methods are too high for non-uniform wind profiles to make any difference on the accuracy of predicted response for the Hardanger Bridge. The non-uniformity of the wind field seems to have less impact on the predictions than other sources of error. Based on the findings in this thesis, the non-uniform profiles of wind speed and turbulence standard deviations should not be included in the dynamic response predictions, as the uniform profiles predict the response just as good or better.

Possible reasons for the low accuracy of the predicted response may be cable forces, admittance functions and uncertainties in the modelling of structural damping. In addition, non-stationarity of the wind field may have impacts on the dynamic response that are not included in the prediction methods used in this thesis, where the wind field is assumed stationary. The effect of skew winds is

another factor that has not been taken into account.

Furthermore, the prediction methods accounting for non-uniformity of the wind field have some simplifications that might have potential for improvement. The coherence model in the cross-spectral densities of the turbulence components (Eq. (2.39)) is dependent on two locations along the bridge, and the wind speed has been taken as the average between those two points. The same has been done for the buffeting load coefficient matrix in Eq. (2.36). In addition, the cross terms in the cross-spectral density matrix have been taken as zero.

A simplification regarding the measured wind data can also be mentioned. To obtain the non-uniform wind profiles from the recordings, linear interpolation has been used between nine wind sensors, which only gives an approximate simulation of the real wind speed profile.

8.2 Recommendations for Further Work

The results in this thesis show that there is large difference between predicted and measured response for the Hardanger Bridge, even when including non-uniformity of the wind field in the response calculations. The study of the prediction models should be continued.

To improve the response predictions, several potential enhancements can be suggested. For instance, FEM programs like Abaqus could be used to predict the bridge response. Some of the uncertainties, such as the cable forces, can be reduced using this approach. In addition, non-stationarity of the wind field can be included when working in the time domain in stead of the frequency domain.

The Kaimal wind spectra are used in this thesis, and other models of wind spectra could be implemented and modified to account for the non-uniform wind field. One could also estimate the wind spectra from measured wind data in stead of using predefined spectra, to better cover the wind characteristics at the site.

Another aspect that has not been studied in this thesis, is how the skew winds influence the response of the bridge. In this thesis all wind data have been set perpendicular to the bridge.

Through the work in this thesis, it has been noticed that the response predictions are good for some recordings and bad for others. In further work, the recordings where the predictions are good can be studied to find common characteristics for these and differences from the recordings where the predictions are worse. In such a study, a larger amount of recordings than used in this thesis should be considered.

References

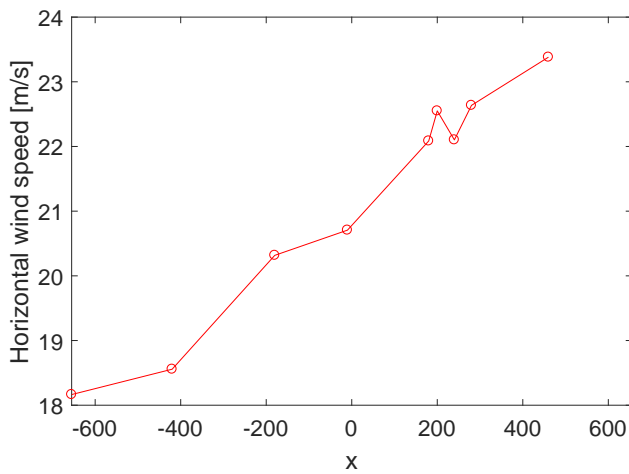
- [1] N.J. Gimsing and C.T. Georgakis. *Cable Supported Bridges: Concept and Design*. Wiley, 3rd edition, 2012.
- [2] A.G. Davenport. *A Statistical Approach to the Treatment of Wind Loading on Tall Masts and Suspension Bridges*. PhD thesis, Department of Civil Engineering, University of Bristol, United Kingdom, 1961.
- [3] A.G. Davenport. Gust loading factors. *Proceedings of the American Society of Civil Engineers. Journal of Structural Division*, 93, 1967.
- [4] R.H. Scanlan and J.J. Tomko. Airfoil and bridge deck flutter derivatives. *Journal of Engineering Mechanics Division*, 97(6):1717–1737, 1971.
- [5] Anurag Jain, Nicholas P. Jones, and Robert H. Scanlan. Coupled flutter and buffeting analysis of long-span bridges. *Structural Engineering*, 122:716–725, 1996b.
- [6] H. Katsuchi, N. P. Jones, and R. H. Scanlan. Multimode coupled flutter and buffeting analysis of the akashi-kaikyo bridge. *Journal of Structural Engineering*, 125(1):60–70, 1999.
- [7] Xinjun Zhang. Influence of some factors on the aerodynamic behavior of long-span suspension bridges. *Wind Engineering and Industrial Aerodynamics*, 95:149–164, 2007.
- [8] Liang Hu, You-Lin Xu, Qing Zhu, Anna Guo, and Ahsan Kareem. Tropical storm-induced buffeting response of long-span bridges: Enhanced nonstationary buffeting force model. *Structural Engineering*, 143, 2017.
- [9] Etienne Cheynet. *Wind-induced vibrations of a suspension bridge*. UiS, 2016.
- [10] A. Arena, W. Lacarbonara, D.T. Valentine, and P. Marzocca. Aeroelastic behavior of long-span suspension bridges under arbitrary wind profiles. *Fluids and Structures*, 50:105–119, 2014.
- [11] Einar Strømmen. *Theory of Bridge Aerodynamics*. Springer, 2006.

- [12] D.E. Newland. *An Introduction to Random Vibrations, Spectral and Wavelet Analysis*. Dover Publications, Inc, 3rd edition, 2005.
- [13] C. Ranieri and G. Fabbrocino. *Operational Modal Analysis of Civil Engineering Structures*. Springer, 2014.
- [14] M.H. Hayes. *Statistical Digital Signal Processing and Modeling*. John Wiley and Sons Inc, 1st edition, 1996.
- [15] Ole Øiseth, Anders Rönnequist, and Ragnar Sigbjörnsson. Simplified prediction of wind-induced response and stability of slender long-span suspension bridges, based on modified quasi-steady theory: A case study. *Wind Engineering and Industrial Aerodynamics*, 98:730–741, 2010.
- [16] Norwegian Public Road Administration. Illustrations. <http://www.vegvesen.no/vegprosjekter/Hardangerbrua/Illustrasjoner>. [cited: 23.03.2017].
- [17] Norwegian Public Road Administration. Teknisk brosjyre. http://www.vegvesen.no/_attachment/113344/binary/206607?fast_title=Teknisk+brosjyre+Hardagerbrua%2C+bokm%C3%A5l+%28pdf%29. [cited: 20.04.2017].
- [18] Ole Øiseth, Anders Rönnequist, Knut Andreas Kvåle, and Ragnar Sigbjörnsson. Monitoring wind velocities and dynamic response of the hardanger bridge. *Dynamics of Civil Structures*, 2:117–125, 2015.
- [19] Aksel Fenerci, Ole Øiseth, and Anders Rönnequist. Long-term monitoring of wind characteristics and dynamic response of a long-span suspension bridge in complex terrain.
- [20] S.O Hansen, M. Lollesgaard, S. Rex, J.B. Jakobsen, and E.H. Hansen. *The Hardanger Bridge: Static and Dynamic Wind Tunnel Tests with a Section Model*. Svend Ole Hansen ApS, Copenhagen, 2006.
- [21] Norwegian Public Road Administration. *The Hardanger Bridge, Design Basis - Wind Characteristics*. NPRA, 2006.

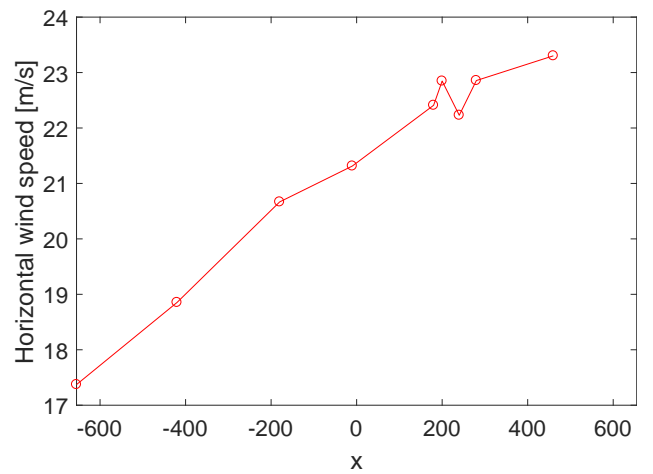
Wind data

The wind and turbulence standard deviation profiles used in this report are shown in this chapter.

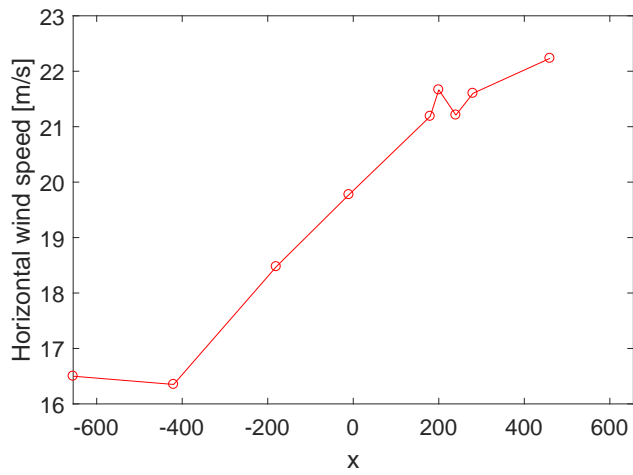
A.1 Horizontal wind profiles



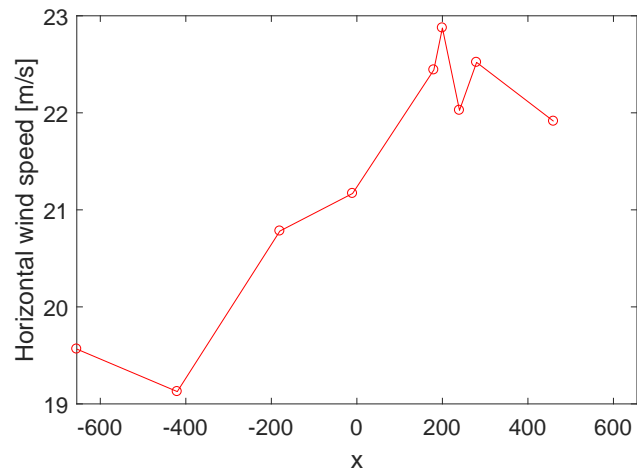
(a) 29-01-2016 13:00:00



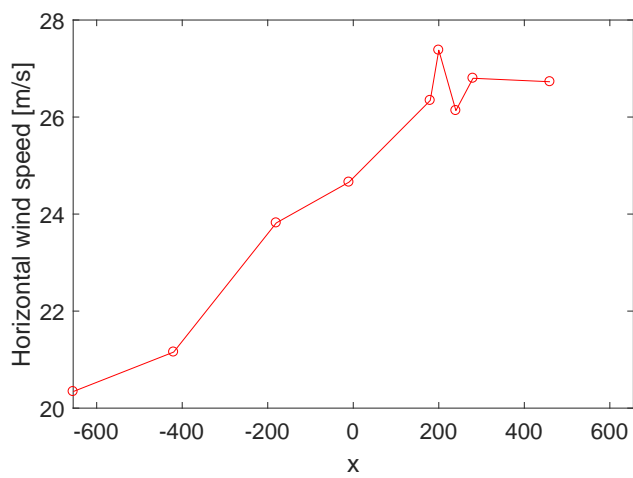
(b) 29-01-2016 13:30:00



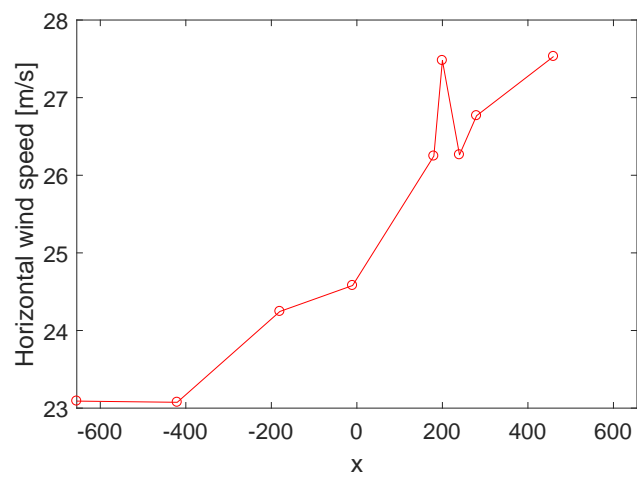
(c) 29-01-2016 14:00:00



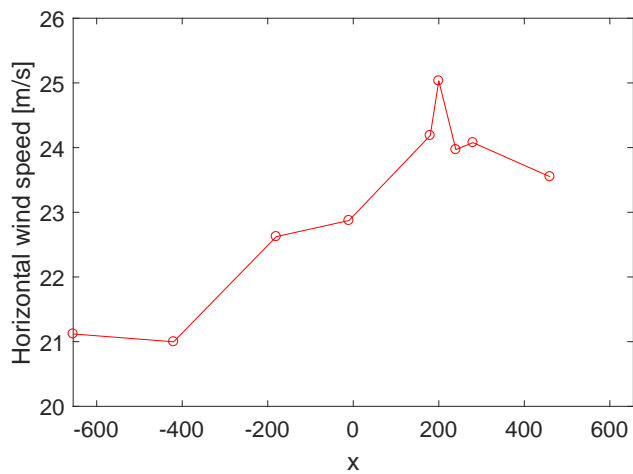
(d) 29-01-2016 15:30:00



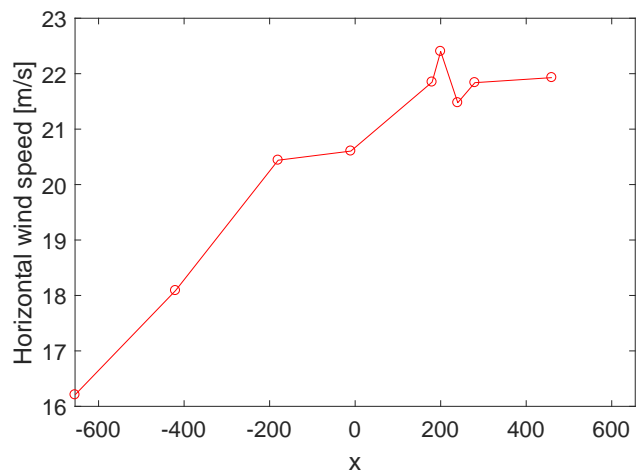
(e) 29-01-2016 17:30:00



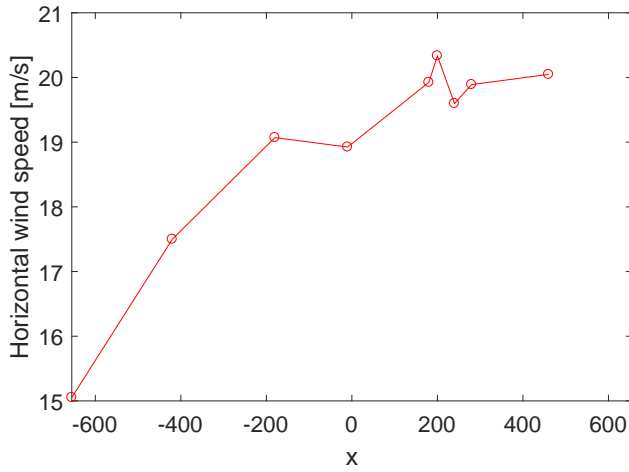
(f) 29-01-2016 19:30:00



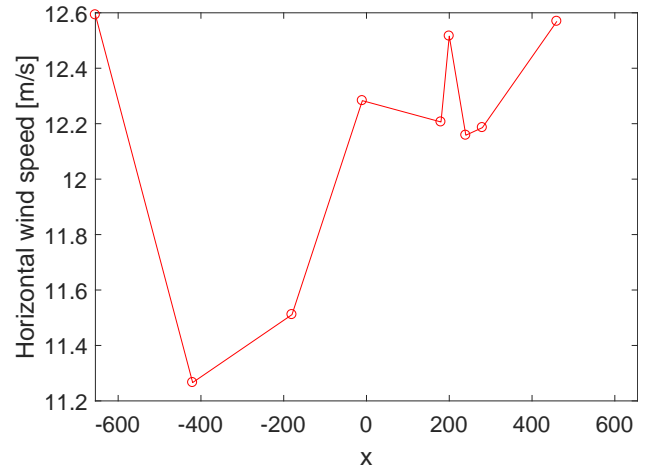
(g) 29-01-2016 20:00:00



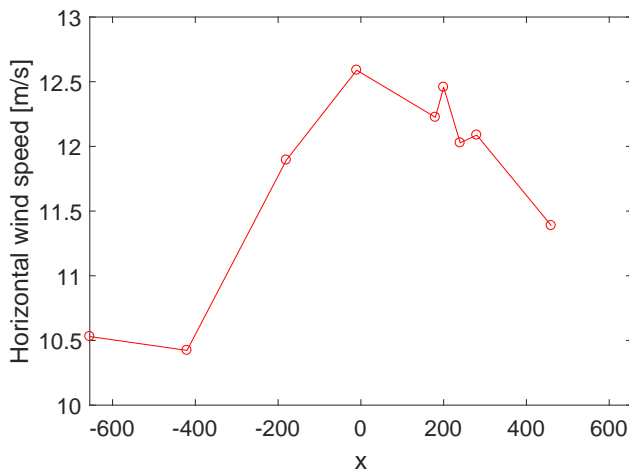
(h) 29-01-2016 20:30:00



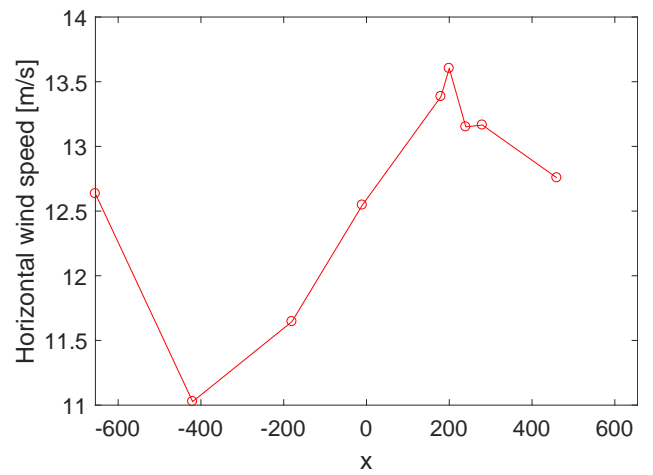
(i) 29-01-2016 21:00:00



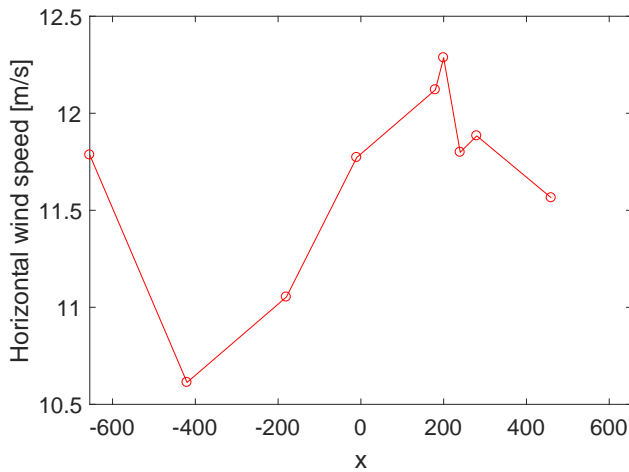
(j) 01-03-2016 22:29:20



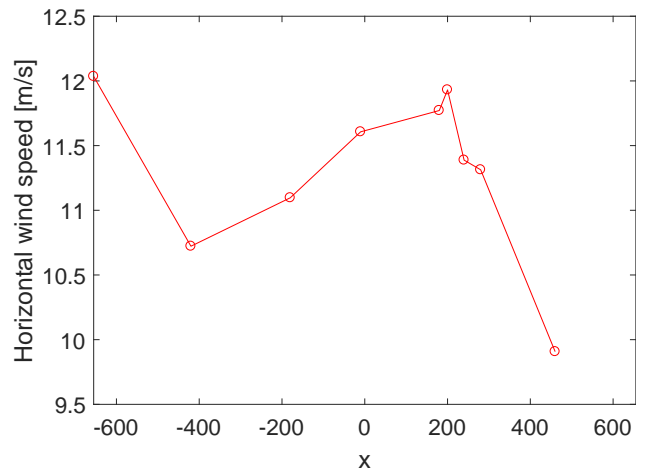
(k) 02-03-2016 02:15:29



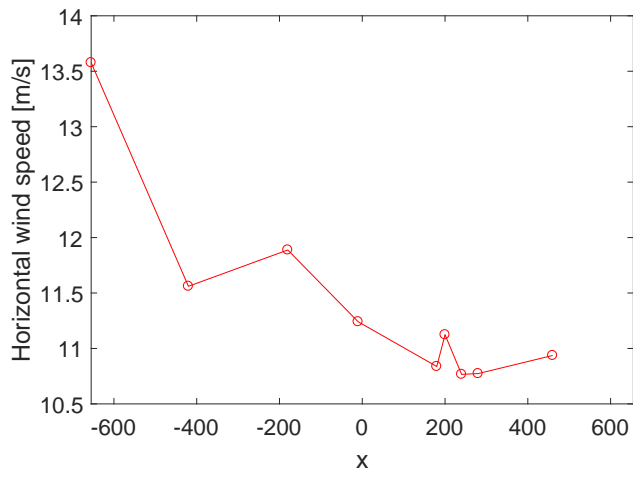
(l) 02-03-2016 02:57:13



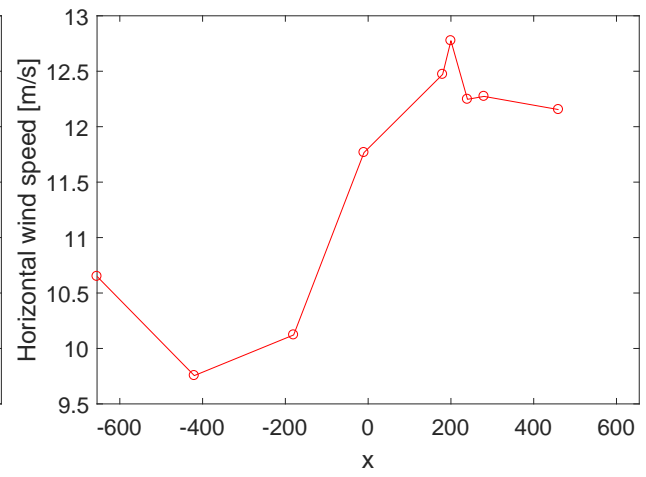
(m) 02-03-2016 03:30:49



(n) 02-03-2016 04:03:08



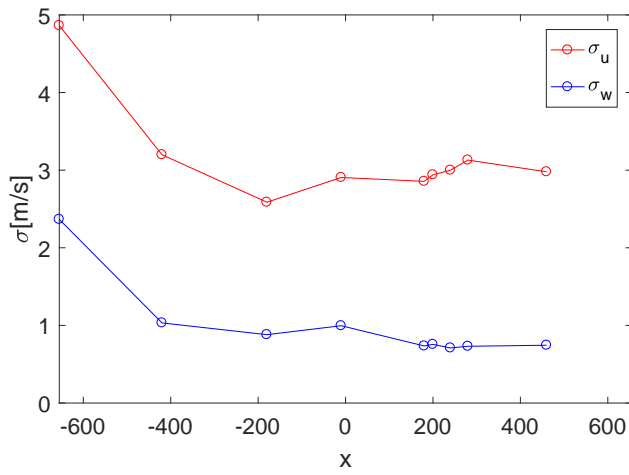
(o) 02-03-2016 04:41:37



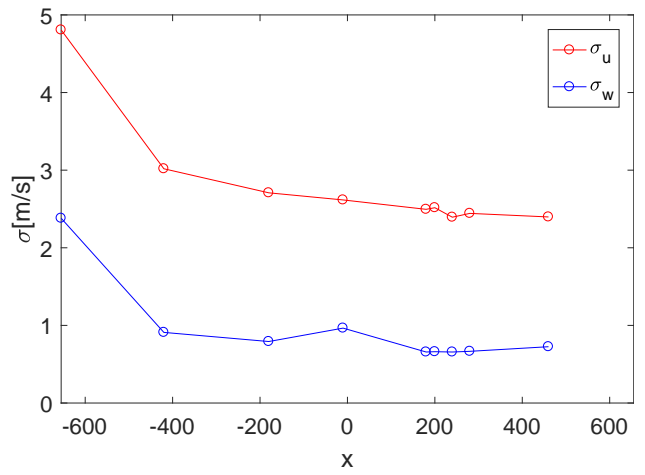
(p) 02-03-2016 05:45:08

Figure A.1: 30-minute horizontal mean wind speed profile using the anemometers.

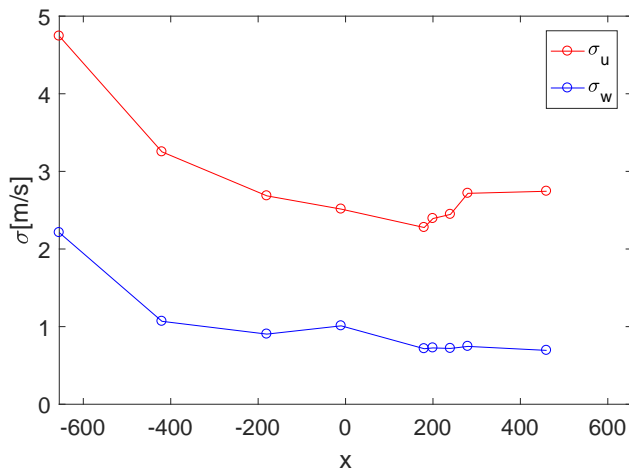
A.2 Standard deviation of turbulence components



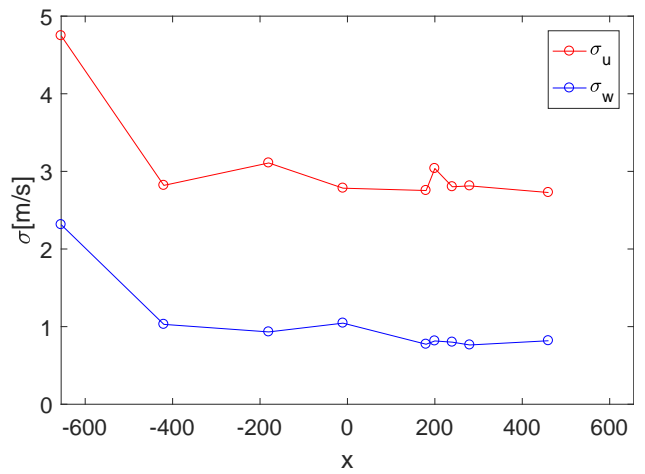
(a) 29-01-2016 13:00:00



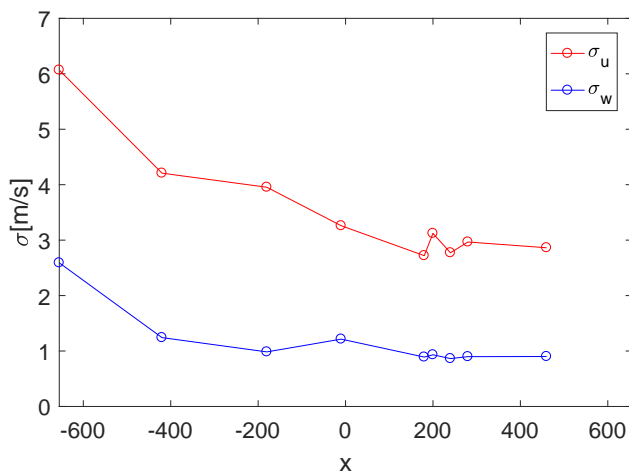
(b) 29-01-2016 13:30:00



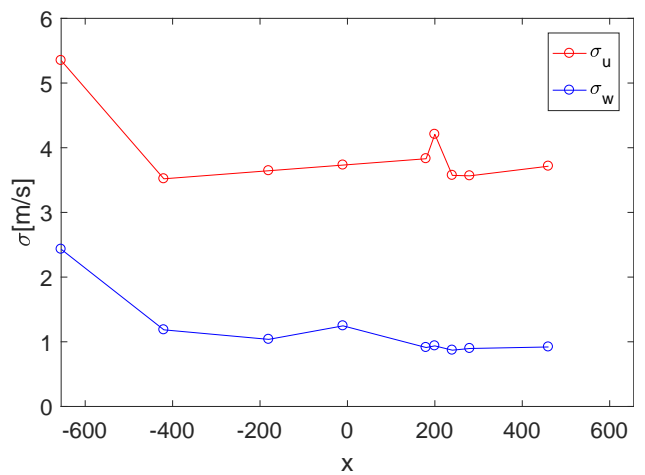
(c) 29-01-2016 14:00:00



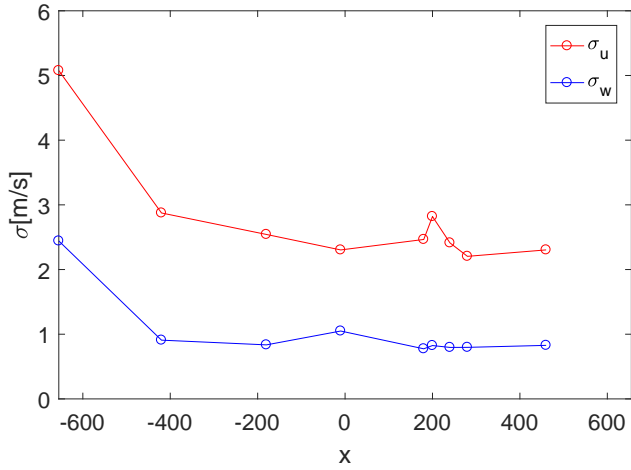
(d) 29-01-2016 15:30:00



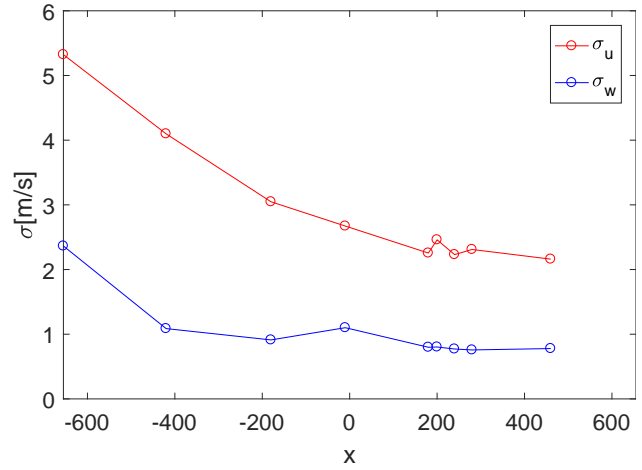
(e) 29-01-2016 17:30:00



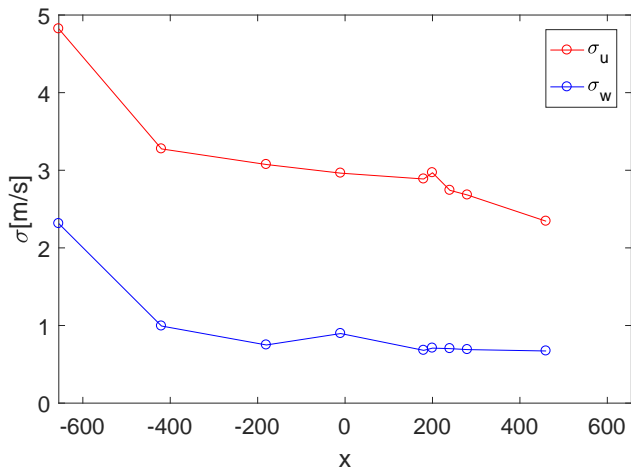
(f) 29-01-2016 19:30:00



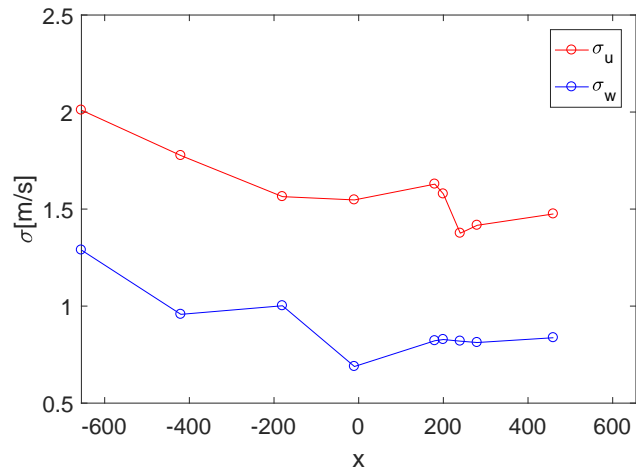
(g) 29-01-2016 20:00:00



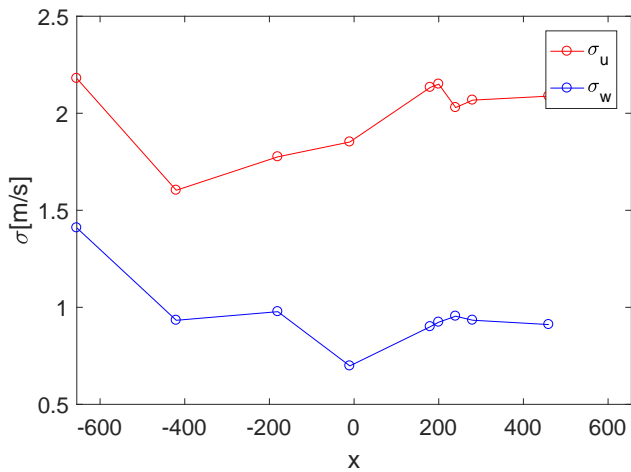
(h) 29-01-2016 20:30:00



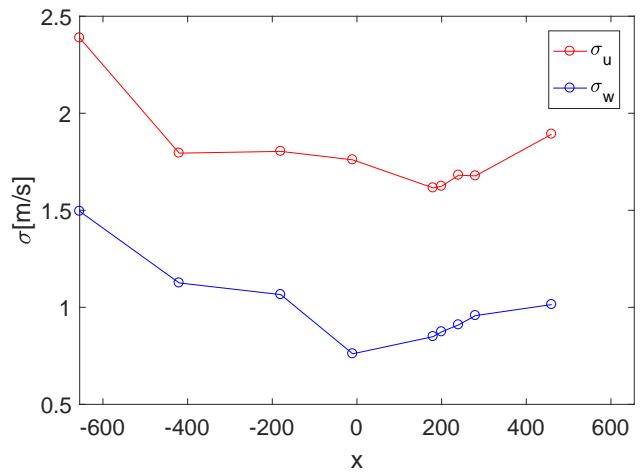
(i) 29-01-2016 21:00:00



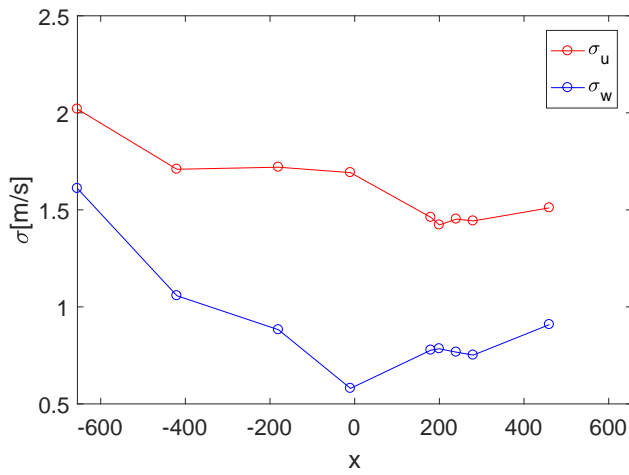
(j) 01-03-2016 22:29:20



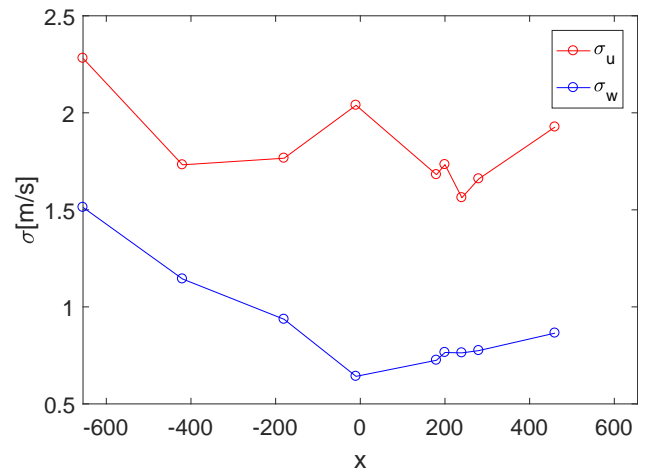
(k) 02-03-2016 02:15:29



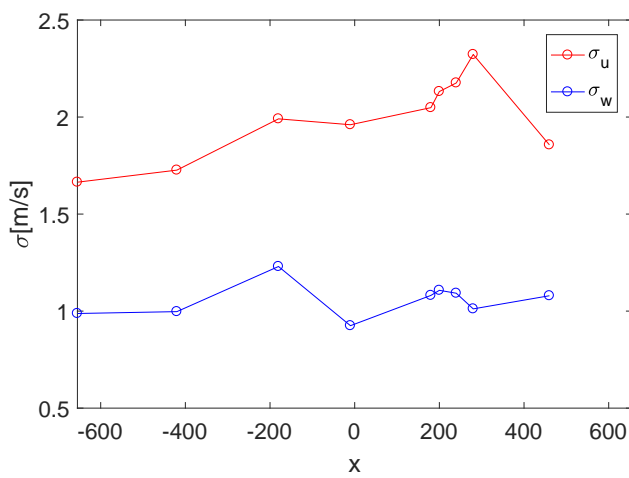
(l) 02-03-2016 02:57:13



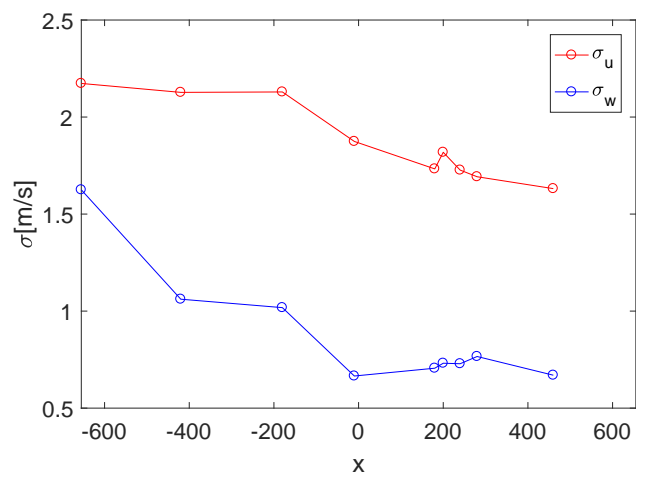
(m) 02-03-2016 03:30:49



(n) 02-03-2016 04:03:08



(o) 02-03-2016 04:41:37



(p) 02-03-2016 05:45:08

Figure A.2: Wind profiles.

A.3 Wind characteristics

Table A.1: Main wind characteristics from the recordings.

Recording name	Span-wise mean wind speed [m/s]		30-minute mean wind speed at midspan [m/s]		Mean wind direction at midspan [°]		Turbulence span-wise mean σ_u [m/s]		Turbulence std midspan σ_w [m/s]	
	speed [m/s]	midspan [m/s]	midspan [m/s]	midspan [m/s]	direction at midspan [°]	direction at midspan [°]	σ_u [m/s]	σ_w [m/s]	σ_u [m/s]	σ_w [m/s]
29-01-2016 13:00:00	21.1	20.7	20.7	101	101	3.1622	0.9945	2.9056	0.9958	
29-01-2016 13:30:00	21.3	21.3	21.3	102	102	2.8216	0.9350	2.6164	0.9650	
29-01-2016 14:00:00	19.9	19.8	19.8	104	104	2.8633	0.9769	2.5139	1.0100	
29-01-2016 15:30:00	21.3	21.2	21.2	102	102	3.0658	1.0321	2.7835	1.0448	
29-01-2016 17:30:00	24.8	24.7	24.7	102	102	3.5481	1.1686	3.2600	1.2145	
29-01-2016 19:30:00	25.5	24.6	24.6	103	103	3.9037	1.1592	3.7318	1.2463	
29-01-2016 20:00:00	23.2	22.9	22.9	98	98	2.7777	1.0283	2.3031	1.0493	
29-01-2016 20:30:00	20.5	20.6	20.6	101	101	2.9507	1.0413	2.6723	1.1009	
29-01-2016 21:00:00	18.9	18.9	18.9	101	101	3.0840	0.9338	2.9628	0.8965	
01-03-2016 22:29:20	12.1	12.3	12.3	284	284	1.5967	0.8950	1.5472	0.6887	
02-03-2016 02:15:29	11.7	12.6	12.6	297	297	1.9866	0.9601	1.8520	0.6981	
02-03-2016 02:57:13	12.7	12.5	12.5	290	290	1.8040	1.0056	1.7601	0.7605	
02-03-2016 03:30:49	11.7	11.8	11.8	296	296	1.6032	0.9020	1.6919	0.5800	
02-03-2016 04:03:08	11.3	11.6	11.6	287	287	1.8202	0.9030	2.0389	0.6419	
02-03-2016 04:41:37	11.4	11.2	11.2	266	266	1.9863	1.0567	1.9604	0.9248	
02-03-2016 05:45:08	11.6	11.8	11.8	291	291	1.8784	0.8857	1.8743	0.6655	

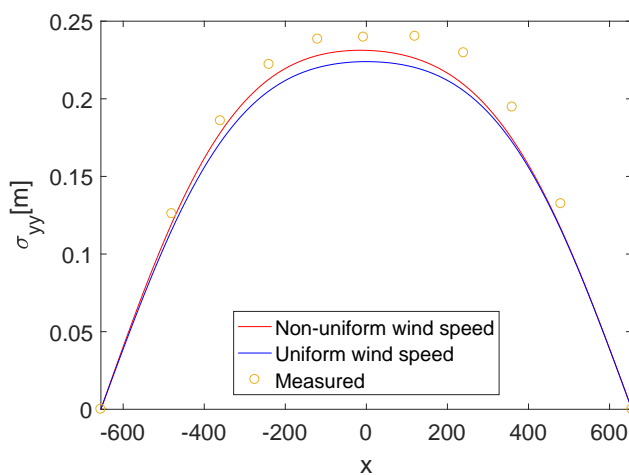
Predicted response

Here will plots of the response along the span be shown for wind characteristics taken from the recordings.

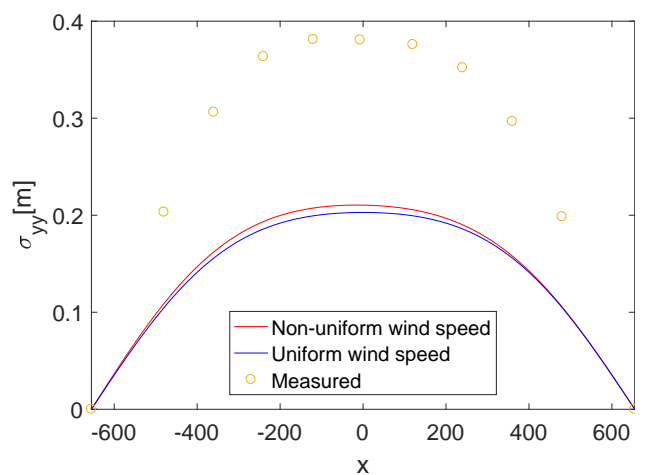
B.1 Uniform compared with non-uniform mean wind speed

The response along the bridge is plotted for the different directions for uniform and non-uniform mean wind speed. The turbulence standard deviation profile used is uniform span-wise mean and uniform self-excited forces along the span.

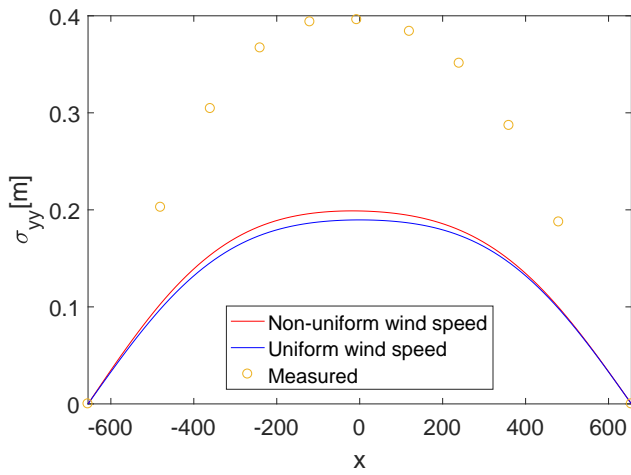
Horizontal response



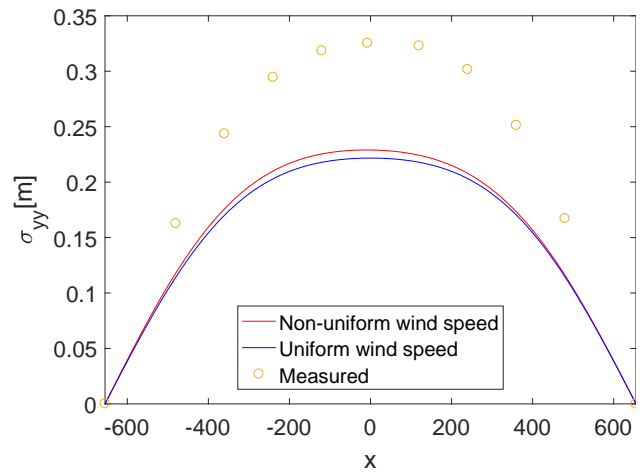
(a) 29-01-2016 13:00:00



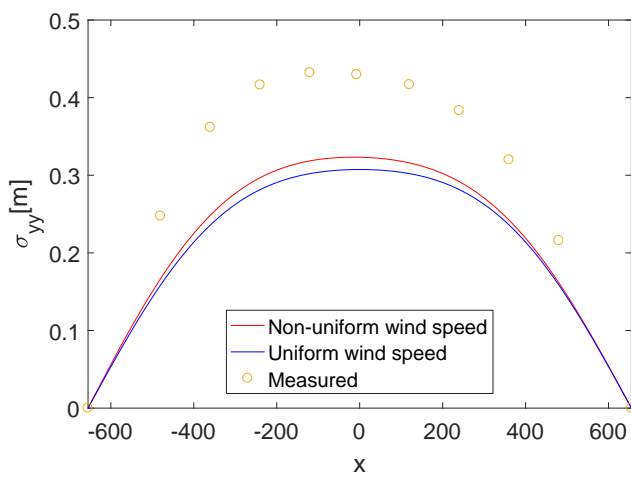
(b) 29-01-2016 13:30:00



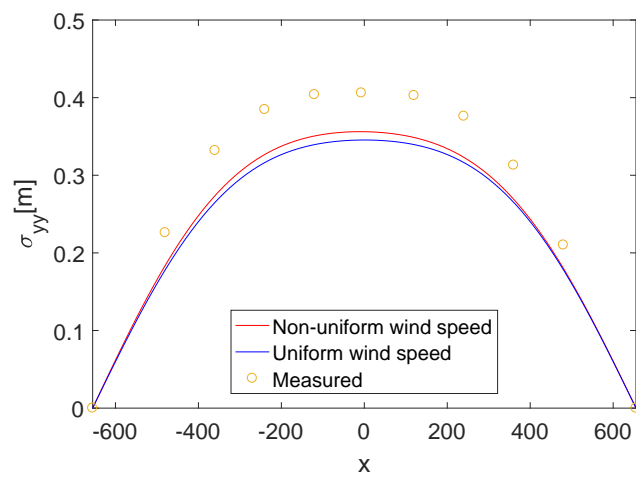
(c) 29-01-2016 14:00:00



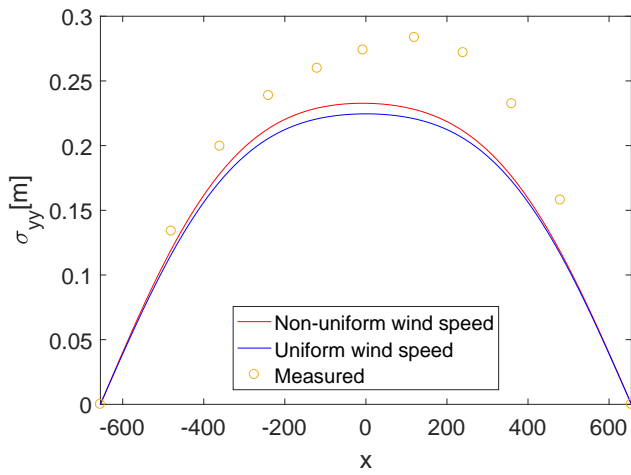
(d) 29-01-2016 15:30:00



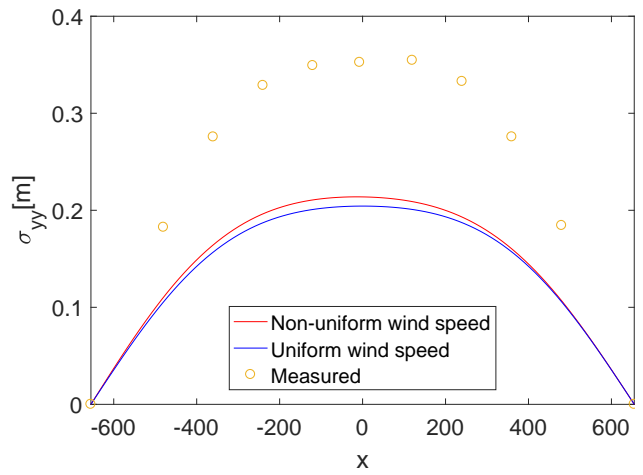
(e) 29-01-2016 17:30:00



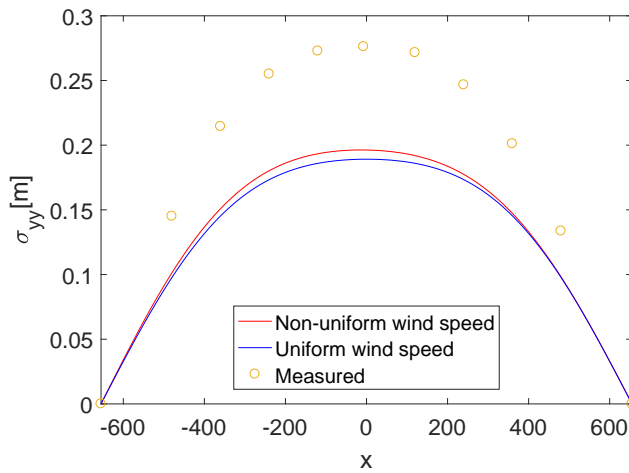
(f) 29-01-2016 19:30:00



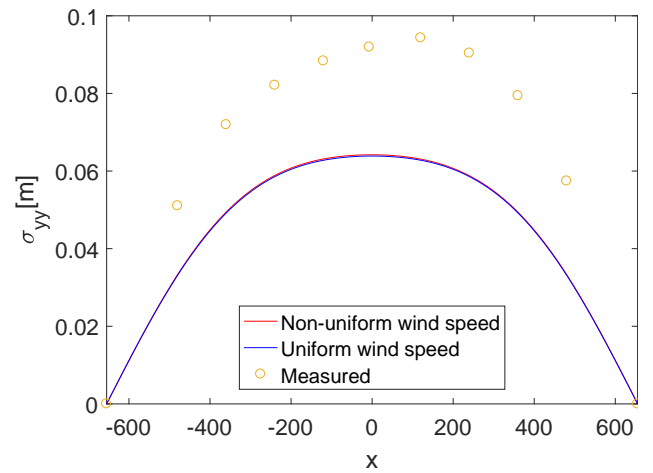
(g) 29-01-2016 20:00:00



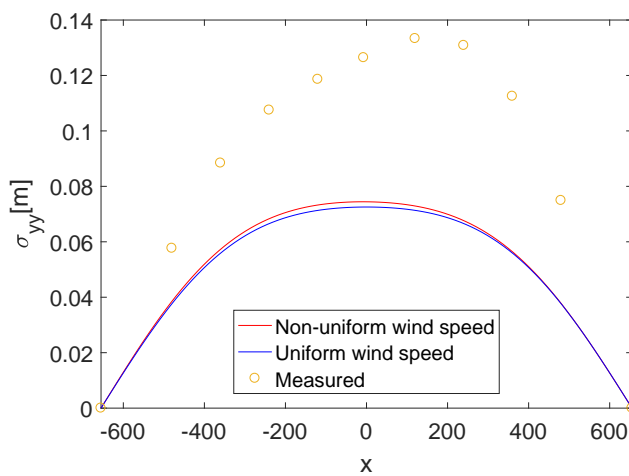
(h) 29-01-2016 20:30:00



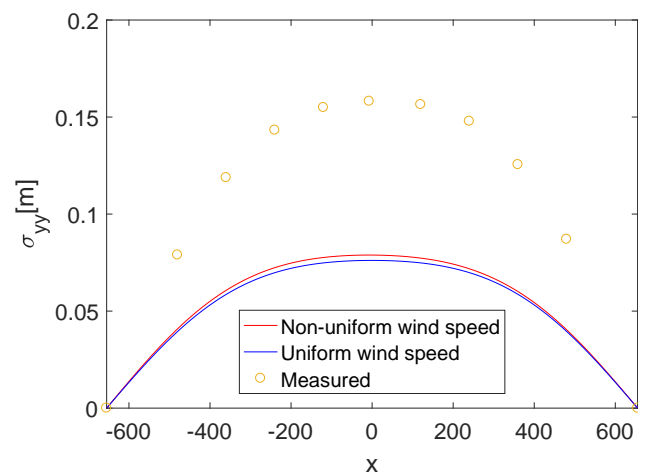
(i) 29-01-2016 21:00:00



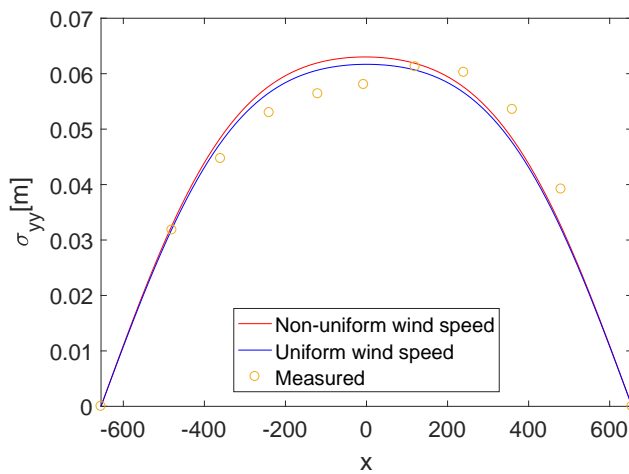
(j) 01-03-2016 22:29:20



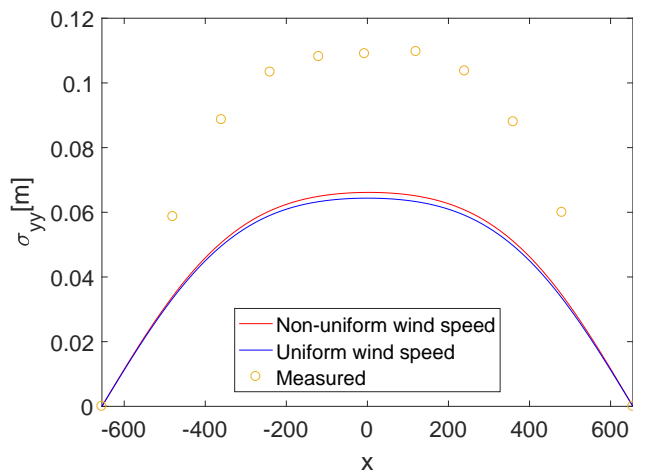
(k) 02-03-2016 02:15:29



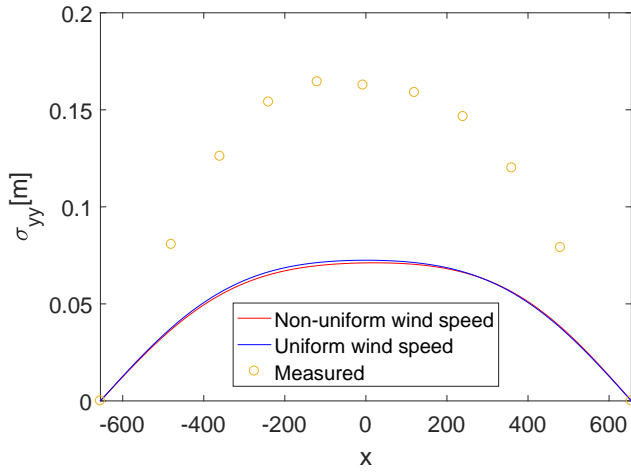
(l) 02-03-2016 02:57:13



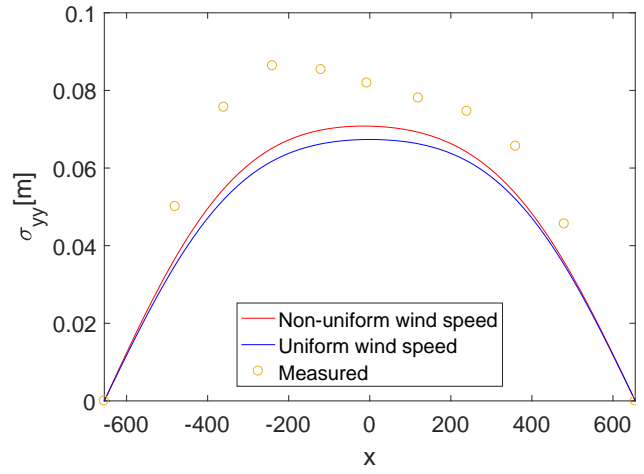
(m) 02-03-2016 03:30:49



(n) 02-03-2016 04:03:08



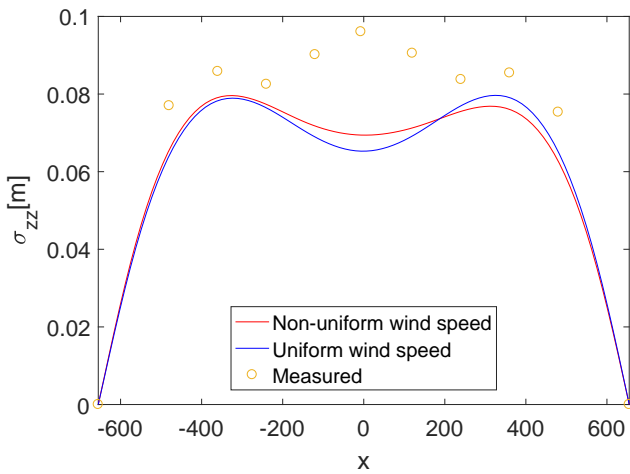
(o) 02-03-2016 04:41:37



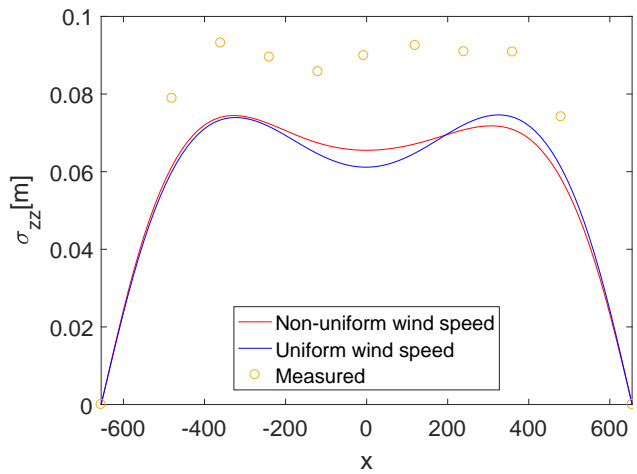
(p) 02-03-2016 05:45:08

Figure B.1: Horizontal response along the span.

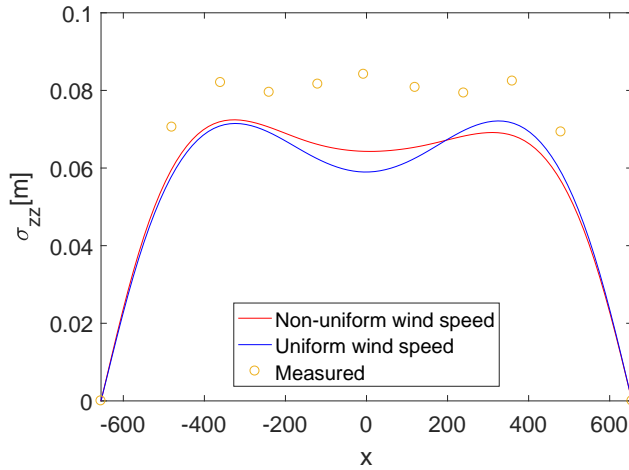
Vertical response



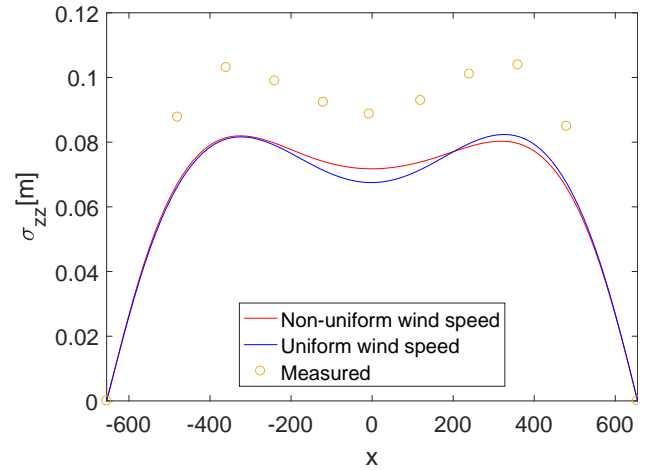
(a) 29-01-2016 13:00:00



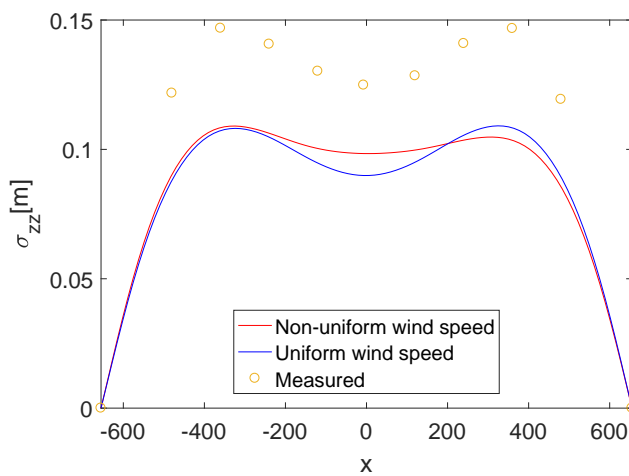
(b) 29-01-2016 13:30:00



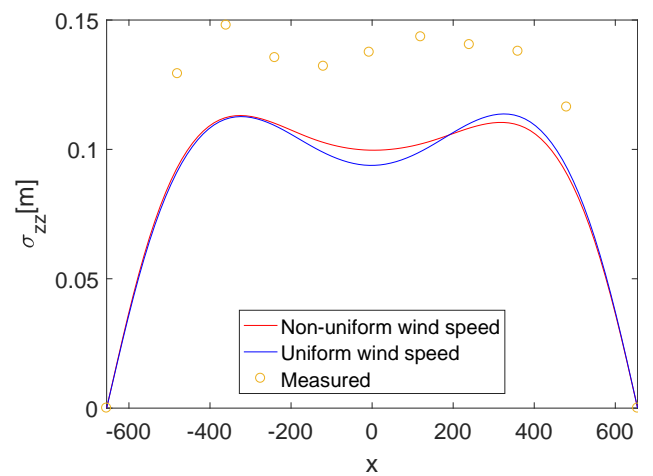
(c) 29-01-2016 14:00:00



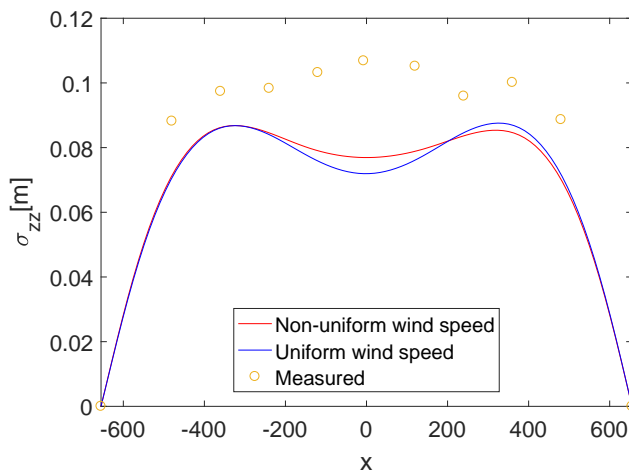
(d) 29-01-2016 15:30:00



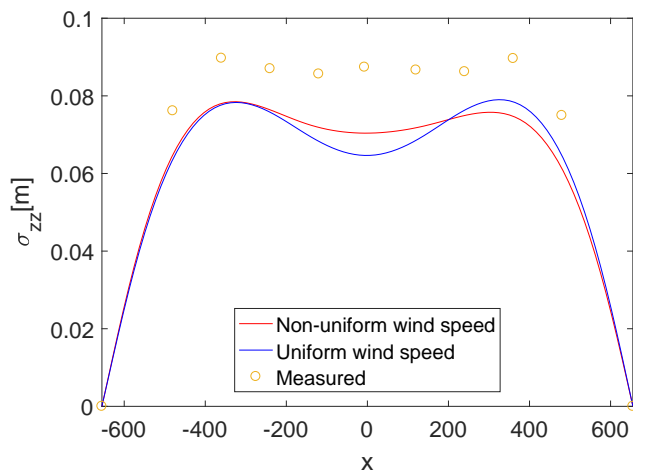
(e) 29-01-2016 17:30:00



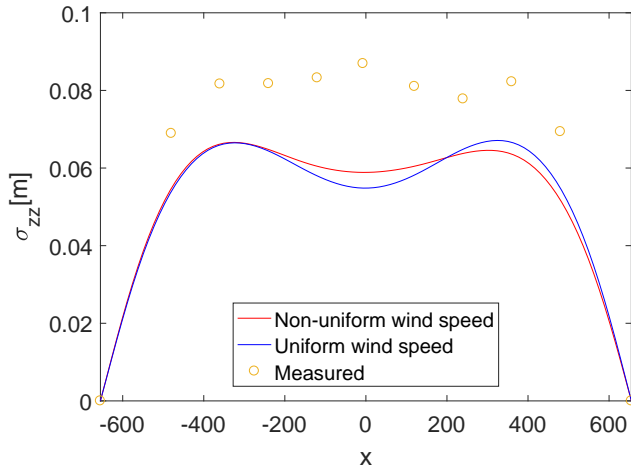
(f) 29-01-2016 19:30:00



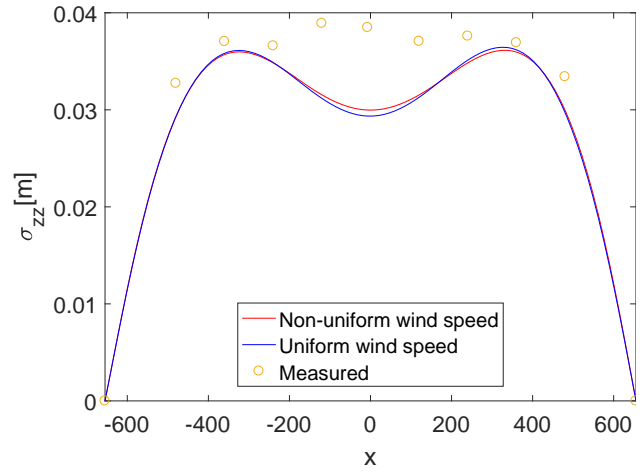
(g) 29-01-2016 20:00:00



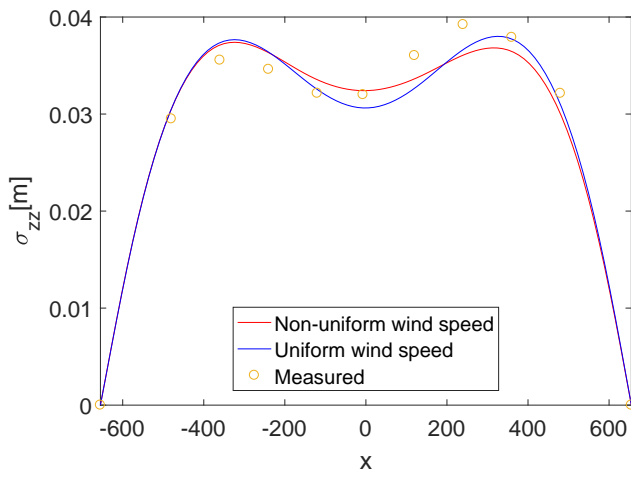
(h) 29-01-2016 20:30:00



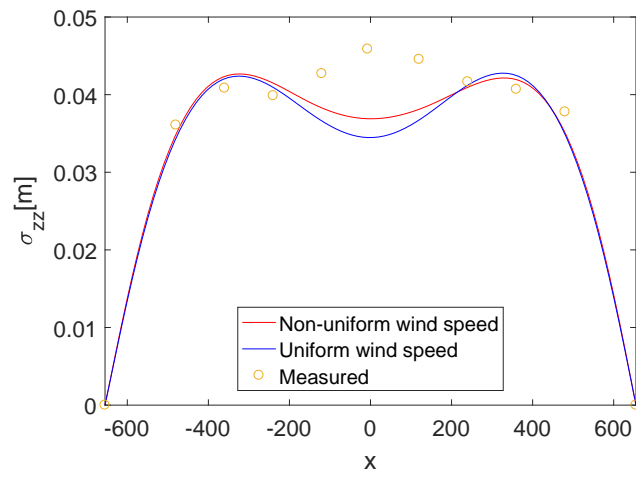
(i) 29-01-2016 21:00:00



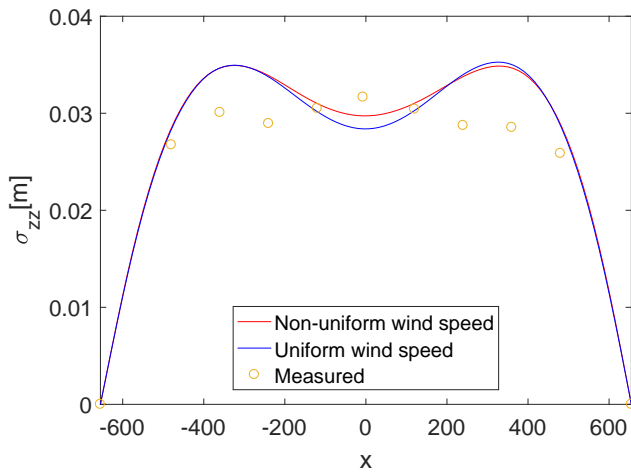
(j) 01-03-2016 22:29:20



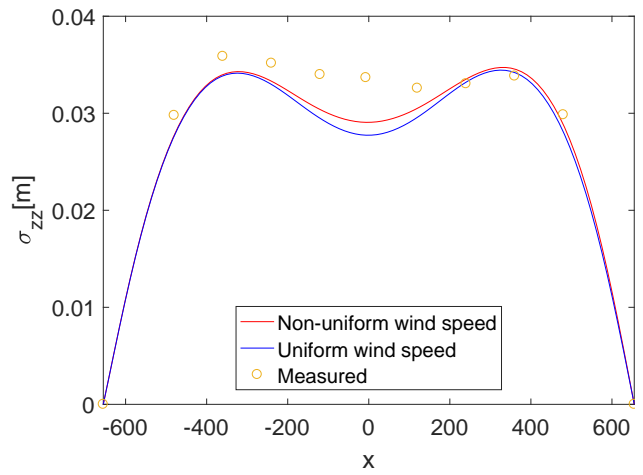
(k) 02-03-2016 02:15:29



(l) 02-03-2016 02:57:13



(m) 02-03-2016 03:30:49



(n) 02-03-2016 04:03:08

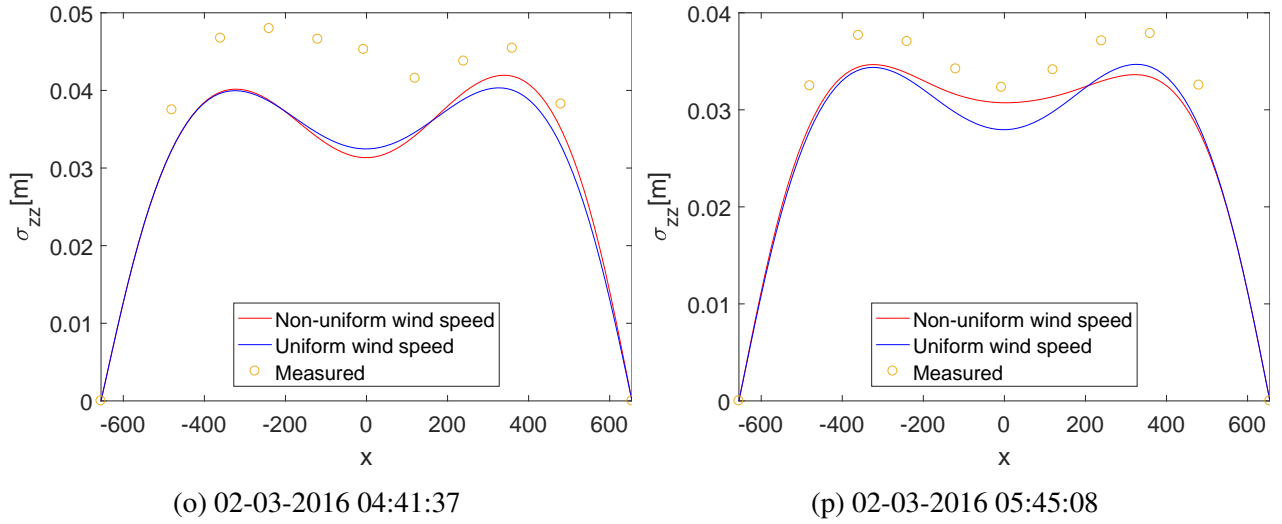
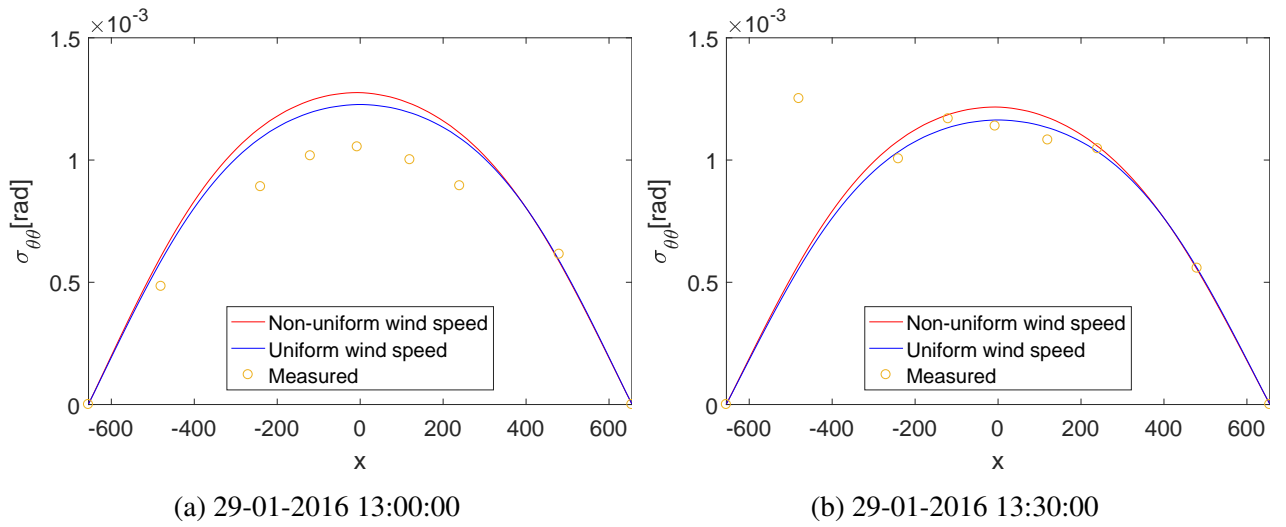
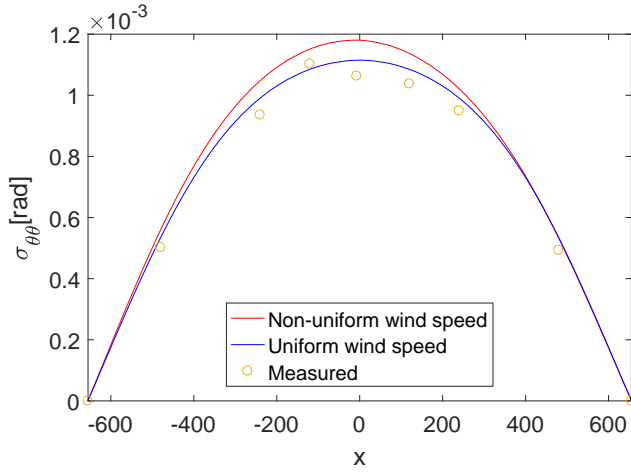


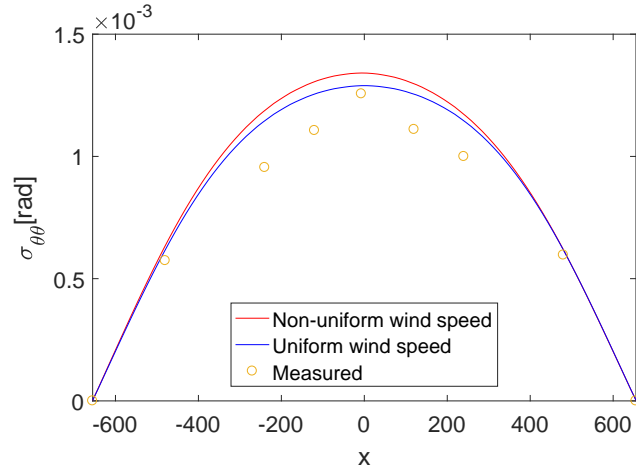
Figure B.2: Vertical response along the span.

Torsional response

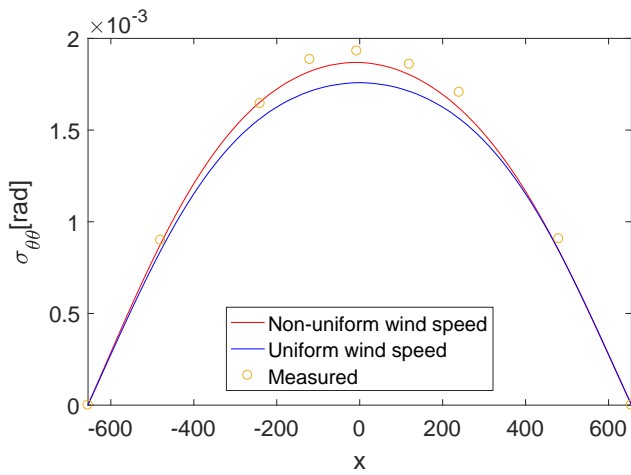




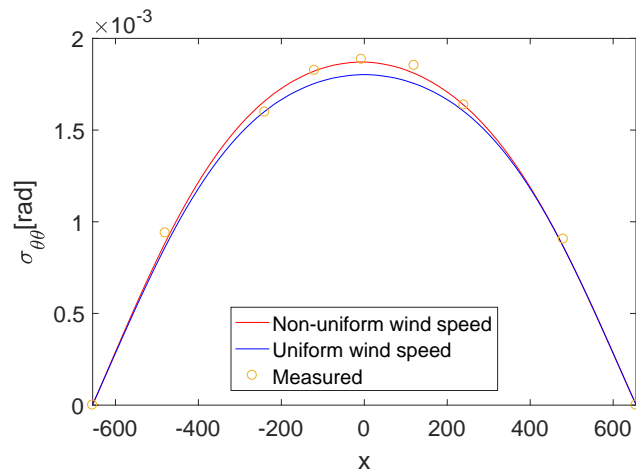
(c) 29-01-2016 14:00:00



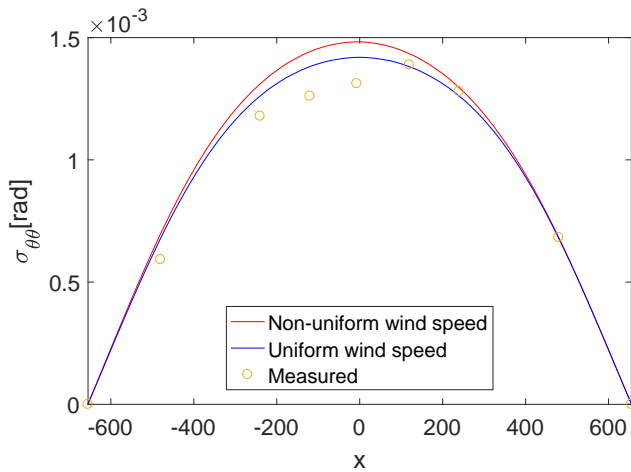
(d) 29-01-2016 15:30:00



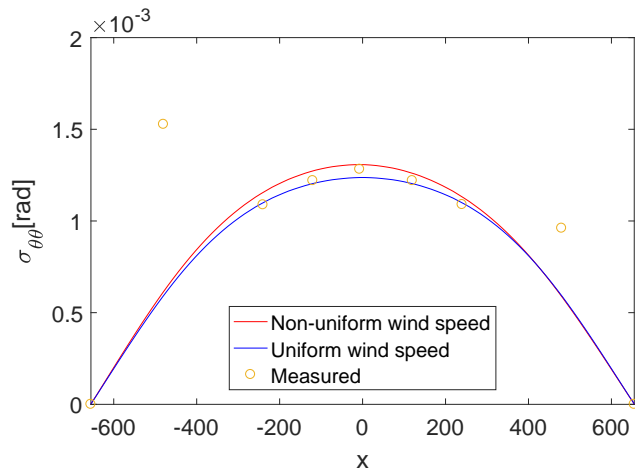
(e) 29-01-2016 17:30:00



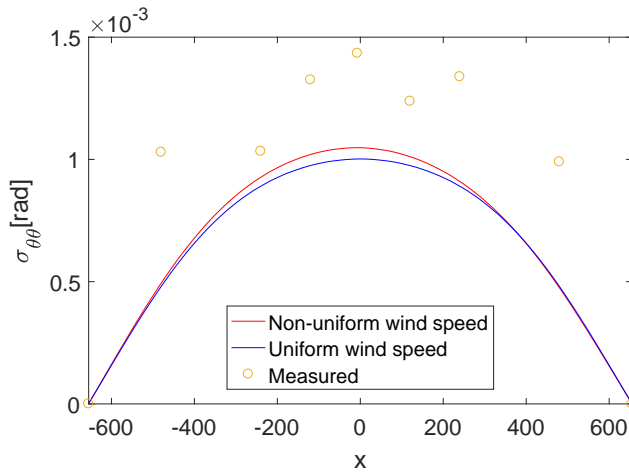
(f) 29-01-2016 19:30:00



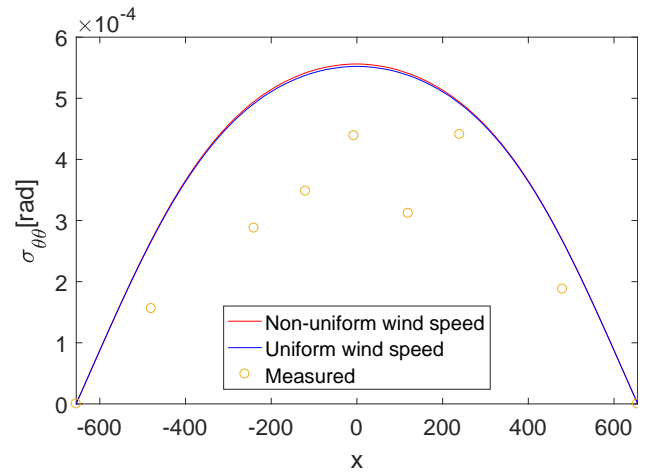
(g) 29-01-2016 20:00:00



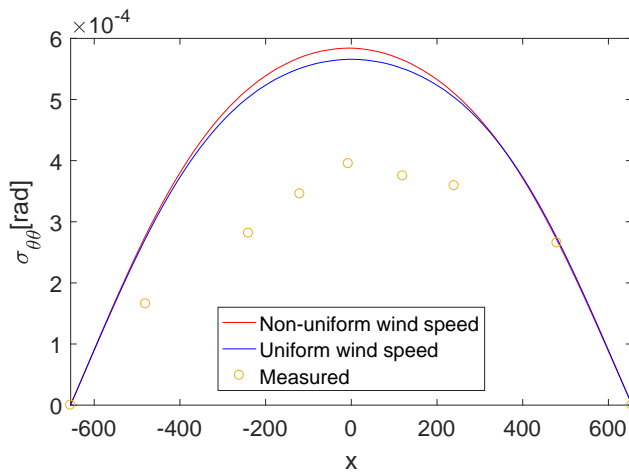
(h) 29-01-2016 20:30:00



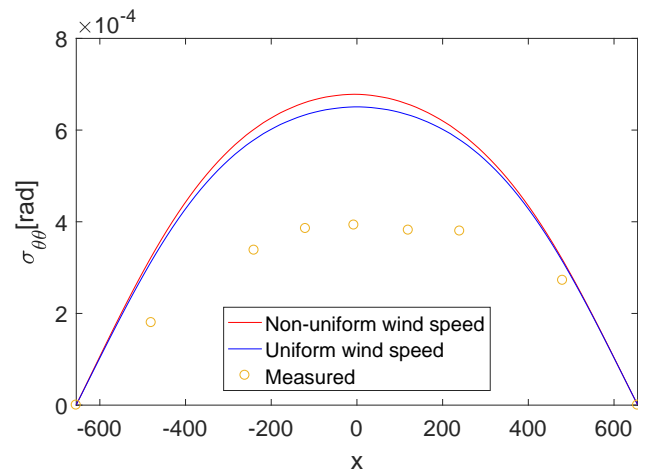
(i) 29-01-2016 21:00:00



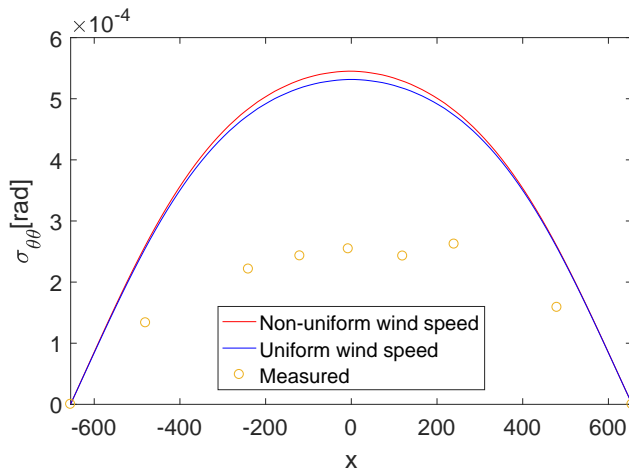
(j) 01-03-2016 22:29:20



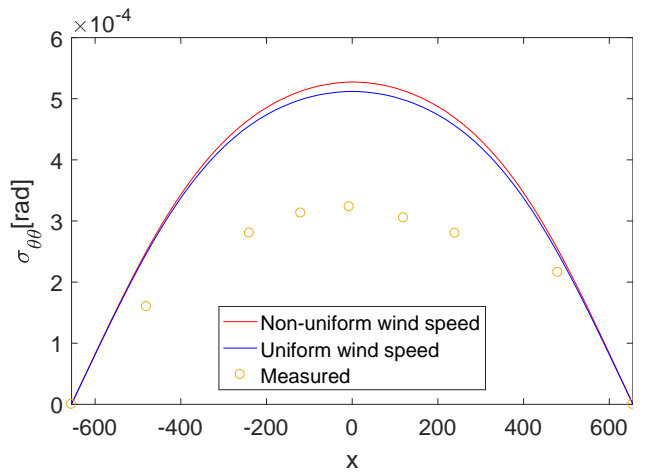
(k) 02-03-2016 02:15:29



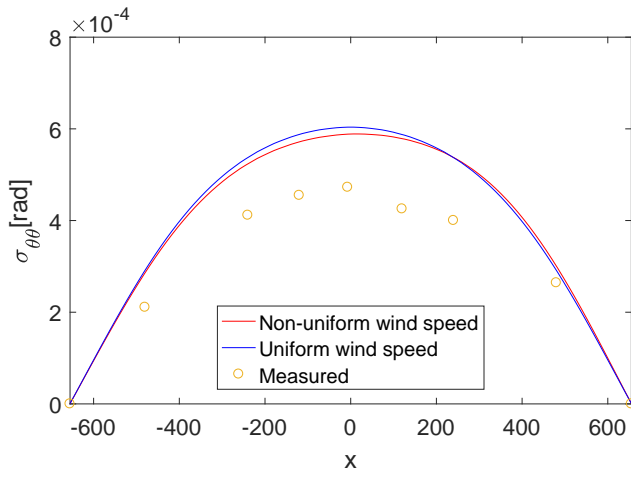
(l) 02-03-2016 02:57:13



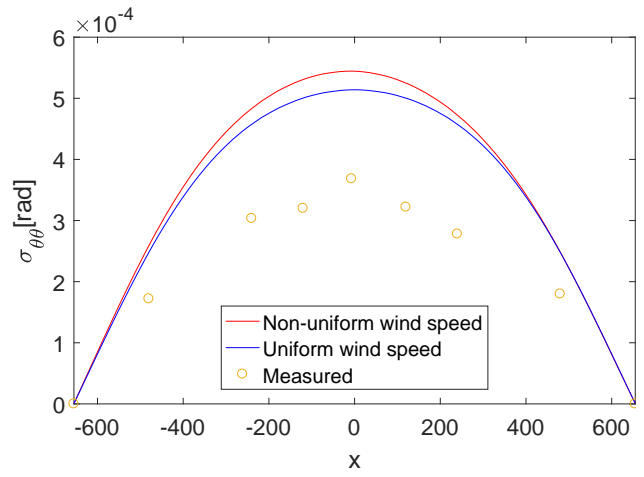
(m) 02-03-2016 03:30:49



(n) 02-03-2016 04:03:08



(o) 02-03-2016 04:41:37



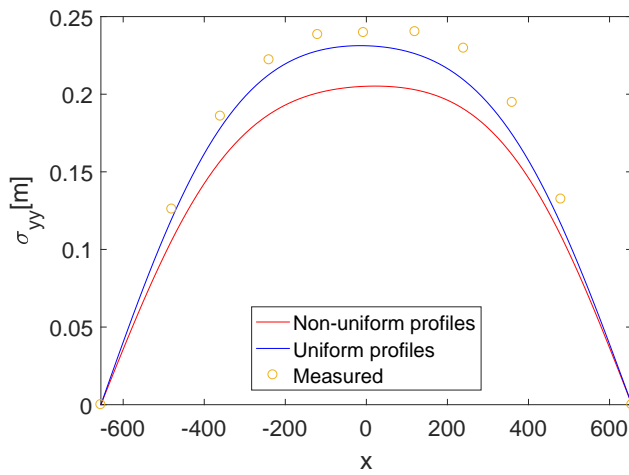
(p) 02-03-2016 05:45:08

Figure B.3: Torsional response along the span.

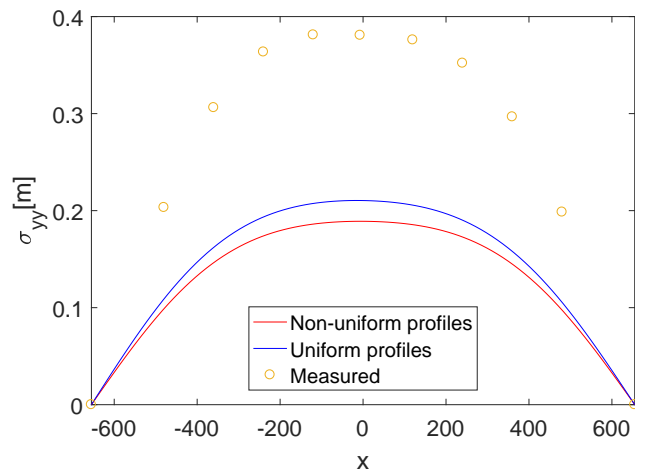
B.2 Uniform compared with non-uniform turbulence std

The response along the bridge is plotted for the different directions for uniform and non-uniform turbulence standard deviation. The non-uniform mean wind speed profiles has been used to calculate the response and the self-excited forces are taken as uniform along the span.

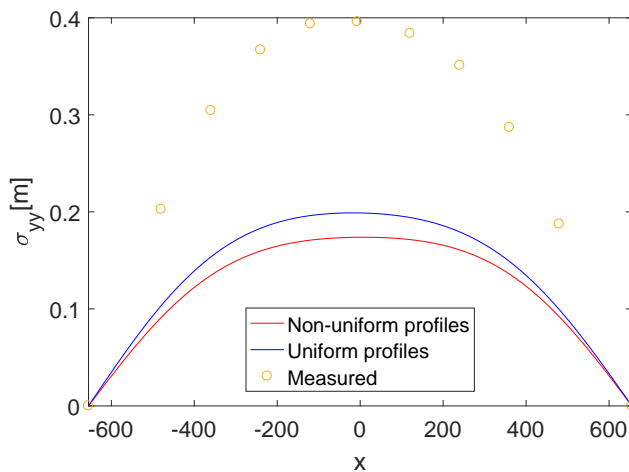
Horizontal response



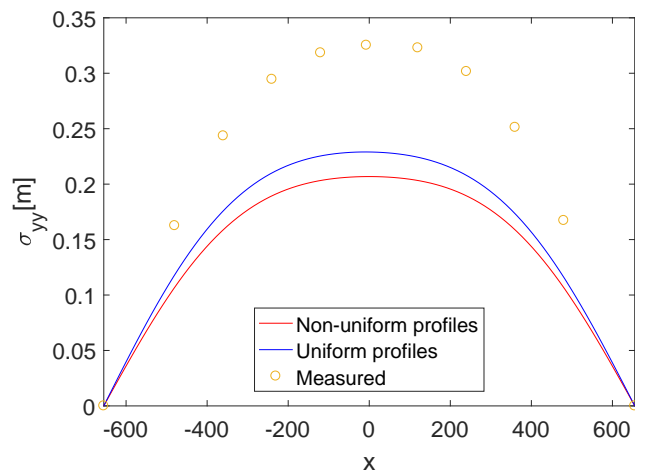
(a) 29-01-2016 13:00:00



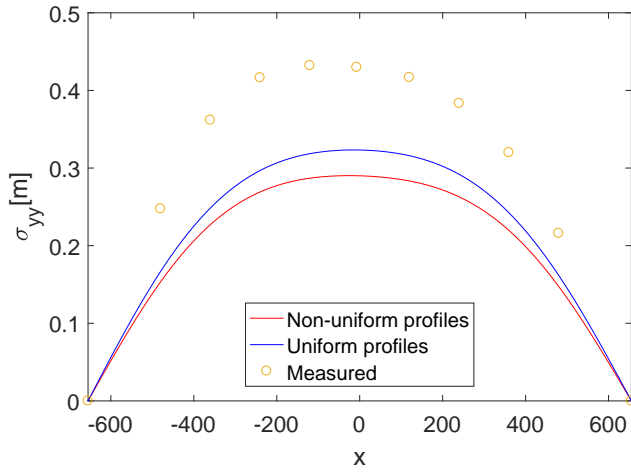
(b) 29-01-2016 13:30:00



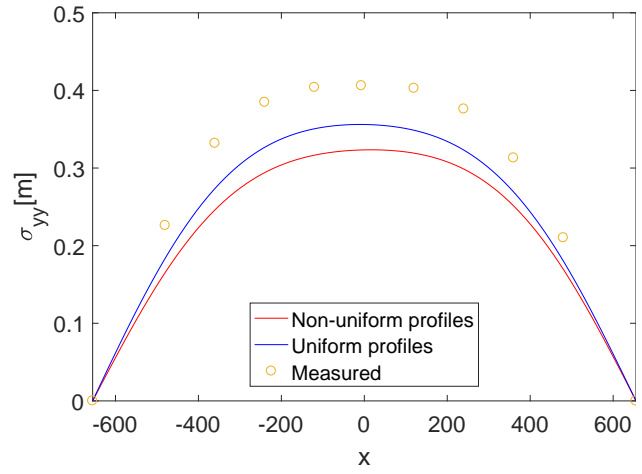
(c) 29-01-2016 14:00:00



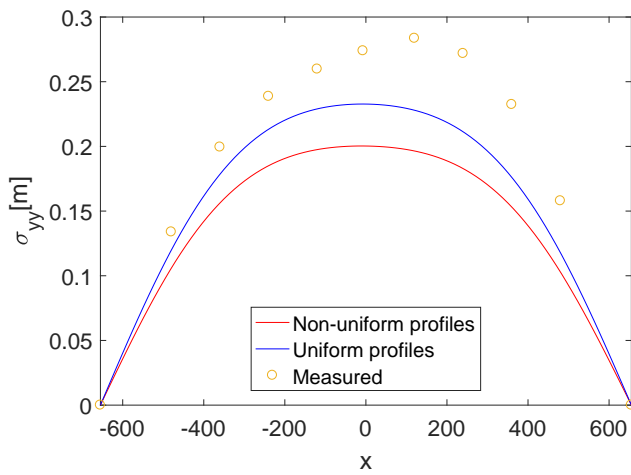
(d) 29-01-2016 15:30:00



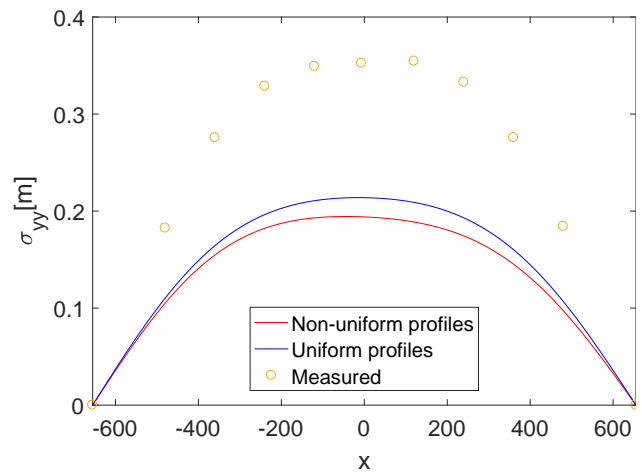
(e) 29-01-2016 17:30:00



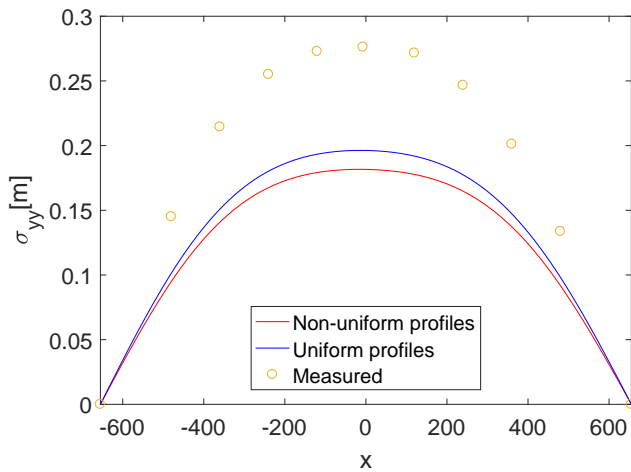
(f) 29-01-2016 19:30:00



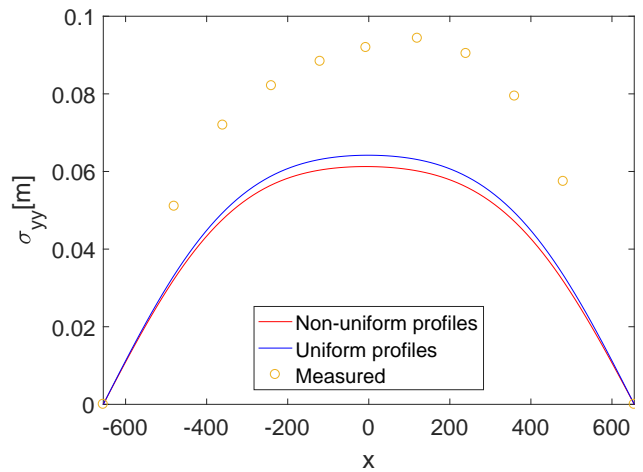
(g) 29-01-2016 20:00:00



(h) 29-01-2016 20:30:00



(i) 29-01-2016 21:00:00



(j) 01-03-2016 22:29:20

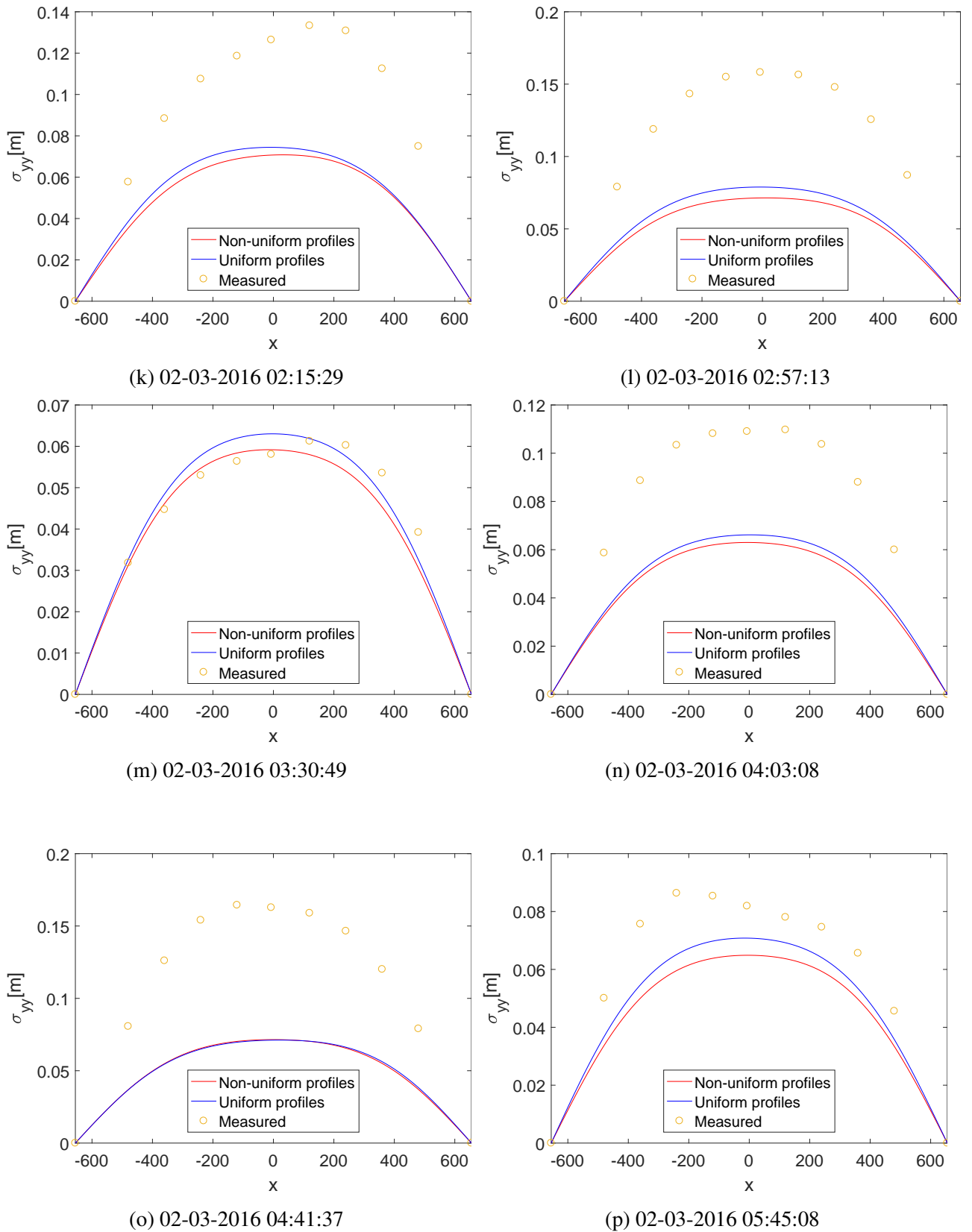
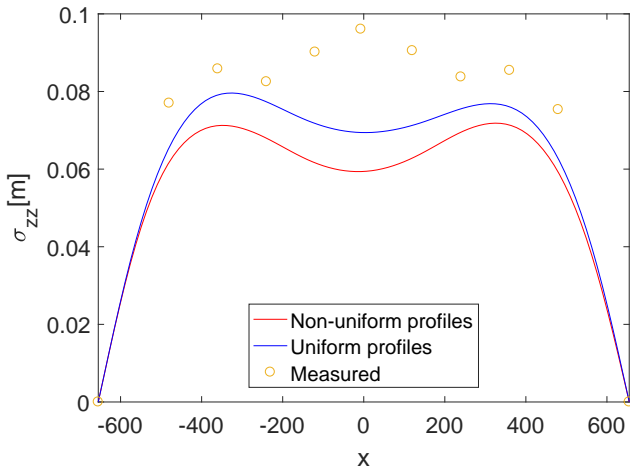
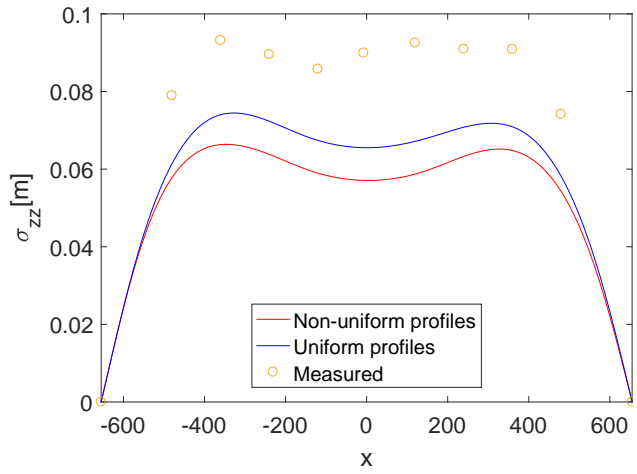


Figure B.4: Horizontal response along the span.

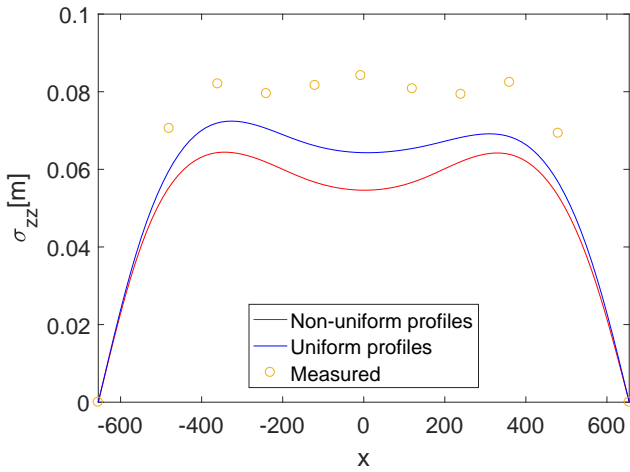
Vertical response



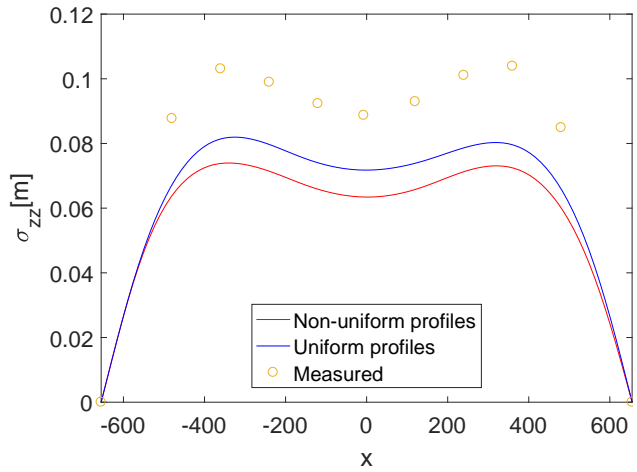
(a) 29-01-2016 13:00:00



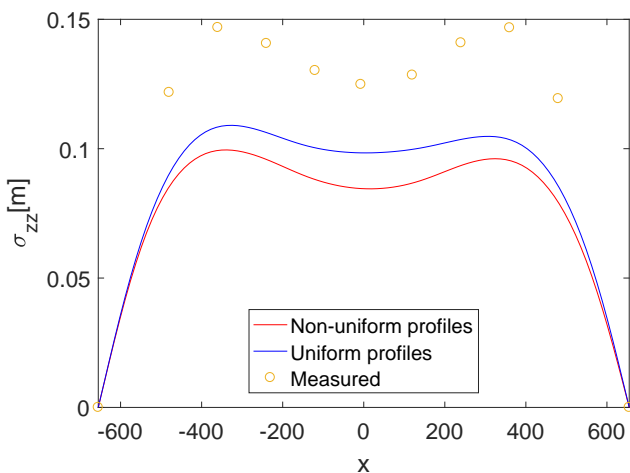
(b) 29-01-2016 13:30:00



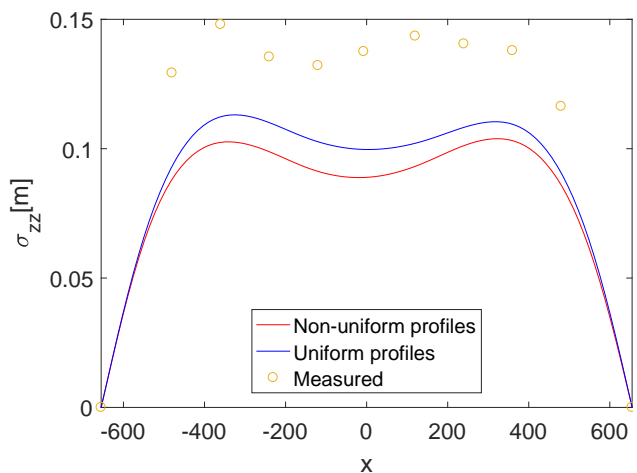
(c) 29-01-2016 14:00:00



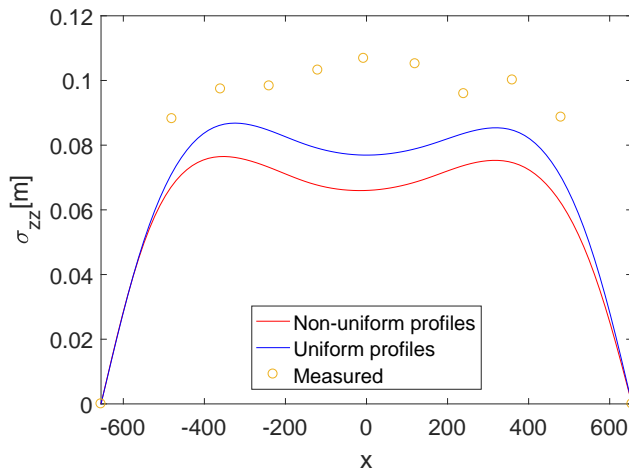
(d) 29-01-2016 15:30:00



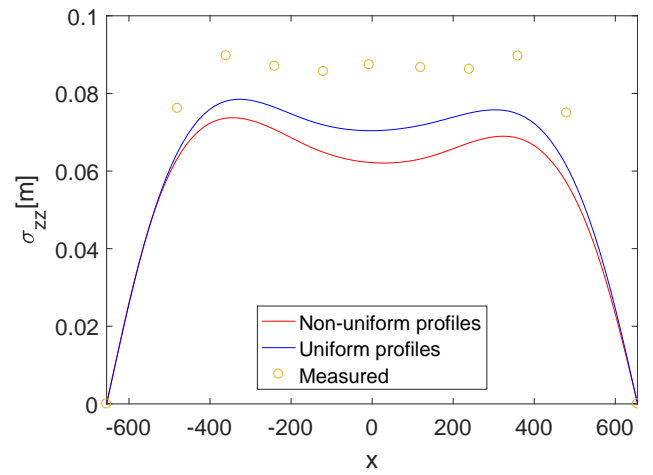
(e) 29-01-2016 17:30:00



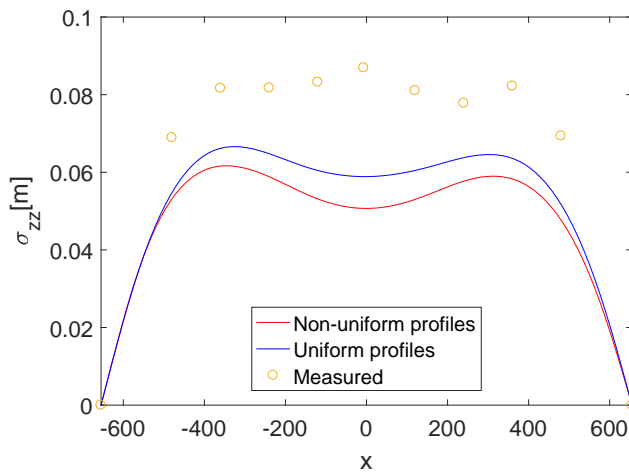
(f) 29-01-2016 19:30:00



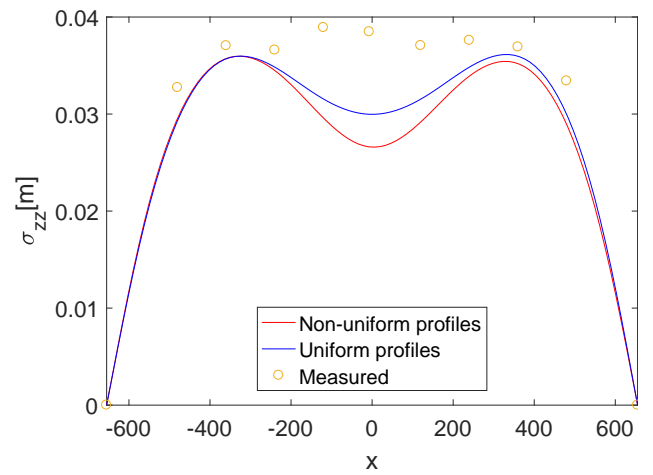
(g) 29-01-2016 20:00:00



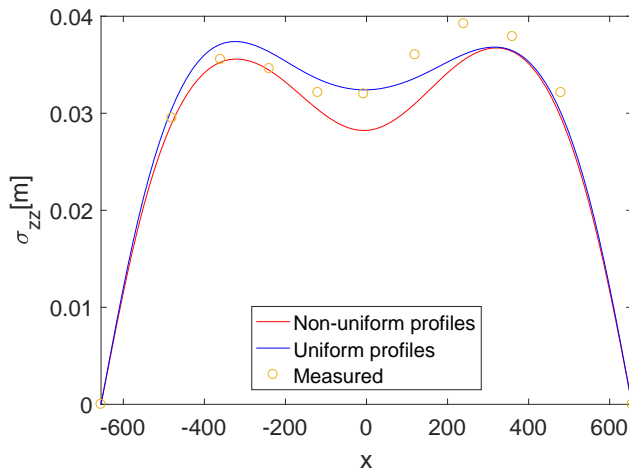
(h) 29-01-2016 20:30:00



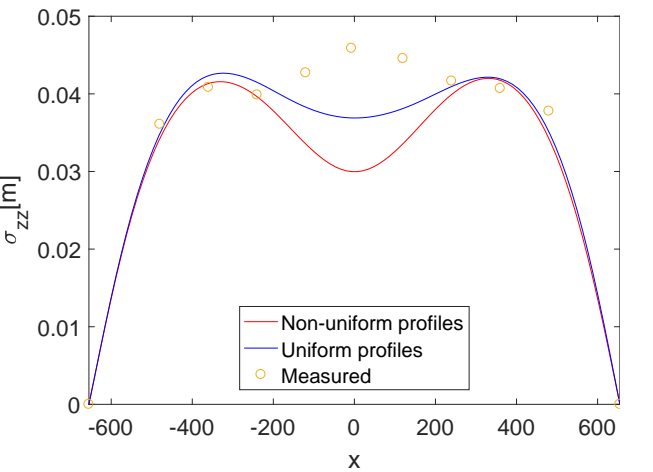
(i) 29-01-2016 21:00:00



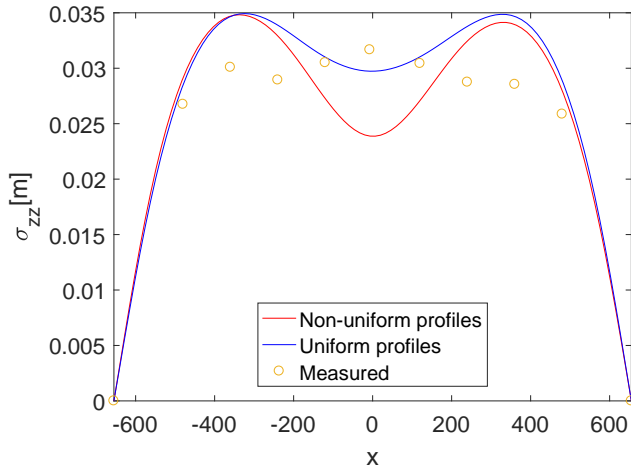
(j) 01-03-2016 22:29:20



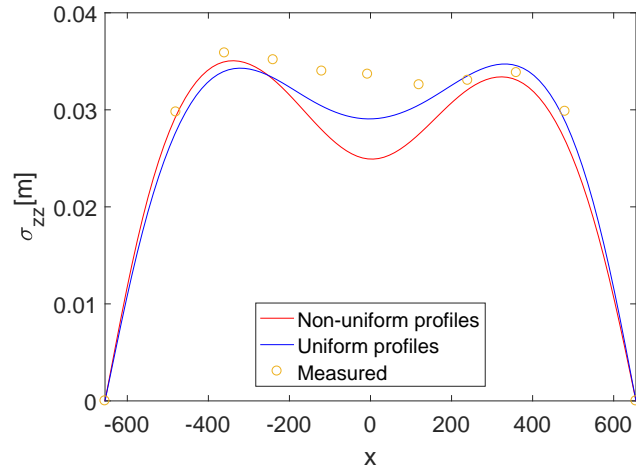
(k) 02-03-2016 02:15:29



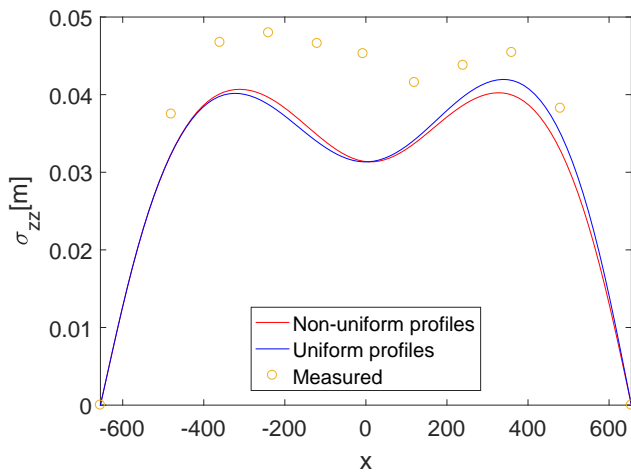
(l) 02-03-2016 02:57:13



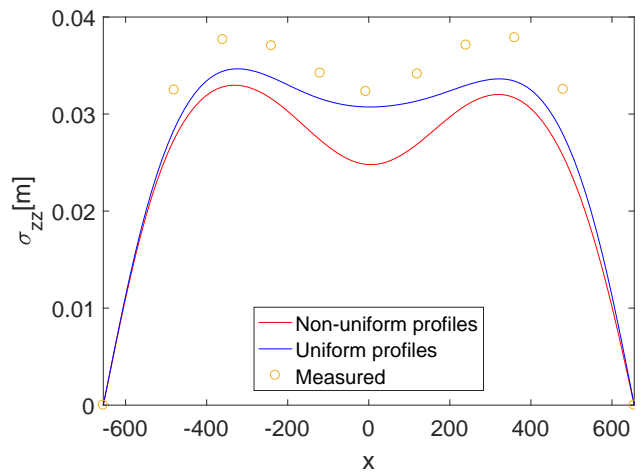
(m) 02-03-2016 03:30:49



(n) 02-03-2016 04:03:08



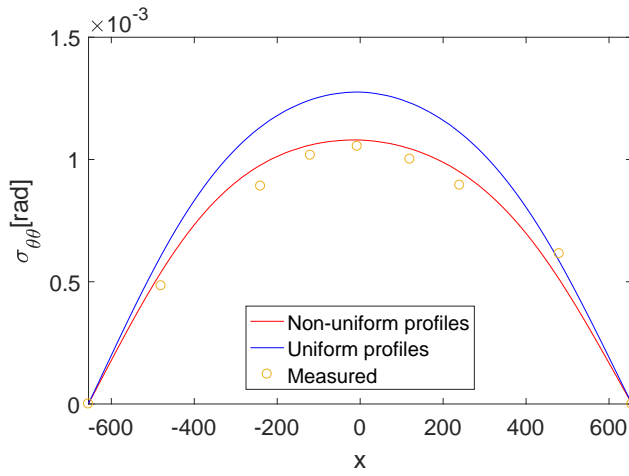
(o) 02-03-2016 04:41:37



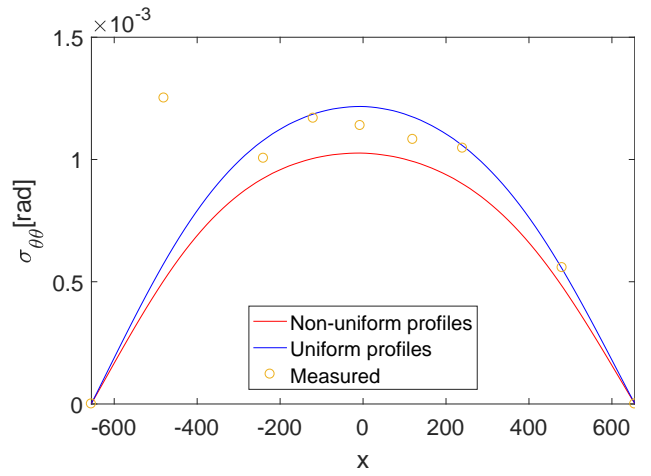
(p) 02-03-2016 05:45:08

Figure B.5: Vertical response along the span.

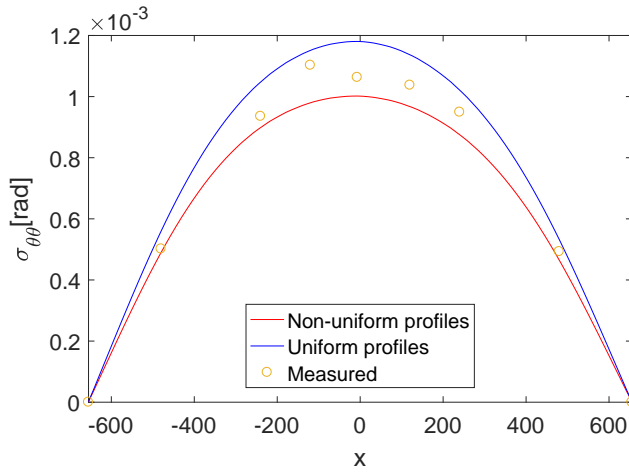
Torsional response



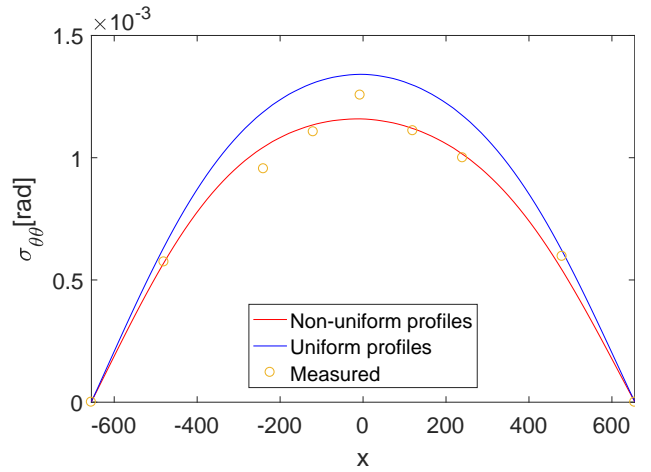
(a) 29-01-2016 13:00:00



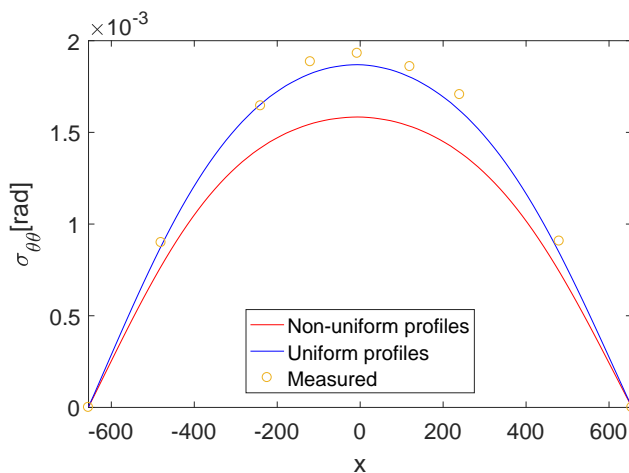
(b) 29-01-2016 13:30:00



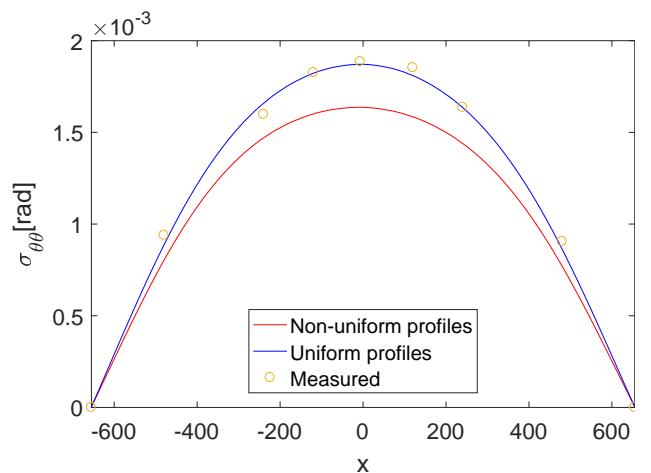
(c) 29-01-2016 14:00:00



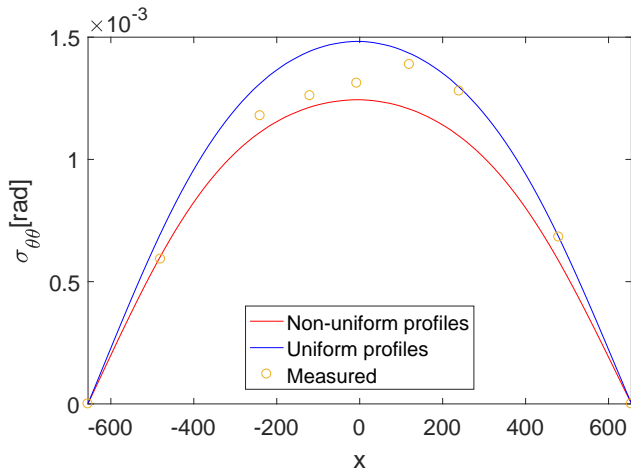
(d) 29-01-2016 15:30:00



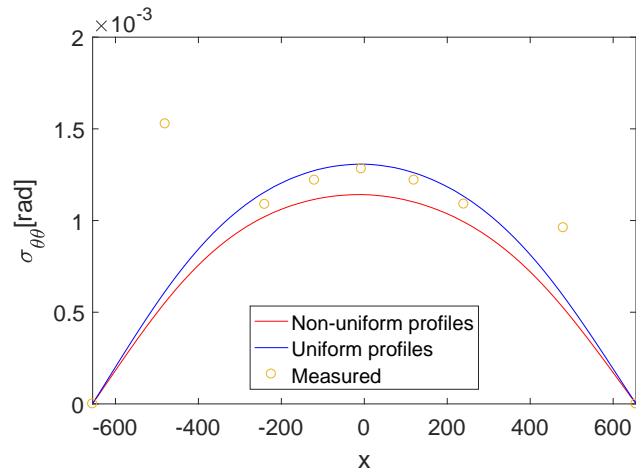
(e) 29-01-2016 17:30:00



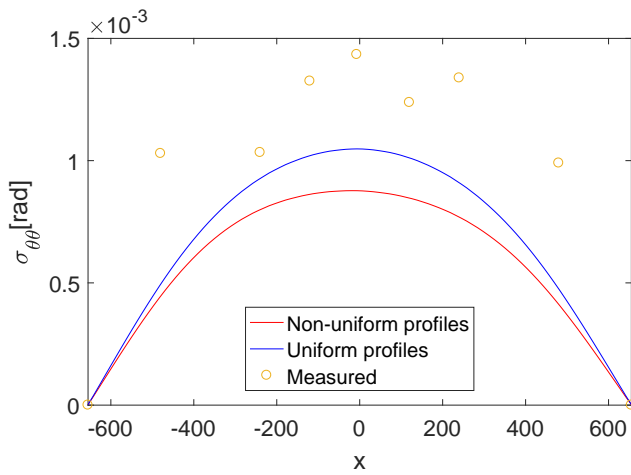
(f) 29-01-2016 19:30:00



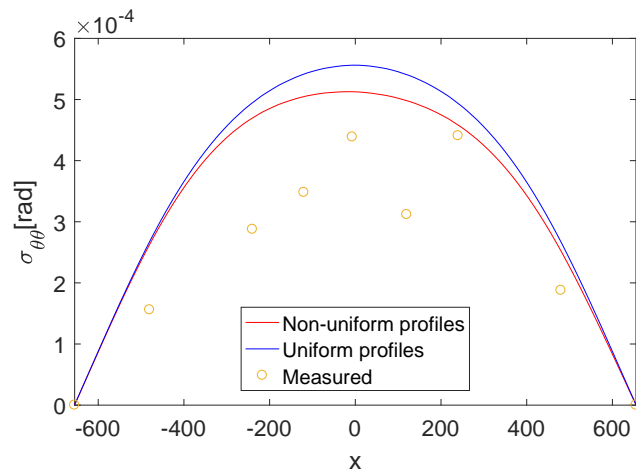
(g) 29-01-2016 20:00:00



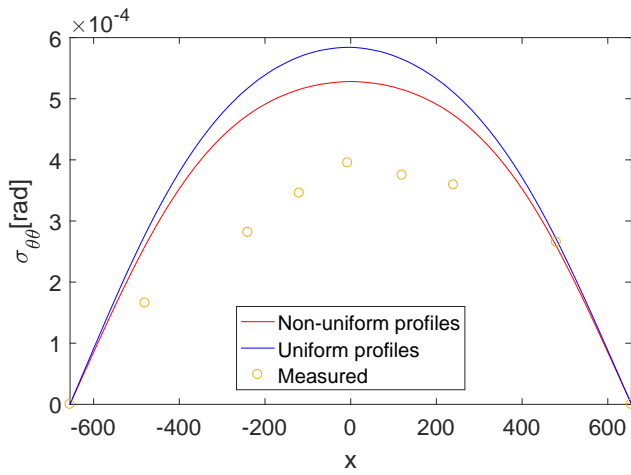
(h) 29-01-2016 20:30:00



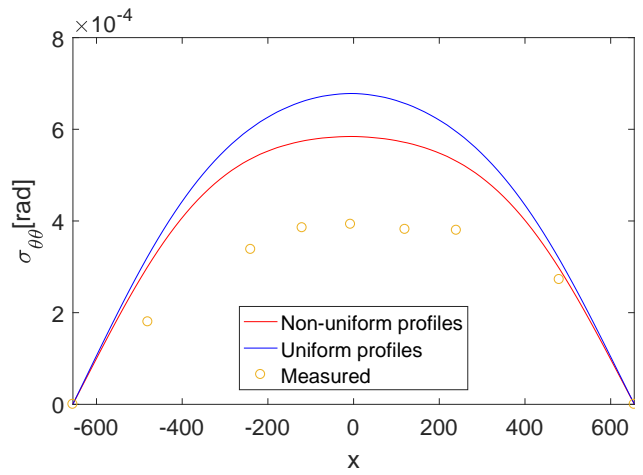
(i) 29-01-2016 21:00:00



(j) 01-03-2016 22:29:20



(k) 02-03-2016 02:15:29



(l) 02-03-2016 02:57:13

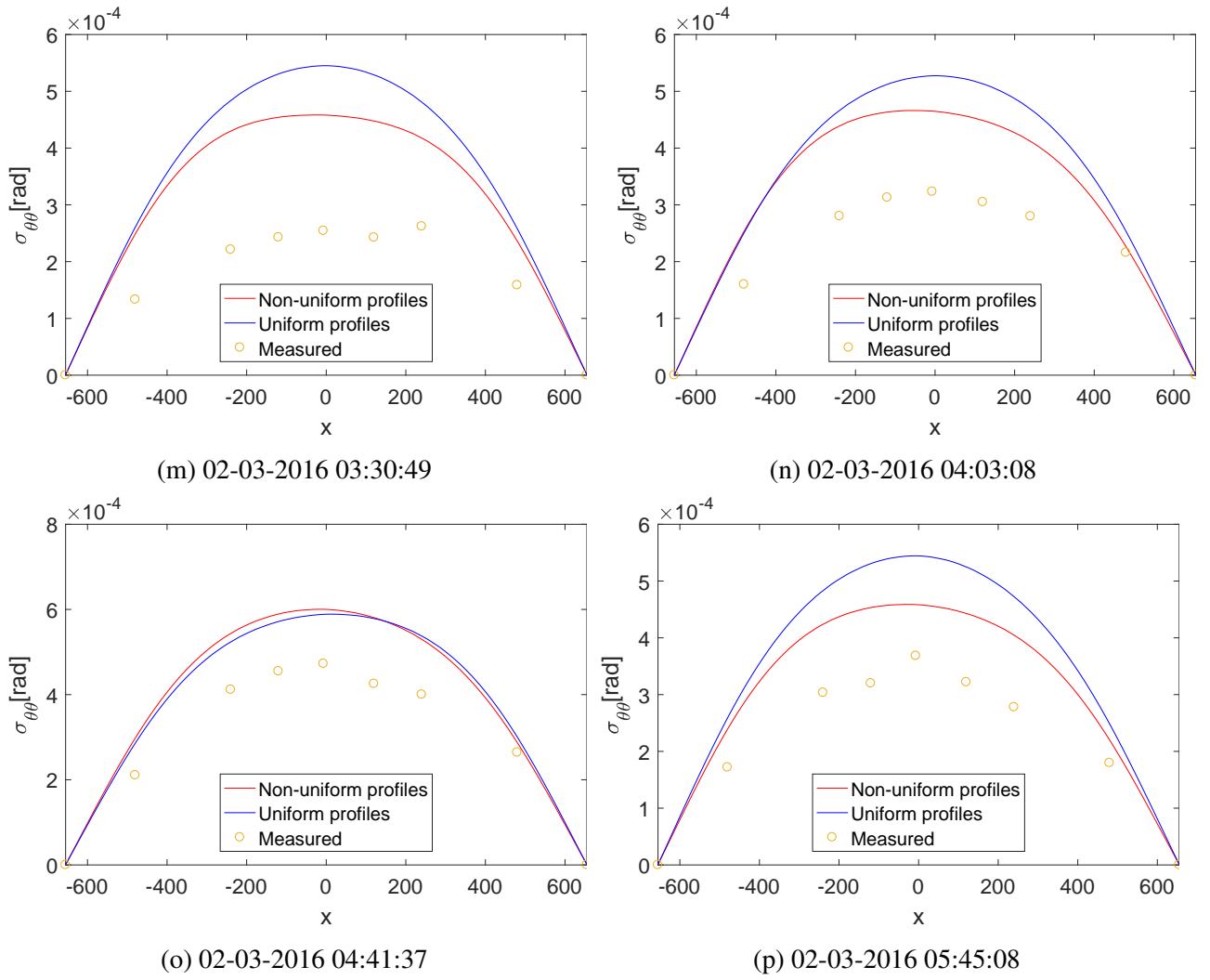


Figure B.6: Torsional response along the span.